Chemotaxis in Microorganism Transport Toward Competing Chemical Stimuli

---

A

Dissertation

Presented to

the faculty of the School of Engineering and Applied Science

University of Virginia

---

in partial fulfillment

of the requirements for the degree

Doctor of Philosophy

by

Xueying Zhao

December 2021

APPROVAL SHEET

This

Dissertation

is submitted in partial fulfillment of the requirements
for the degree of

Doctor of Philosophy

Author: Xueying Zhao

This Dissertation has been read and approved by the examining committee:

Advisor: Roseanne M. Ford

Advisor:

Committee Member: Bryan W. Berger

Committee Member: Liheng Cai

Committee Member: Matthew J. Lazzara

Committee Member: Lisa Colosi Peterson

Committee Member:

Committee Member:

Accepted for the School of Engineering and Applied Science:

Jennifer L. West, School of Engineering and Applied Science

December 2021

Abstract

Bioremediation is a clean-up technology that has been used to degrade hydrocarbon contaminants in soil and sediments. However, bioremediation in the ocean in the context of an oil spill is not well studied. The heterogeneous and ephemeral hydrocarbon distribution increases the challenges for marine bacteria to navigate the ocean in search of favorable locations for survival. Therefore, transport properties, such as motility and chemotaxis provide marine bacteria a way to locate and swim preferentially toward the hydrocarbons. Studies have shown that chemotaxis has the potential to increase bioavailability and enhance biodegradation efficiency. However, most studies have focused on bacteria chemotaxis to a single stimulus, while bacteria are commonly exposed to multiple stimuli with competing effects. Bacteria chemotactic responses to multiple stimuli are not fully understood. A mathematical model can give us insights into the chemosensory mechanism that bacteria use to integrate their overall response to multiple inputs. In this work, the chemotactic responses of the well-studied bacterium *Escherichia coli* (*E. coli*) were first measured to validate a mathematical model. Then, the model was adapted and used to study marine bacteria *Halomonas* sp. chemotactic responses.

The mathematical model for *E. coli* chemotactic responses to multiple stimuli was evaluated with experimental data. In the model, *E. coli* chemotactic velocities were derived from the transport equations for an attractant α-methylaspartate alone, repellent nickel ion alone, and several combinations of the two. The multi-scale model related the individual bacterium response to the population level response. At the individual level, the model incorporated the signal transduction mechanism as the stimuli bind to the receptor that crosses the cell membrane and the subsequent signaling reactions inside the cell. Values for the chemotactic parameters (stimuli sensitivity coefficient σ, signaling efficiency γ, and repellent sensitivity coefficient κ) were obtained by fitting the model to experimental results. The experimental data were collected using a microfluidic

device designed to create a constant concentration gradient. For *E. coli*, the model correctly predicted the overall attraction or repulsion outcomes of the mixtures. However, quantitatively the prediction showed a slightly greater repellent response of the mixture than the experimental results.

The mathematical model was then used to evaluate marine bacteria *Halomonas* sp. 10BA chemotactic responses to multiple stimuli. It was assumed that *Halomonas* sp. have the same run-and-tumble motility pattern as *E. coli* because they have the same flagella arrangement. However, published studies suggested that the chemotactic mechanism for marine bacteria is different from *E. coli*. This difference was also supported from the experimental results because direct application of the model used for *E. coli* failed to correctly capture the chemotactic response of *Halomonas* sp. Since marine bacteria exhibit faster chemotactic responses than *E. coli*, instead of using only a single receptor for sensing a stimulus, we assumed that *Halomonas* sp. can use multiple receptors. The model was then updated using two chemotactic receptors for sensing attractant decane and one chemotactic receptor for sensing repellent copper. This change resulted in *Halomonas* sp. responding more quickly to stimuli. The updated model predicted *Halomonas* sp. response to multiple stimuli well at the low repellent Cu concentration, while it overpredicted bacteria repulsion at high Cu concentration of 2 mM. This discrepancy may be due to a high association constant for the reaction of Cu bound receptor and the phosphate group at high Cu concentration, altering the value for the repellent sensitivity coefficient κ. This underperformance may also possibly result from the increased swimming speed of marine bacteria at a higher repellent concentration. This increased swimming speed further changes the strength of chemotactic responses to both repellent and attractant. This work suggests that the signaling pathway adapted from *E. coli* can be applied to qualitatively describe marine bacteria chemotactic response to multiple stimuli. However, further modification should be applied to the model to accurately predict the response quantitatively. Regardless, this model can provide qualitatively estimation on the naturally occurring marine

bacteria respond to the oil given the oil composition. This can provide some information on whether bioremediation should be considered or the conventional interventions should be enforced in oil spill cleanup.

Acknowledgement

First and foremost, I would like to acknowledge my advisor, Dr. Roseanne Ford. For all your patience, advice, support, and encouragement. Your passion for research always drives me to learn more about the topic and it is such fun to discuss research with you. You also care for me and my family, and care about whether we are happy as a graduate student. Thank you for all of it!

I would like to thank all the members of my committee: Dr. Bryan W. Berger, Dr. Liheng Cai, Dr. Matthew Lazzara, Dr. Lisa Colosi Peterson for all their time, suggestions during my proposal, and making time for my defense. I would like to thank the most to Dr. Matthew Lazzara for letting me join your group meeting while Professor Ford was on her sabbatical. Your group provided a good environment for me when I was the only graduate student in the lab.

Thank you to all of the past and present Chemical Engineering staff: Ricky Buchanan, Jennifer Davis, Vickie Faulconer, Jen Lamb, Teresa Morris, April Spencer, Angela Skubon, and Ryan Thompson. Thank you for moving things for me, ordering and following up on my orders, scheduling space for my presentation, fixing my computer, and all other things.

This work was funded by The Gulf of Mexico Research Initiative. I appreciate Dr. Doug Bartlett from Scripps Institute of Oceanography for sharing us marine bacteria strains and Kelly Mullane for discussing new findings. I am thankful for the discussions with other graduate students who also work on the project in the conferences and the information shared by other professors.

Thank you, Dr. Periasamy in the Keck Center for Cellular Imaging for your advice, your care, and mentorship over the years. Thanks, Ruofan and other staff for the discussion and guidance.

I would like to thank all the past and present members of the Ford lab: Dr. Xiaopu Wang, Dr. Joanna Adadevoh, Dr. Shun Zheng, Beibei Gao, Tracy Kuper, Rhea Braun, and Sanha Kim, for your support, discussion, and your help editing my documents. Thank you, Gabrielle Chen, for sharing with me your work on the experimental setup. I would also want to thank Kenton Weigel for your

time and ideas when working with me. Nushaba Rashid, I cannot say how much support you gave me when I was the only graduate student in the lab. You are also a good friend to me. Thank you for sharing your ideas on work and life with me!

Thank you to the members of Dr. James P. Landers' lab for your help with the plasma treatment machine and laser cutter. Thanks to Scott Karas for scheduling the laser cutter, changing the gas tank, and fixing equipment for me. I'm always inspired by your cheerful attitude. I also appreciate members from other research labs who helped me with the equipment.

The support from the UVA Engineering Writing Lab is invaluable. Thank you, Dr. Kelly Cunningham, for organizing such a wonderful program. Thank you to all the past and present peer review group members, Dr. Bonnie Doughert, Dr. Christopher Rawls, Adrienne Williams, Dr. Billy Lamberti, Areli Rodriguez, Carolina Moraes, Maria Rossetti for providing feedback to my written documents and presentations. Thank you for your support both in research and graduate life.

I would also want to acknowledge Dr. Amy Clobes and Dr. Marlit Hayslett, you taught me how to communicate a complex research question in a simple way that can be easily understood by the public. I am also inspired by your attitude toward both work and life.

Thank you to all my classmates. Thank you for your academic and emotional support. I feel so lucky to have you all in graduate school and I treasured all the time we spent together.

Thanks for all my other friends: Fangwei, Lauren, Rachel, Renqin, Yan and Zhangfan. Thank you for spending time with me and making me a better person in your own ways.

I also appreciate everyone who creates such an amazing environment at UVA. Walking around the grounds always makes me happy and relaxed, and feels the better in life even though it might not one for me at the moment.

I would really like to thank my parents for always supporting, encouraging, and believing in me. Thank you for your unconditional love!

List of Symbols

Symbols

a	attractant concentration
b	bacterial concentration
I	gray level value
k	reaction rate constant of the phosphate transfer reaction
K_1	dissociation constant of phosphorylation of the unbound receptor complex
K_2	dissociation constant of phosphorylation of the repellent bound receptor complex
K_c	chemotaxis receptor constant
K_{dA}	dissociation constant of α-methyl aspartate binding
K_{dC}	dissociation constant of copper ions binding
K_{dD}	dissociation constant of decane binding
K_{dN}	dissociation constant of nickel ions binding
L	length of the channel
t	time
v	individual bacterial swimming speed
V_c	chemotactic velocity
x	distance in x-direction

Greek letters

γ	signaling efficiency
κ	repellent sensitivity coefficient
μ_0	bacterial random motility coefficient

σ	stimuli sensitivity coefficient
τ	mean run time
χ_0	chemotactic sensitivity coefficient

List of Figures

Figure 1.1 Bacteria trajectories under conditions with (a) no attractant gradient, bacteria run and tumble, performing a random walk behavior, (b) attractant gradient, bacteria tumble less, performing biased random walk toward the gradient direction. 3

Figure 1.2 Schematic of the signaling transduction mechanism in *E. coil*. (a) Receptor reaction inside cell membrane when there is no stimulus, (b) Receptor reaction inside cell membrane when the receptor is bound to attractant α-methylaspartate (Asp), (c) Receptor reaction inside cell membrane when the receptor is bound to repellent nickel ion (Ni). 4

Figure 2.1 Expected trajectories of CheY-P concentration for cells running in one dimension, either up (green) or down（red）in a gradient. Adapted from Dufour et al. (2014). 19

Figure 2.2 Switching frequency as a function of CheY-P concentration. Adapted from Cluzel et al. (2000). 20

Figure 2.3 Dependence of the phosphorylation reaction on the concentration of CheA. Open symbols indicate wild type bacteria and closed symbols indicate controls, circles indicate the amount of CheY-phosphate and squares indicate CheA-phosphate with 1000 cpm/pmol (red dashed lines indicate the values used in the calculation: $[\mathrm{CheA_T}]$ is 40 pmol and CheA-P is 2000 cpm or 2 pmol). Adapted from Borkavich et al. (1989). 21

Figure 2.4 Response of *E. coli* to addition of attractant and repellent. The concentrations shown are (proceeding from the lowest curve to the highest): 10 mM Ni^{2+}, 1 mM Ni^{2+}, 100 μM Ni^{2+}, 10 μM Ni^{2+}, 0.01 μM Asp, 0.1 μM Asp, 1 μM Asp, 10 μM Asp, 100 μM Asp. Adapted from Hauri and Ross (1995). 22

Figure 2.5 CW bias of *E. coli* plotted as a function of CheY-P concentration. Adapted from Cluzel et al. (2000). 23

Figure 2.6 Plot of the effect of different concentrations of aspartate and Ni^{2+} (plotted as fraction of receptors with stimulatory ligand bound). The peak excitation plotted as a function of the difference between the fraction of receptors with aspartate bound (f_{asp}) and the fraction with Ni^{2+} (f_{Ni}) bound. Adapted from Hauri and Ross (1995). 24

Figure 3.1 Photo of microfluidic device (top-down view) with *E. coli* flow path colored green and chemoeffector colored blue and an enlarged cross-sectional view (not drawn to scale in order to emphasize the diffusion in the channel) showing connections between the top and bottom channels. 36

Figure 3.2 (a) GFP-labeled *E. coli* distribution in a cross channel at steady state. There is a constant source of bacteria on the left-hand side of the channel, and a constant attractant source of 0.2 mM α-methylaspartate on the right-hand side; the fluorescence intensity is proportional to bacterial concentration. Red rectangular box indicates the region over which data was analyzed. (b) Normalized bacteria intensity along the channel (scattered data) and the model results (solid lines). The black line indicates the expected bacterial distribution at steady state for the control case without chemoattractant. The blue shading from right to left represents the attractant gradient. 39

Figure 3.3 (a) GFP-labeled *E. coli* distribution in a cross channel at steady state. There is a constant source of bacteria on the left-hand side of the channel, and a constant attractant source of 0.4 mM α-methylaspartate on the right-hand side; the fluorescence intensity is proportional to bacterial concentration. Red rectangular box indicates the region over which data was analyzed. (b) Normalized bacteria intensity along the channel (scattered data) and the model results (solid lines). The black line indicates the expected bacterial distribution at steady state for the control case without chemoattractant. The blue shading from right to left represents the attractant gradient.

..... 40

Figure 3.4 (a) GFP-labeled *E. coli* distribution in a cross channel at steady state. There is a constant source of bacteria on the left-hand side of the channel, and a constant repellent source of 0.01 mM nickel sulfate on the right-hand side; the fluorescence intensity is proportional to bacterial concentration. Red rectangular box indicates the region over which data was analyzed. (b) Normalized bacteria intensity along the channel (scattered data) and the model results (solid line). The red line indicates the expected bacterial distribution at steady state for the control case without chemorepellent. The red shading from right to left represents the repellent gradient.

..... 41

Figure 3.5 (a) GFP-labeled *E. coli* distribution in a cross channel at steady state. There is a constant source of bacteria on the left-hand side of the channel, and a constant

repellent source of 0.05 mM nickel sulfate on the right-hand side; the fluorescence intensity is proportional to bacterial concentration. Red rectangular box indicates the region over which data was analyzed. (b) Normalized bacteria intensity along the channel (scattered data) and the model results (solid line). The red line indicates the expected bacterial distribution at steady state for the control case without chemorepellent. The red shading from right to left represents the repellent gradient.

..... 42

Figure 3.6 GFP-labeled *E. coli* distribution in a cross channel at steady state. There is a constant source of bacteria on the left-hand side of the channel, and a constant source of chemoeffector on the right-hand side: (a) 0.2 mM α-methyl aspartate, (b) 0.2 mM α-methyl aspartate and 0.01 mM nickel ions, and (c) 0.2 mM α-methyl aspartate and 0.05 mM nickel ions. The fluorescence intensity is proportional to bacterial concentration and is plotted as normalized intensity as a function of location for bacteria response to (d) 0.2 mM α-methyl aspartate, (e) 0.2 mM α-methyl aspartate and 0.01 mM nickel ions, and (f) 0.2 mM α-methyl aspartate and 0.05 mM nickel ions. Note that although the bacteria concentrations in the images are not the same, the gray level value in each image is calibrated itself using the methods described in 3.4.3..... 44

Figure 3.7 GFP-labeled *E. coli* distribution in a cross channel at steady state for a constant source of bacteria on the left-hand side of the channel and a constant source of chemoeffector on the right-hand side with (a) 0.05 mM nickel ions (b) 0.05 mM nickel ions and 0.2 mM α-methyl aspartate and (c) 0.05 mM nickel ions and 0.4 mM α-methyl aspartate). The fluorescence intensity is proportional to bacterial concentration and is plotted as normalized intensity as a function of location for bacteria response to (d) 0.05 mM nickel ions, (e) 0.05 mM nickel ions and 0.2 mM α-methyl aspartate, and (f) 0.05 mM nickel ions and 0.4 mM α-methyl aspartate. Note that although the bacteria concentrations in the images are not the same, the gray level value in each image is calibrated itself using the methods described in 3.4.3. 45

Figure 3.8 GFP-labeled *E. coli* distribution in a cross channel at steady state. There is a constant source of bacteria on the left-hand side of the channel, and a constant source of attractant α-methyl aspartate or/and repellent nickel ions on the right-hand side (a: buffer only; b-c 0.2 mM and 0.4 mM α-methyl aspartate; d-f 0.01 mM nickel ions, addition of 0.2 mM, and addition of 0.4 mM α-methyl aspartate;

g-i 0.05 mM nickel ions, addition of 0.2 mM, and addition of 0.4 mM α-methyl aspartate). The fluorescence intensity is proportional to bacterial concentration. 46

Figure 4.1 Transmission Electron Micrograph of *Halomonas titanicae* BH1, showing flagellar arrangement. (From Sánchez-Porro et al., 2010)..... 56

Figure 4.2 Schematic of the signal transduction mechanism in (a) *E. coli*, where the Tar receptor is used to sense both stimuli (blue indicates attractant and red indicates repellent); (b) *Halomonas* sp., where there are two Receptor 1s (m=2) for sensing attractant, and for each Receptor 2 (n=1), which is associated with sensing repellent..... 60

Figure 4.3. (a) Microscopic images of the cross channel in the microfluidic device, where *Halomonas* sp. 10BA migrate from a constant source at the left-hand side toward 0.06 μM decane from a constant source at the right-hand side. The red rectangular box indicates the region over which the data was analyzed. (b) Normalized bacterial intensity profile from the experiment (scattered blue line) and model results (solid blue line). The blue shading indicates the concentration of decane which decreases from right to left. 64

Figure 4.4 (a) Microscopic images of the cross channel in the microfluidic device, where *Halomonas* sp. 10BA form a constant source at the left-hand side and 0.2 μM decane form a constant source at the right-hand side. The red rectangular box indicates the region over which the data was analyzed. (b) Normalized bacterial intensity profile from the experiment (scattered blue line) and model results (solid line). The blue gradient shade indicates the constant gradient of decane from right to left. 65

Figure 4.5 (a) Microscopic images of the bottom channel in the microfluidic device, where *Halomonas* sp. 10BA form a constant source at the left-hand side and 0.5 mM Cu form a constant source at the right-hand side. The red rectangular box indicates the region over which the data was analyzed. (b) Normalized bacterial intensity profile from the experiment (scattered blue line) and model results (solid line). The blue gradient shade indicates the constant gradient of Cu from right to left. 66

Figure 4.6 (a) Microscopic images of the bottom channel in the microfluidic device, where *Halomonas* sp. 10BA form a constant source at the left-hand side and 2 mM Cu form a constant source at the right-hand side. The red rectangular box indicates the region over which the data was analyzed. (b) Normalized bacterial intensity

profile from the experiment (scattered blue line) and model results (solid line). The blue gradient shade indicates the constant gradient of Cu from right to left. 67

Figure 4.7 Effect of the addition of Cu to *Halomonas* sp. 10BA response to chemoeefector. Microscopic images of the bottom channel in the microfluidic device, where *Halomonas* sp. 10BA form a constant source at the left-hand side and (a) 0.2 μM decane (b) 0.2 μM decane and 0.5 mM Cu (c) 0.2 μM decane and 2 mM Cu form a constant source at the right-hand side; normalized bacterial intensity profile from the experiment (scattered blue line) and model results (solid line). The blue gradient shade indicates the constant gradient of chemoeffector from right to left. 69

Figure 4.8 Effect of the addition of decane to *Halomonas* sp. 10BA response to chemoeefector. Microscopic images of the bottom channel in the microfluidic device, where *Halomonas* sp. 10BA form a constant source at the left-hand side and (a) 0.5 mM decane (b) 0.5 mM Cu and 0.06 μM decane and (c) 0.5 mM Cu and 0.2 μM decane form a constant source at the right-hand side; normalized bacterial intensity profile from the experiment (scattered blue line) and model results (solid line). The blue gradient shade indicates the constant gradient of chemoeffector from right to left. 70

Figure 4.9 Normalized bacterial intensity profile from the experiment (scattered blue line) and model results (solid line). (a) buffer only; (b-c) 0.06 μM decane and 0.2 μM decane; (d) 0.5 mM Cu; (e) 2 mM Cu; (f) 0.06 μM decane and 0.5 mM Cu; (g) 0.2 μM decane and 0.5 mM Cu; (h) 0.06 μM decane and 2 mM Cu; (i) 0.2 μM decane and 2 mM Cu. The blue gradient shade indicates the constant gradient of chemoeffector from right to left. 71

Table of Contents

Chapter 1. Introduction **1**

1.1 Motivation and Background 1

1.1.1 Motility and chemotaxis 2

1.1.2 Marine bacteria motility and chemotaxis 5

1.2 Hypothesis and Objectives 6

1.3 Outline 8

Chapter 2. Mathematical Model and Chemotactic Parameters **11**

2.1 Signal Transduction Kinetics 11

2.2 Tumbling Probability 13

2.3 Derivation of the Chemotactic Velocity under Different Conditions 14

2.3.1 Phosphorylation of histidine kinase in the absence of chemoeffectors 14

2.3.2 Chemotactic velocity in presence of attractant 14

2.3.3 Chemotactic velocity in the presence of repellent 16

2.3.4 Chemotactic velocity in the presence of combined chemoeffectors 17

2.4 Parameter Values as Deduced from Published Literature 17

Chapter 3. *Escherichia coli* Chemotactic to Multiple Stimuli in a Microfluidic Device with a Constant Gradient **27**

3.1 Abstract 27

3.2 Introduction 28

3.3 Mathematical Model 31

3.3.1 Bacteria transport processes at the population level 31

3.3.2 Signal transduction kinetics for chemotaxis 33

3.4 Experimental Methods 34

3.4.1 Preparation of bacteria cultures 34

3.4.2 Microfluidic design, fabrication and operation 35

3.4.3 Microscopy and image analysis 36

3.5 Results and Discussion 37
3.5.1 *E. coli* HCB1 chemotactic response to an attractant α-methylaspartate 37
3.5.2 *E. coli* HCB1 chemotactic response to a repellent nickel 40
3.5.3 *E. coli* response to chemoeffector mixtures 42
Chapter 4. Marine Bacteria *Halomonas* sp. 10BA Chemotactic to Multiple Stimuli 51
4.1 Abstract 51
4.2 Introduction 53
4.3 Methods and Model 57
4.3.1 Preparation of bacteria cultures 58
4.3.2 Mathematical Model 59
4.4 Results and Discussion 63
4.4.1 *Halomonas* sp. 10BA chemotactic response to decane 63
4.4.2 *Halomonas* sp. 10BA chemotactic response to copper 65
4.4.3 *Halomonas* sp. 10BA chemotactic response to chemoeffector mixtures 67
Chapter 5. Conclusions and Future Directions 76
Appendix A: Validation of diffusion only in the device using 10% uranine solution 81
Appendix B: Random Motility Coefficient for *E. coli* HCB1 83
Appendix C: Random Motility Coefficient for *Halomonas* sp. 10BA 85

Chapter 1. Introduction

1.1 Motivation and Background

In the 2000s, 181 large oil tanker spills occurred, with each oil spill over 7 tonnes, resulting in 196,000 tonnes of oil released accidently into the ocean (ITOPF, 2020). Even though in the 2010s, the number of large oil spills declined to 64 spills, the total oil released was still as high as 164,000 tonnes (ITOPF, 2020). Cleanup techniques such as using booming and skimming are typically used for surface water. However, some spills occur from wells on the ocean floor. A recent example was the oil spill near Orange County on the Southern California coast, caused by a pipeline rupture from the offshore well. The Deepwater Horizon Oil Spill, which released around 225,000 tonnes of oil in 2010, occurred at approximately 1500 m depth and is the deepest oil spill on record. Oil droplets were found at different depths, and the fate of those oil droplets depended largely on hydrocarbon degrading bacteria. This technique to use microorganisms to remove pollutants from contaminated sites is called bioremediation.

Bioremediation was shown to occur naturally after the 2010 oil spill in the Gulf of Mexico (King et al., 2015; Maruyama et al., 2003; Teramoto et al., 2009). However, the natural rate of bioremediation is slow. While most interventions to increase bioremediation rate have been applied to soil systems and reactors, a recent study by Eliora and Eugene (2014) proposed increasing the bioremediation rate in the ocean by adding uric acid as a potential fertilizer. However, even with fertilizer to increase the amount of biomass generated to degrade hydrocarbons, mass transfer limitations still limit the apparent rate of degradation. Bioremediation can proceed at a much faster rate if these marine organisms are in close contact with the components of the oil. Interestingly, bacteria can also adapt in response to an oil plume in the ocean. For example, King et al. (2015) found after the Gulf of Mexico oil spill, genes for hydrocarbon degradation were expressed in

marine bacteria. They also noted that genes for motility and chemotaxis were enriched and expressed. These observations suggest that marine organisms' motility and chemotaxis properties play an important role in hydrocarbon degradation in the ocean. In addition, it is important to understand how these properties affect bacterial responses to the mixtures of chemical compounds, because crude oil is a mixture of hydrocarbons and heavy metals. More details on bacteria response to multiple stimuli will be introduced in Chapter 2.

1.1.1 Motility and chemotaxis

Bacteria motility is the independent movement of bacteria. Flagella are involved in some types of motility, for example, swarming (2D movement over a surface) and swimming (in liquid environments). In this study, motility specifically refers to bacteria swimming. For some bacteria, such as *Escherichia coli* (*E. coli*), the trajectory of their swimming motion consists of straight "runs", which are interrupted by "tumbles", to change swimming direction. This random walk is similar to diffusive motion. Analogous to the diffusion coefficient, the random motility coefficient is used to describe this random walk of bacteria. The random motility coefficient μ_0 is related to individual cellular properties: cell swimming speed, run time, and the turn angle distribution between two successive runs (Lovely and Dalquist, 1975).

Chemotactic bacteria can sense the chemical gradient, moving toward the attractant (food or energy sources) and moving away from repellent (harmful or poison chemicals). When facing the higher concentration of attractant, chemotactic bacteria will decrease tumble probability, which result in a biased random walk that favors the attractant direction. An illustration of bacteria run-and-tumble behavior with and without attractant gradient is shown in Figure 1.1.

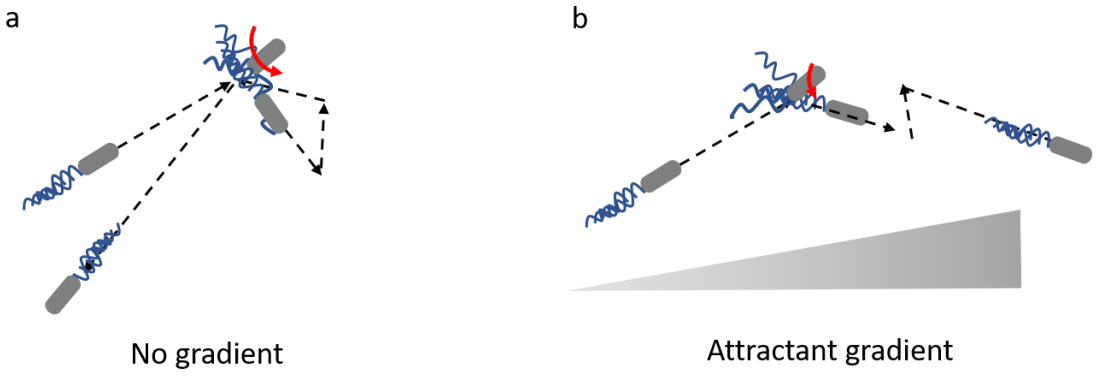

Figure 1.1 Bacteria trajectories under conditions (a) with no attractant gradient, where bacteria exhibit run-and-tumble behavior, tracing out a random walk behavior, and (b) with an attractant gradient, where bacteria tumble less frequently, and perform a biased random walk toward the attractant gradient. The triangle indicates an increasing attractant gradient from left to right.

Some established devices to measure bacteria motility and chemotaxis at the population scale are introduced here. One widely used assay is a simple capillary assay developed by Adler (1967). In this assay, bacteria were introduced at one end of a capillary tube filled with buffer, and the number of bacteria that accumulated in the capillary was recorded at several different times. For chemotactic parameter measurements, the number of bacteria that entered the capillary tubes filled with an attractant was compared to the number of bacteria that accumulated in the presence of buffer. However, the difficulty of determining the exact concentration gradient made it hard for mathematical modeling. The development of the stopped-flow diffusion chamber (SFDC) made it possible to mathematically model bacteria chemotaxis, because it created a defined step-change of the chemical concentration (Ford and Lauffenburger, 1991). However, the concentration gradient in the SFDC will eventually relax over time. Another step in developing these devices was the constant gradient microfluidic device (Wang et al., 2015), which provided a well-maintained constant gradient throughout the experiment. New techniques such as differential dynamic microscopy that was used for analyzing Brownian motion of colloids was also adapted to measure bacteria motility

(Germain et al., 2016). Though in this work, we adapted the constant gradient device and made a few improvements such as image quality and device maintenance.

While these populational scale measurements will give us certain chemotactic information, it is also important to understand the individual-level mechanism controlling the overall chemotactic behavior. The signaling response in *E. coli* chemotaxis (Figure 1.2) is well studied, which depends on the phosphate transfer between a histidine kinase and a response regulator (Sourjik et al., 2010). In the absence of a chemoattractant, the kinase CheA has autophosphorylation activity, the CheA phosphoryl group is further transferred to response regulator CheY, which will diffuse through the cytoplasm and transmit the signal to the flagellar motor, enhance the probability of clockwise (CW) rotation and cause the bacteria to tumble. In the presence of a chemoattractant, the binding of attractant causes CheA inactivation and decreases the tumble probability, which will lead to the cell continually moving in this direction. The binding of repellent does not inactivate CheA, rather it increases the likelihood of a tumble, resulting in the net movement of the cell away from that direction. However, the chemotactic response to multiple stimuli is not well studied, which is the focus of this work and will be introduced in more detail in Chapter 2 and Chapter 3.

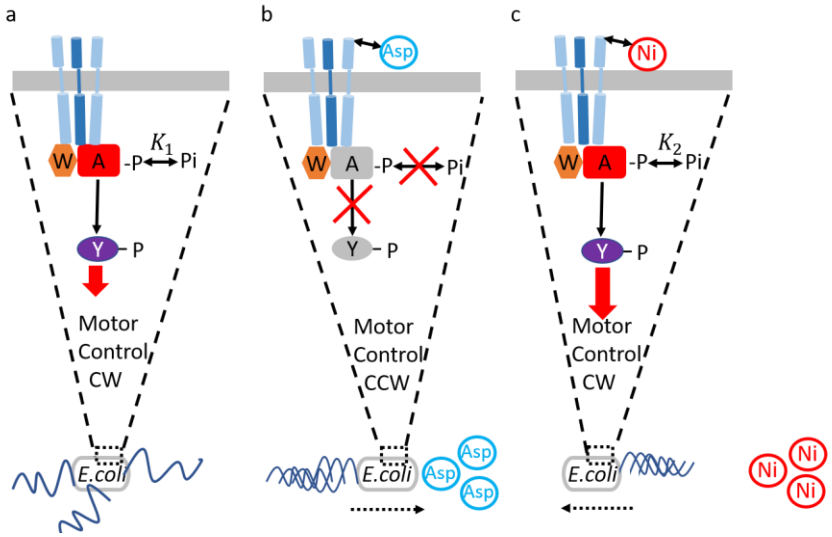

Figure 1.2 Schematic of the signaling transduction mechanism in *E. coil*. (a) Receptor reaction inside cell membrane when there is no stimulus, (b) Receptor reaction inside cell membrane when

the receptor is bound to attractant α-methylaspartate (Asp), (c) Receptor reaction inside cell membrane when the receptor is bound to repellent nickel ion (Ni).

1.1.2 Marine bacteria motility and chemotaxis

Even though less studied, motility and chemotaxis are more important for marine bacteria because of the heterogeneous environment of the ocean and transient release of nutrient pulses (Stocker and Seymour, 2012). Swimming is an energy-consuming cost; however, studies show that marine bacteria usually swim faster than *E. coli*, which are indigenous to a richer nutrient environment. The mean swimming speed for marine bacteria varies between 45 to 230 μm/s based on observations of natural communities and isolates (Mitchell et al., 1995), while the swimming speed for *E. coli* is typically between 15 to 30 μm/s. This higher swimming speed allows marine bacteria to quickly navigate around the temporal changes in nutrient concentration and enhance their survival.

Marine bacteria also show different motility patterns from *E. coli*. Some marine bacteria have only a single flagellum and trace out a run-and-reverse pattern, instead of run-and-tumble like *E. coli*. Xie et al. (2011) observed a unique reorientation "flick" within marine bacteria, where it reoriented with a mean of 90 degrees, however, the underlying cellular process for this behavior is unknown. The "flick" creates a random exploration of the environment for single flagellum marine bacteria, while effectively saving the synthesis energy costs of flagella (Stocker and Seymour, 2012), compared to bacteria with multiple flagella, such as *E. coli*. In this dissertation, the *Halomonas* sp. have multiple flagella (Sánchez-Porro et al., 2010), similar to *E. coli*. Since there is not enough evidence from the literature, we assumed *Halomonas* sp. 10BA apply the same run-and-tumble mechanism because they have the same flagella arrangement with *E. coli*.

In addition to the motility pattern differences between marine bacteria and *E. coli*, the

chemotactic responses of marine bacteria were also found to be greater and faster compared to *E. coli*. Son et al. (2016) found that the chemotactic migration coefficient (CMC) of marine bacteria *Vibrio alginolyticus* was twofold than that of *E. coli*, where CMC = 0 signifies no chemotactic response, CMC = 1 is maximum attraction, and CMC = -1 is maximum repulsion. It was also suggested that chemotaxis was faster for marine bacteria than *E. coli*. Stocker et al. (2008) tested the chemotaxis of bacteria toward a nutrient patch in a microfluidic device and found that marine bacteria *P. haloplanktis* migrated ten times faster than *E. coli* into the nutrient patch. This response would largely increase the nutrient uptake of motile bacteria over nonmotile bacteria (Smriga et al., 2016) and advance marine chemical cycling processes.

These greater performances of marine bacteria chemotaxis may correspond to differences in signal transduction processes compared to *E. coli*. Previous studies (Mitchell et al., 1996; Brumley et al., 2020) suggested that marine bacteria have faster signal processing time to allow sensing of chemical gradients at higher swimming speeds. In order to study the unknown chemotactic response of marine bacteria, we modified a mathematical model from *E. coli*. This updated model suggests *Halomonas* sp. responds independently to attractant and repellent, which will be explained in more detail in Chapter 4.

1.2 Hypothesis and Objectives

The release of oil from the Macondo well blowout produced a large amount of undissolved oil droplets within large plumes near the ocean floor. Microorganisms in the vicinity of these plumes that were capable of degrading hydrocarbons had a competitive advantage in their quest to survive and proliferate. It is important to increase the biodegradation rate to facilitate oil spill cleanup, which can be achieved by increasing bacteria concentration. The bacteria population increases when they degrade and grow on hydrocarbons, which take days. In contrast, motile bacteria can concentrate

around hydrocarbon droplets via chemotaxis in a shorter time before growth increases the bacteria population, which further increases the biodegradation rate. However, little is known about the marine bacteria mass transfer coefficient. Therefore, I am interested to answer the research question: To what extent does chemotaxis contribute to increasing the transport process of hydrocarbon-degrading marine bacteria to oil droplets? To answer this question, I measure bacteria diffusive mass transfer coefficient (random motility coefficient) in the absence of hydrocarbons and directed mass transfer coefficient (chemotactic parameters) in the presence of hydrocarbons using a microfluidic device.

To mainly focus on the transport of bacteria, I assume that there is no hydrocarbon degradation during the experiment. In this work, I first used GFP labeled *E. coli* HCB1 to test the chemotactic response to different concentrations of α-methylaspartate (attractant) and nickel (repellent). By fitting the transport model to the experimental data, I then obtained bacteria transport coefficients (random motility coefficient and chemotactic parameters). Bacteria chemotactic response in the presence of multiple stimuli was predicted using the parameters obtained from single stimuli and compared with experimental results. After validating the model for how multiple inputs are integrated within the signal transduction mechanism in *E. coli*, I studied marine bacteria response to multiple stimuli. Decane was selected as an attractant, and copper ions, a component in crude oil, was selected as a repellent. For the marine bacteria chemotactic model, Gasperotti et al. (2018) studied the organization of chemotactic genes in *Halomonas* sp. and found that they are almost identical to that observed in the *E. coli* Che cluster. However, for *E. coli*, each receptor is responsible for multiple compounds (e.g. Tar for both aspartate and nickel). Therefore, the response of *E. coli* to the attractant depends on the concentration of the repellent as well because they compete for the same receptor. *Halomonas* sp. has three methyl-accepting chemotactic proteins in the chemosensory cluster. There are several possibilities for *Halomonas* sp. chemotactic mechanism: 1) similar to *E.*

coli, attractant and repellent compete for the same receptor, 2) attractant and repellent are independently bind to separate receptor, 3) attractant and repellent can bind to multiple receptors (m receptor for attractant binding and n receptor for repellent binding). To investigate these possibilities, I adapted the mathematical model of *E. coli* chemotactic responses to quantify marine bacteria chemotactic responses. The specific objectives are outlined below:

1. Quantify the motility and chemotactic response of *E. coli* to multiple stimuli;
2. Quantify the motility and chemotactic response of marine bacteria (*Halomonas* sp. 10BA) to a single hydrocarbon stimulus and a single repellent stimulus;
3. Apply marine bacteria chemotactic model in the presence of multiple stimuli.

1.3 Outline

Chapter 2 describes the chemosensory pathway in an individual bacterium and the parameters used in this study, to help understand the key concepts in the following chapters. Chapter 3 and 4 are the main contents of this dissertation. Chapter 3 focuses on the quantification of the chemotactic parameters of *E. coli* by using a constant gradient microfluidic device. Chapter 4 concentrates on adapting the chemotactic model for marine bacteria *Halomonas* sp. 10BA and quantification of the chemotactic parameters. Chapter 5 concludes the dissertation and recommends directions for future studies.

References

Adler, J., Dahl, M. M. (1967). A method for measuring the motility of bacteria and for comparing random and non-random motility. *J. gen. Microbiol*, *46*, 161.

Barbara, G. M., Mitchell, J. G. (2003). Marine bacterial organisation around point-like sources of amino acids. *FEMS microbiology ecology*, *43*(1), 99-109.

Brumley, D. R., Carrara, F., Hein, A. M., Hagstrom, G. I., Levin, S. A., Stocker, R. (2020). Cutting through the noise: Bacterial chemotaxis in marine microenvironments. *Frontiers in Marine Science*, *7*, 527.

Ford, R. M., Lauffenburger, D. A. (1991). Analysis of chemotactic bacterial distributions in population migration assays using a mathematical model applicable to steep of shallow attractant gradients. *Bull Math Biol*, *53*, 721-749.

Germain, D., Leocmach, M., & Gibaud, T. (2016). Differential dynamic microscopy to characterize Brownian motion and bacteria motility. *American Journal of Physics*, *84*(3), 202-210.

ITOPF, 2020. The data is taken from https://www.itopf.org/knowledge-resources/data-statistics/statistics/

King, G. M., Kostka, J. E., Hazen, T. C., Sobecky, P. A. (2015). Microbial responses to the Deepwater Horizon oil spill: from coastal wetlands to the deep sea. *Annual review of marine science*, *7*, 377-401.

Lovely P. S., Dahlquist F. W. (1975). Statistical measures of bacterial motility and chemotaxis. J *Theor Biol*, *50*, 477-496.

Maruyama, A., Ishiwata, H., Kitamura, K., Sunamura, M., Fujita, T., Matsuo, M., Higashihara, T. (2003). Dynamics of microbial populations and strong selection for *Cycloclasticus pugetii* following the Nakhodka oil spill. *Microb Ecol*, *46*, 442-445.

Mitchell, J. G., Pearson, L., Dillon, S., Kantalis, K. (1995). Natural assemblages of marine bacteria exhibiting high-speed motility and large accelerations. *Applied and environmental microbiology*, *61*(12), 4436-4440.

Mitchell, J. G., Pearson, L, Dillon, S. (1996). Clustering of marine bacteria in seawater enrichments. *Applied and environmental microbiology*, *62*, 3716-3721.

Stocker, R., Seymour, J. R. (2012). Ecology and physics of bacterial chemotaxis in the ocean.

Microbiology and Molecular Biology Reviews, *76*(4), 792-812.

Sánchez-Porro, C., Kaur, B., Mann, H., Ventosa, A. (2010). *Halomonas titanicae* sp. nov., a halophilic bacterium isolated from the RMS Titanic. *International journal of systematic and evolutionary microbiology*, *60*(12), 2768-2774.

Smriga, S., Fernandez, V. I., Mitchell, J. G., Stocker, R. (2016). Chemotaxis toward phytoplankton drives organic matter partitioning among marine bacteria. *Proceedings of the National Academy of Sciences*, *113*(6), 1576-1581.

Stocker, R., Seymour, J. R., Samadani, A., Hunt, D. H., Polz, M. F. (2008). Rapid chemotactic response enables marine bacteria to exploit ephemeral microscale nutrient patches. *Proc. Natl. Acad. Sci. U. S. A.*, *105*, 4209-4214.

Teramoto, M., Suzuki, M., Okazaki, F., Hatmanti, F. A., Harayama, S. (2009). Oceanobacter-related bacteria are important for the degradation of petroleum aliphatic hydrocarbons in the tropical marine environment. *Microbiology*, *155*, 3362-3370.

Wang, X., Atencia, J., Ford, R. M., (2015). Quantitative Analysis of Chemotaxis Towards Toluene by *Pseudomonas putidau* in a convection-free device. *Biotechnology and Bioengineering*, *112*, 896-904.

Xie, L., Altindal, T., Chattopadhyay, S., Wu, X-L. (2011). Bacterial flagellum as a propeller and as a rudder for efficient chemotaxis. *Proc. Natl. Acad. Sci. U. S. A.*, *108*, 2246-2251.

Chapter 2 Mathematical Model and Chemotactic Parameters

Section 2.4 was published as: Middlebrooks, S. A., Zhao, X., Ford, R. M., & Cummings, P. T. (2021). A mathematical model for Escherichia coli chemotaxis to competing stimuli. Biotechnology and Bioengineering, 118(12), 4678-4686.

2.1 Signal Transduction Kinetics

This section introduces the signal transduction kinetics of *E. coli* chemotaxis in the absence and presence of chemoeffector. In the absence of a chemoeffector, the autophosphorylation of histidine kinase when the ternary receptor complex (Tar-CheW-CheA) is unbound is represented as

$$\text{CheA} + \text{P} \overset{K_1}{\Leftrightarrow} \text{CheA-P} \tag{2.1}$$

$$\text{CheA}_\text{T} = \text{CheA} + \text{CheA-P} \tag{2.2}$$

where CheA_T a fixed value, is the summation of CheA and CheA-P, CheA is the unbound receptor complex, CheA-P is the phosphorylated receptor complex, and $K_1 = 0.2$ mM (Surette et al., 1996) is the dissociation constant of phosphorylation of the unbound receptor complex.

In the presence of chemoeffectors, we assume that the binding of α-methylaspartate (Asp) and nickel ion (Ni) to the receptor CheA can be regarded as a competitive adsorption equilibrium, represented as

$$\text{CheA} + \text{Asp} \overset{K_{dA}}{\Leftrightarrow} \text{Asp-CheA} \tag{2.3}$$

$$\text{CheA} + \text{Ni} \overset{K_{dN}}{\Leftrightarrow} \text{Ni-CheA} \tag{2.4}$$

$$\text{Ni-CheA} + \text{P} \overset{K_2}{\Leftrightarrow} \text{CheA- P} \tag{2.5}$$

$$[\text{CheA}_\text{T}] = [\text{CheA}] + [\text{Asp-CheA}] + [\text{Ni-CheA}] + [\text{CheA- P}] + [\text{Ni-CheA- P}] \tag{2.6}$$

In the above Equations (2.3-2.6), Asp-CheA and Ni-CheA represent bound receptor complexes of α-methylaspartate and nickel ions, $CheA_T$ is the total amount of receptor and is a fixed number, $K_{dA} = 0.64$ mM (Clarke and Koshland, 1979) is the dissociation constant of α-methylaspartate and $K_{dN} = 0.54$ mM (Middlebrooks, 1993) is the dissociation constant of nickel ions, and K_2 is the dissociation constant of phosphorylation of the nickel bound receptor complex.

The transfer of phosphate to the response regulator CheY is represented as

$$\text{CheA-P} \xrightarrow{k} \text{CheY-P} \tag{2.7}$$

where CheY-P is the phosphorylated CheY.

The concentration of phosphorylated CheY in the absence of chemoattractant could be obtained since the total amount of receptor is fixed, and is shown in Equation (2.8)

$$[\text{CheY-P}]_0 = \frac{CheA_T k}{\gamma+1} \tag{2.8}$$

where k is the reaction rate constant of the phosphate transfer reaction, and $\gamma = \frac{K_1}{[P]}$ is the signaling efficiency.

Similarly, the amount of signal in the presence of α-methylaspartate alone and nickel alone are expressed in Equations (2.9-2.10)

$$[\text{CheY- P}]_{\text{Asp}} = \frac{CheA_T k}{(\gamma+1)+\gamma\frac{[Asp]}{K_{dA}}} \tag{2.9}$$

$$[\text{CheY- P}]_{\text{Ni}} = \frac{CheA_T k}{1+\gamma(1+\frac{[Ni]}{K_{dN}})/(1+\kappa\frac{[Ni]}{K_{dN}})} \tag{2.10}$$

where $\kappa = \frac{K_1}{K_2}$ is the dissociation constant ratio for phosphorylation.

We assume that the binding of aspartate and nickel to the Tar receptor is competitive. We know that aspartate binds to the periplasmic domain of the Tar receptor (Park et al., 2011) and nickel doesn't need the periplasmic NikA binding protein for the chemotaxis reaction (Englert et al., 2010). However, the specific site on the Tar receptor that nickel binds is still debated. Englert et al. (2010)

suggested that Ni binds specifically to the periplasmic domain of the Tar receptor, and that Ni uptake is not required for repellent taxis in response to Ni. However, Bi et al. (2018) suggested that Ni is detected not by the periplasmic domain, but most likely by the HAMP domain (in the cytoplasm region) and its junction with the transmembrane domain of the Tar receptor. The reason for their conclusion is that they observed that a Tar mutant that completely lacks the periplasmic domain still showed a repellent response to Ni.

After binding to aspartate, the Tar receptor undergoes conformational changes, including a piston motion in the periplasmic domain and a bending in the transmembrane domain. These conformational changes will partially hinder the binding of nickel. However, we don't fully understand the mechanism of nickel binding. There is also a chance that aspartate and nickel can bind to the Tar receptor independently. Gardina et al. (1998) suggested that the binding of aspartate and maltose can be independent if the ligands are restricted to a particular orientation. Even though we assumed that the binding of aspartate and Ni is competitive, we also plotted the theoretical data for the independent addition model to account for the results from other studies. However, we don't have enough experimental data to differentiate between these two possibilities.

2.2 Tumbling Probability

Berg and Brown (1972) suggested that the logarithm of mean run time increases with respect to the time rate of change in the number of bounded receptors according to

$$\ln \tau = \ln \tau_0 + \alpha \frac{dN_b}{dt} \tag{2.11}$$

where τ is the mean run time, τ_0 is the mean run time in absence of the chemoattractant gradient, α is the ratio constant, and N_b is the number of bound receptors in presence of chemoattractant.

In our model, we use the amount of signaling complex CheA-P to represent the number of bound receptors. The mean run time is the reciprocal of the tumbling probability $\tau = 1/p_t$, and after substitution into Equation (2.11), we get

$$\frac{p_t^{+/-}}{p_0} = \exp\left(-\varepsilon \frac{D\frac{[CheA-P]}{[CheA-P]_0}}{Dt}\right) \tag{2.12}$$

where p_0 is the tumbling probability in the absence of a chemoattractant gradient, ε is a ratio constant, $[CheA-P]$ is the amount of signaling complex in the presence of chemoeffectors, and $[CheA-P]_0$ is the amount of signaling complex in the absence of chemoeffectors.

Furthermore, bacteria population migration velocity caused by chemotaxis is defined as

$$V_c = v\frac{p^- - p^+}{p^- + p^+} \tag{2.13}$$

where *v* is the bacterium swimming speed. However, to evaluate the chemotactic velocity, Dufour et al. (2014) suggested that the maximum chemotactic drift velocity is achieved not by optimizing motor directional change (e.g. CW bias), but by maximizing contrast between the run time up and down the gradient. Rivero et al. (1989) defines the equation of chemotactic velocity using the cell swimming velocity, probability per unit time that a "+"-moving cell will become a "-"-moving cell, and the probability per unit time that a "-"-moving cell will become a "+"-moving cell.

2.3. Derivation of the Chemotactic Velocity Under Different Conditions

2.3.1 Phosphorylation of histidine kinase in the absence of chemoeffectors

From Equation (2.1), we know

$$K_1 = \frac{[CheA][P]}{[CheA-P]} \tag{2.14}$$

And we know that $[CheA] = [CheA_T] - [CheA-P]$ from Equation (2.2). Therefore, we can get

$$[CheA-P] = \frac{[CheA_T][P]}{K_1+[P]} = \frac{[CheA_T]}{\frac{K_1}{[P]}+1} = \frac{[CheA_T]}{\gamma+1} \tag{2.15}$$

where $\gamma = \frac{K_1}{P}$ is the signaling efficiency.

2.3.2 Chemotactic velocity in presence of attractant

From Equation (2.3), we know that $K_{dA} = \frac{[CheA][Asp]}{[CheA-Asp]}$ (2.16)

So $[CheA - Asp] = \frac{[CheA][Asp]}{K_{dA}}$ (2.17)

We assume receptors bound by aspartate produce much fewer signaling complex (Borkovich and Simon, 1990), which leads to

$$[CheA_T] = [CheA] + [CheA - P] + [CheA - Asp] \quad (2.18)$$

Substitute Equations (2.16-2.17) into (2.18), and we can get

$$[CheA] = \frac{[CheA_T]}{1+\frac{[P]}{K_1}+\frac{[Asp]}{K_{dA}}} \quad (2.19)$$

Therefore, substitute Equation (2.19) into Equation (2.15), we can get

$$[CheA - P] = \frac{[CheA_T][P]}{K_1+[P]+K_1\frac{[Asp]}{K_{dA}}} = \frac{[CheA_T]}{1+\frac{K_1}{[P]}+\frac{K_1[Asp]}{[P]K_{dA}}} = \frac{[CheA_T]}{1+\gamma+\gamma\frac{[Asp]}{K_{dA}}} \quad (2.20)$$

where $\gamma = \frac{K_1}{P_i}$, is the signaling efficiency, K_{dA} is the dissociation constant for Asp binding.

From Equation (2.11), $\frac{DN_b^{+/-}}{Dt} = \frac{\partial N_b}{\partial t} \pm v\frac{\partial N_b}{\partial x}$, and we use $[CheA - P]$ as representative of the signaling complex, to replace the number of bound receptors N_b, then

$$p_t^{+/-} = p_0 \exp\left[-\alpha\left(\frac{\partial[CheA-P]}{\partial t} \pm v\frac{\partial[CheA-P]}{\partial x}\right)\right] \quad (2.21)$$

We can also write Equation (S21) as $\frac{p_t^{+/-}}{p_0} = \exp\left(-\sigma\left(\frac{\partial\frac{[CheA-P]}{[CheA-P]_0}}{\partial t} \pm v\frac{\partial\frac{[CheA-P]}{[CheA-P]_0}}{\partial x}\right)\right)$. Because the equation of $[CheA - P]$ is a function of $[Asp]$, and $[Asp]$ is independent of time when the experiment is measured at steady state, so Equation (2.21) can be simplified into

$$p_t^{+/-} = p_0 \exp\left[\mp\alpha\left(v\frac{\partial\frac{[CheA-P]}{[CheA-P]_0}}{\partial x}\right)\right] \quad (2.22)$$

Substitute the above equation into Equation (2.13), we can get the chemotactic velocity of bacteria in the presence of attractant

$$V_c = v\frac{e^{\sigma v\frac{\partial\frac{[CheA-P]}{[CheA-P]_0}}{\partial x}} - e^{+\sigma v\frac{\partial\frac{[CheA-P]}{[CheA-P]_0}}{\partial x}}}{e^{\sigma v\frac{\partial\frac{[CheA-P]}{[CheA-P]_0}}{\partial x}} - e^{+\sigma v\frac{\partial\frac{[CheA-P]}{[CheA-P]_0}}{\partial x}}} = v\tanh\left(\sigma v\frac{\partial\frac{[CheA-P]}{[CheA-P]_0}}{\partial x}\right) \sim v\sigma v\frac{\partial\frac{[CheA-P]}{[CheA-P]_0}}{\partial x}$$

when $\sigma v \frac{\partial \frac{[CheA-P]}{[CheA-P]_0}}{\partial x}$ is small. Therefore,

$$V_c = \sigma v^2 \frac{\partial \frac{1+\gamma}{1+\gamma+\gamma\frac{[Asp]}{K_{dA}}}}{\partial x} = \sigma v^2 \frac{(\frac{\gamma+1}{\gamma})K_{dA}}{((\frac{\gamma+1}{\gamma})K_{dA}+[Asp])^2}\frac{\partial([Asp])}{\partial x} \quad (2.23)$$

2.3.3 Chemotactic velocity in the presence of repellent

Because receptors bound to nickel are able to be phosphorylated as shown in Equation (2.5), therefore,

$$[CheA_T] = [CheA] + [CheA-P] + [Ni-CheA] + [Ni-CheA-P] \quad (2.24)$$

From Equation (2.1), we know that $[CheA-P] = \frac{[CheA][P]}{K_1}$ (2.25)

From Equation (2.4), we can get

$K_{dN} = \frac{[Ni][CheA]}{[Ni-CheA]}$, so $[Ni-CheA] = \frac{[Ni][CheA]}{K_{dN}}$ (2.26)

From Equation (2.5), we know that

$K_2 = \frac{[Ni-CheA][P]}{[Ni-CheA-P]}$, so $[Ni-CheA-P] = \frac{[Ni-CheA][P]}{K_2}$ (2.27)

Substitute Equations (2.25-2.27) into Equation (2.24), we can get $[CheA] = \frac{[CheA_T]}{1+\frac{[P]}{K_1}+(1+\frac{[P]}{K_2})\frac{[Ni]}{K_{dN}}}$

Therefore $[CheA-P] = \frac{[CheA_T]}{1+\frac{K_1}{[P]}+\frac{[Ni]K_1}{K_{dN}[P]}+\frac{K_1[Ni]}{K_2K_{dN}}}$

$$[Ni-CheA-P] = \frac{[CheA_T]}{1+\frac{[P]}{K_1}+(1+\frac{[P]}{K_2})\frac{[Ni]}{K_{dN}}}\frac{[Ni][P]}{K_{dN}K_2} = \kappa[CheA-P]\frac{[Ni]}{K_{dN}}$$

So $[CheA-P]_{total} = (1+\kappa\frac{[Ni]}{K_{dN}})[CheA-P] = (1+\kappa\frac{[Ni]}{K_{dN}})\frac{[CheA_T]}{1+\frac{K_1}{[P]}+\frac{[Ni]K_1}{K_{dN}[P]}+\frac{K_1[Ni]}{K_2K_{dN}}} = (1+\kappa\frac{[Ni]}{K_{dN}})\frac{[CheA_T]}{1+\gamma+(k+\gamma)\frac{[Ni]}{K_{dN}}}$

where $\gamma = \frac{K_1}{[P]}$, is the signaling efficiency, $\kappa = \frac{K_1}{K_2}$ is the repellent sensitivity coefficient, K_{dN} is the dissociation constant for nickel ion binding.

Substitute $[CheA-P]_{total}$ into Equation (2.22), and then Equation (2.13), we can get the

chemotactic velocity in the presence of repellent,

$$V_c = \sigma v^2 \frac{\partial \frac{[CheA-P]}{[CheA-P]_0}}{\partial x} = \sigma v^2 \frac{\partial \frac{(1+\gamma)(1+\kappa\frac{[Ni]}{K_{dN}})}{1+\gamma+(k+\gamma)\frac{[Ni]}{K_{dN}}}}{\partial x} = -\sigma(\kappa-1)v^2 \frac{(\frac{\gamma+1}{\gamma})K_{dN}}{[(\frac{\gamma+1}{\gamma})K_{dN}+(\frac{\kappa+\gamma}{\gamma})[Ni]]^2} \frac{\partial([Ni])}{\partial x} \quad (2.28)$$

2.3.4 Chemotactic velocity in the presence of combined chemoeffectors

When both stimuli exist, the total amount of receptors can be represented as

$$[CheA_T] = [CheA] + [CheA-P] + [Asp-CheA] + [Ni-CheA] + [Ni-CheA-P] \quad (2.29)$$

Substitute Equations (2.17) and (2.25-2.27) into Equation (2.29), and we can get

$$[CheA] = \frac{[CheA_T]}{1 + \frac{[P]}{K_1} + \frac{[Asp]}{K_{dA}}(1 + \frac{[P]}{K_2})\frac{[Ni]}{K_{dN}}}$$

Therefore $[CheA-P] = \frac{[CheA_T]}{1+\frac{K_1}{[P]}+\frac{[Asp]K_1}{K_{dA}[P]}+(\frac{K_1}{[P]}+\frac{K_1}{K_2})\frac{[Ni]}{K_{dN}}}$

$$[Ni-CheA-P] = \frac{[CheA_T]}{1 + \frac{K_1}{[P]} + \frac{[Asp]}{K_{dA}}\frac{K_1}{[P]} + (\frac{K_1}{[P]} + \frac{K_1}{K_2})\frac{[Ni]}{K_{dN}}} \frac{[Ni][P]}{K_{dN}K_2} = \kappa[CheA-P]\frac{[Ni]}{K_{dN}}$$

So $[CheA-P]_{total} = \left(1+\kappa\frac{[Ni]}{K_{dN}}\right)[CheA-P] = (1+\kappa\frac{[Ni]}{K_{dN}})\frac{[CheA_T]}{1+\frac{K_1}{[P]}+\frac{[Asp]K_1}{K_{dA}[P]}+(\frac{K_1}{[P]}+\frac{K_1}{K_2})\frac{[Ni]}{K_{dN}}} =$

$(1+\kappa\frac{[Ni]}{K_{dN}})\frac{[CheA_T]}{1+\gamma+\gamma\frac{[Asp]}{K_{dA}}+(k+\gamma)\frac{[Ni]}{K_{dN}}}$

where $\gamma = \frac{K_1}{[P]}$, is the signaling efficiency, $\kappa = \frac{K_1}{K_2}$ is the repellent sensitivity coefficient, K_{dA} is the dissociation constant for aspartate ion binding, K_{dN} is the dissociation constant for nickel ion binding.

Substitute $[CheA-P]_{total}$ into Equation (2.22), and then Equation (2.13), we can get the chemotactic velocity in the presence of combined chemoeffectors,

$$V_c = \sigma v^2 \frac{\partial \frac{[CheA-P]}{[CheA-P]_0}}{\partial x} = \frac{\partial \frac{(1+\gamma)(1+\kappa\frac{[Ni]}{K_{dN}})}{1+\gamma+\gamma\frac{[Asp]}{K_{dA}}+(k+\gamma)\frac{[Ni]}{K_{dN}}}}{\partial x} = \frac{\sigma v^2(1+\gamma)\gamma}{[1+\gamma+\gamma\frac{[Asp]}{K_{dA}}+(k+\gamma)\frac{[Ni]}{K_{dN}}]^2}\{(1+\kappa\frac{[Ni]}{K_{dN}})\frac{\partial\frac{[Asp]}{K_{dA}}}{\partial y} - (\kappa-1+$$

$$\kappa\frac{[Asp]}{K_{dA}})\frac{\partial\frac{[Ni]}{K_{dN}}}{\partial y}\} \quad (2.30)$$

2.4 Parameter Values as Deduced from Published Literature

In this section, the steps to deduce the theoretical values of three parameters (σ, the stimuli sensitivity coefficient; γ, the signaling efficiency and κ, the repellent sensitivity coefficient) are described. The purpose of this was to use theoretical models and experimental data reported previously in the literature to provide an independent assessment of these parameter values.

Theoretical value of σ as deduced from literature data

In our model

$$\ln\left(\frac{p_t}{p_0}\right) = \sigma \frac{D(\frac{[CheY-P]}{[CheY-P]_0})}{Dt} \tag{2.31}$$

where σ is the stimuli sensitivity coefficient, p_t is the probability of tumble per unit time in the presence of chemoeffector (Rivero et al., 1989), p_0 is the probability of tumble per unit time in the absence of chemoeffectors, [*CheY-P*] is the concentration of phosphorylated CheY in the presence of chemoeffector and $[CheY-P]_0$ is the concentration of phosphorylated CheY in the absence of chemoeffector.

Because p_0, σ and $[CheY-P]_0$ are constant and the internal spatial gradients are considered indistinguishable to the cells, Equation (2.31) can be reduced to

$$\ln\left(\frac{p_t}{p_0}\right) = \frac{\sigma}{[CheY-P]_0} \frac{d([CheY-P])}{dt} \tag{2.32}$$

From the green line in Figure 2B of Dufour et al. (2014) (shown in Figure 2.1), $[CheY-P]_0 = 2.4\ \mu$M, and $[CheY-P] = 2.3\ \mu$M in the presence of attractant. $[CheY-P]$ is a function of time and we estimate the derivative as $\frac{d([CheY-P])}{dt} = -0.02\ \mu$M/s.

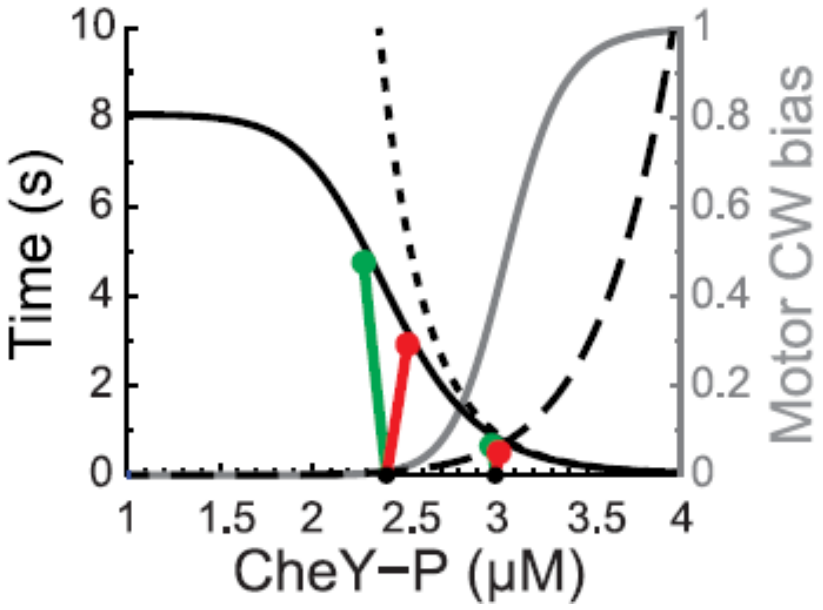

Figure 2.1 Expected trajectories of CheY-P concentration for cells running in one dimension, either up (green) or down（red）in a gradient. Adapted from Dufour et al. (2014).

Cluzel et al. (2000) measured the switching frequency as a function of CheY-P concentration, where they defined switching frequency as the number of times that a motor switched its direction of rotation divided by the duration of the recording. Therefore, we can view the switching frequency of Cluzel et al. (2000) to be defined as twice the tumble probability we used in our model. From Figure 2B in Cluzel et al. (2000) (shown in Figure 2.2 below), $2p_t(2.3\ \mu\text{M})$ =0.72 and $2p_0(2.4\ \mu\text{M})$ =0.77. Therefore, rearrangement of Equation (2.32) yields

$$\sigma = \frac{\ln\left(\frac{p_t}{p_0}\right)}{\frac{d([CheY-P])}{dt}} \cdot [CheY-P]_0 = 8\ \ s.$$

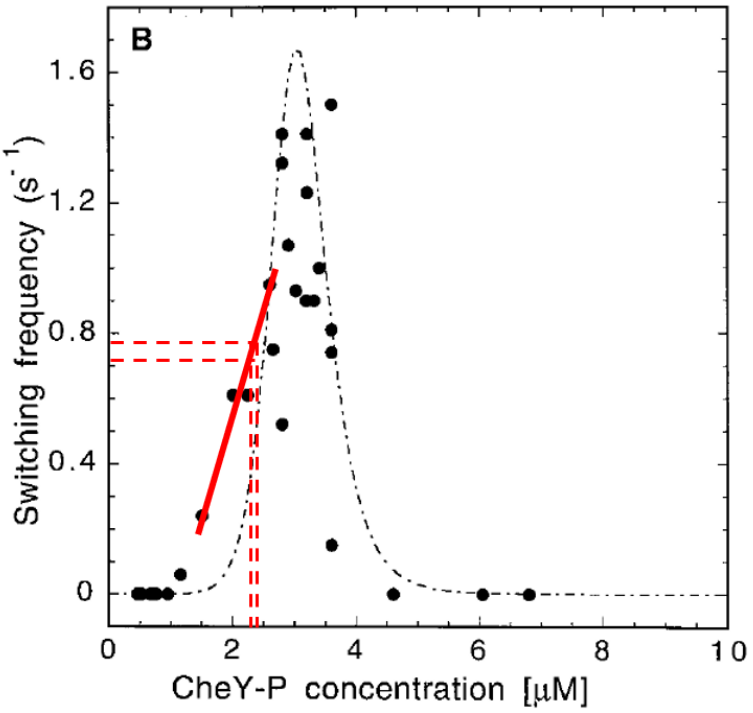

Figure 2.2 Switching frequency as a function of CheY-P concentration. Adapted from Cluzel et al. (2000).

Theoretical value of γ *as deduced from Borkavich et al (1989)*

γ is defined as

$$\gamma = \frac{K_1}{[P]} \tag{2.33}$$

where $K_1 = \frac{[CheA][P]}{[CheA-P]}$.

We define $[\mathrm{CheA_T}] = [CheA] + [CheA-P]$, so $[CheA] = [\mathrm{CheA_T}] - [CheA-P]$, then

$$\gamma = \frac{K_1}{[P]} = \frac{[CheA]}{[CheA-P]} = \frac{[\mathrm{CheA_T}]}{[CheA-P]} - 1 \tag{2.34}$$

From the Figure 2A in Borkavich et al. (1989) (shown in Figure 2.3), we can get the ratio of $\frac{[\mathrm{CheA_T}]}{[CheA-P]}$, therefore,

$$\gamma = \frac{[\mathrm{CheA_T}]}{[CheA - P]} - 1 = \frac{40}{2} - 1 = 19$$

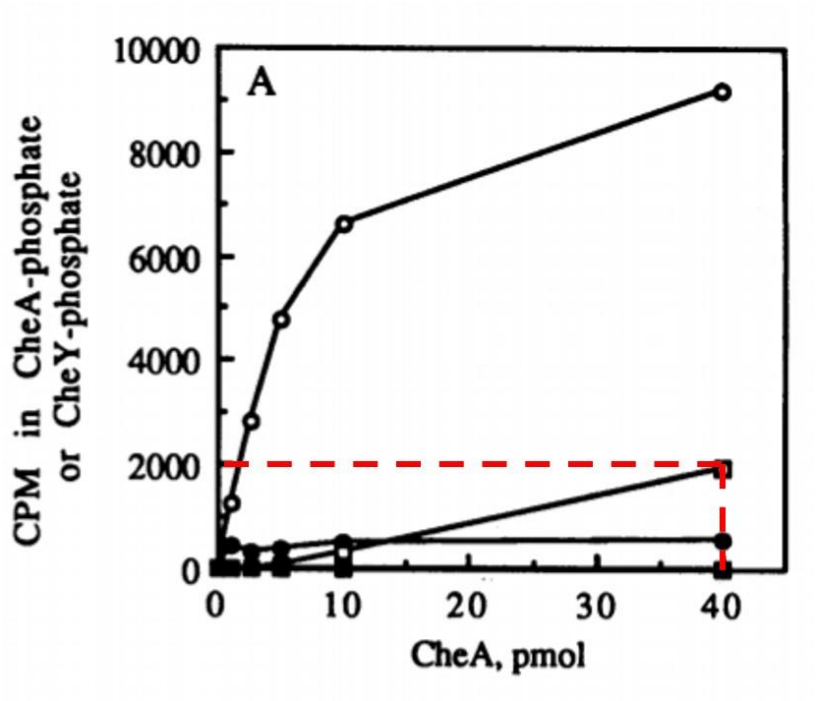

Figure 2.3 Dependence of the phosphorylation reaction on the concentration of CheA. Open symbols indicate wild type bacteria and closed symbols indicate controls, circles indicate the amount of CheY-phosphate and squares indicate CheA-phosphate with 1000 cpm/pmol (red dashed lines indicate the values used in the calculation: $[\mathrm{CheA_T}]$ is 40 pmol and CheA-P is 2000 cpm or 2 pmol). Adapted from Borkavich et al. (1989).

Theoretical value of κ *as deduced from Hauri and Ross (1995)*

κ is defined as

$$\kappa = \frac{K_1}{K_2} \tag{2.35}$$

$$\kappa = \frac{K_1}{K_2} \frac{\frac{[CheA][P]}{[CheA-P]}}{\frac{[Ni-CheA][P]}{[Ni-CheA-P]}} = \frac{[CheA]}{[Ni-CheA]} \frac{[Ni-CheA-P]}{[CheA-P]} \tag{2.36}$$

The transfer of phosphate from the kinase CheA to the response regulator CheY is represented as

$$\text{CheA-P} \xrightarrow{k_1} \text{CheY-P} \tag{2.37}$$

$$\text{Ni-CheA-P} \xrightarrow{k_2} *\text{CheY-P} \tag{2.38}$$

where CheY-P is the phosphorylated CheY.

We assume the reaction rate constants are the same in the phosphate transfer step, $k_1 = k_2 = k$, and observation times Δt are the same. Then Equation (2.36) can be written as

$$\kappa = \frac{K_1}{K_2} = \frac{\frac{[CheA][P]}{[CheA-P]}}{\frac{[Ni-CheA][P]}{[Ni-CheA-P]}} = \frac{[CheA]}{[Ni-CheA]}\frac{[Ni-CheA-P]}{[CheA-P]}$$

$$= \frac{[CheA]}{[Ni-CheA]}\frac{\frac{[*CheY-P]}{k\Delta t}}{\frac{[CheY-P]}{k\Delta t}} = \frac{[CheA]}{[Ni-CheA]}\frac{[*CheY-P]}{[CheY-P]} \tag{2.39}$$

Hauri and Ross (1995) plotted the fraction of CCW bias in response to the addition of Ni^{2+} (shown in Figure 2.4). The third curve from the bottom captures the response to 100 μM concentration of Ni^{2+} and the trough corresponds to $f_{ccw} = 0.47$ (or CW bias=0.53). We can also read from the figure that $f_{ccw} = 0.65$ (or CW bias=0.35) without the presence of any chemoeffector.

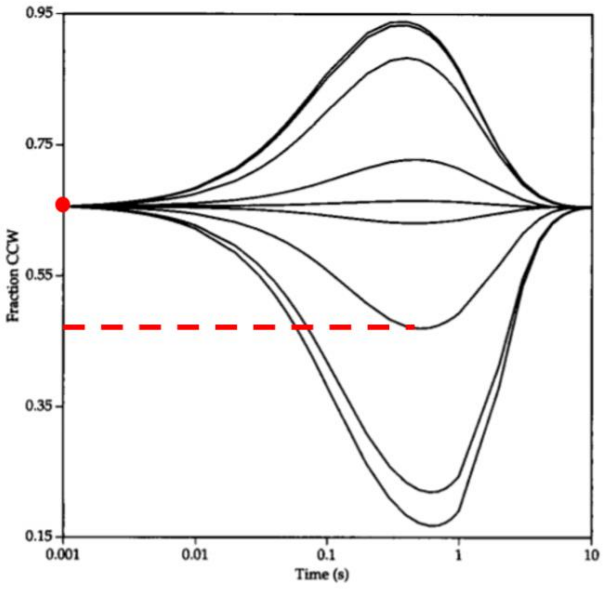

Figure 2.4 Response of *E. coli* to addition of attractant and repellent. The concentrations shown are (proceeding from the lowest curve to the highest): 10 mM Ni^{2+}, 1 mM Ni^{2+}, 100 μM Ni^{2+}, 10 μM Ni^{2+}, 0.01 μM Asp, 0.1 μM Asp, 1 μM Asp, 10 μM Asp, 100 μM Asp. Adapted from Hauri and Ross (1995).

From the curve fit in Figure 2A of Cluzel et al. (2000) (shown in Figure 2.5), we estimated $[CheY-P]$ (0.53) = 3.2 μM and $[CheY-P]_0$(0.35) = 3.0 μM.

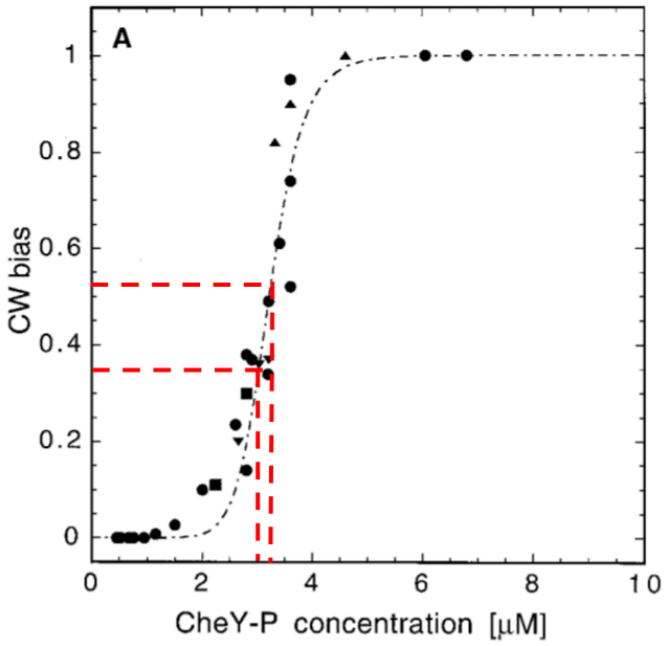

Figure 2.5 CW bias of *E. coli* plotted as a function of CheY-P concentration. Adapted from Cluzel et al. (2000).

Therefore, we calculate the ratio of $\frac{[*CheY-P]}{[CheY-P]} = \frac{3.2}{3.0}$. For the other ratio in Equation (2.39), $\frac{[CheA]}{[Ni-CheA]}$, we know that $\gamma = \frac{[CheA]}{[CheA-P]} = 19$. We also know that

$$[\text{CheA}_\text{T}] = [\text{CheA}] + [\text{CheA-P}] \tag{2.40}$$

So, $[CheA] = 0.95 CheA_T$ in the absence of Ni^{2+}.

The fraction of receptors bound with chemoeffector can be related to the change in f_{ccw} from Figure 2.6. The peak response as change in % CCW$= 47 - 65 = -18$ when comparing the situations with or without 100 μM Ni^{2+}. However, the data in Figure 2.6 is for when both attractant and repellent are present. We can then read from Figure 2.6 that $f_{asp} - f_{Ni} = -0.31$.

For the situation with nickel only and no aspartate, $f_{Ni} = 0.31$. Therefore, $\frac{[CheA]}{[Ni{-}CheA]} = \frac{0.95[\mathrm{CheA_T}]}{0.31[\mathrm{CheA_T}]} = 3.1$.

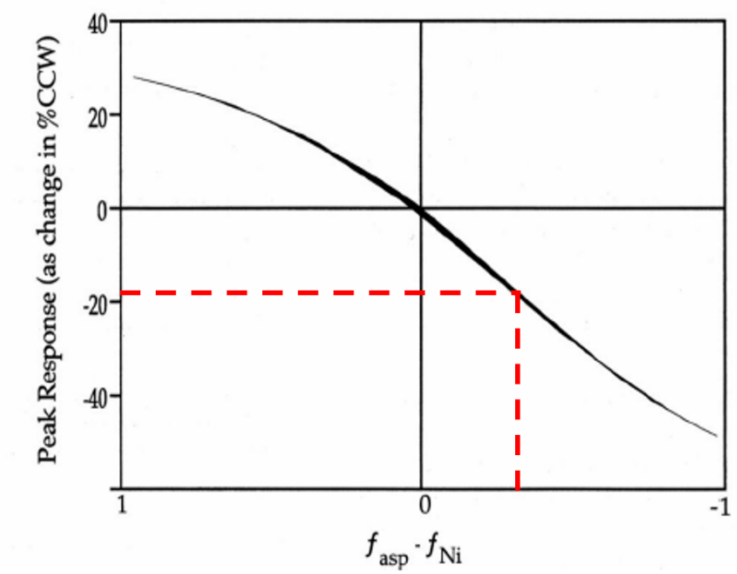

Figure 2.6 Plot of the effect of different concentrations of aspartate and Ni^{2+} (plotted as fraction of receptors with stimulatory ligand bound). The peak excitation plotted as a function of the difference between the fraction of receptors with aspartate bound (f_{asp}) and the fraction with Ni^{2+} (f_{Ni}) bound. Adapted from Hauri and Ross (1995).

So, $\kappa = \frac{K_1}{K_2} = \frac{\frac{[CheA][P]}{[CheA-P]}}{\frac{[Ni-CheA][P]}{[Ni-CheA-P]}} = \frac{[CheA]}{[Ni-CheA]}\frac{[Ni-CheA-P]}{[CheA-P]} = \frac{[CheA]}{[Ni-CheA]}\frac{[Ni-CheY-P]}{[CheY-P]} = \frac{3.2}{3.0} \times 3.1 = 3.3.$

References

Berg, H. C., Brown, D. A. (1972). Chemotaxis in *Escherichia coli* analysed by three-dimensional tracking. *Nature*, *239*(5374), 500-504.

Bi, S., Jin, F., & Sourjik, V. (2018). Inverted signaling by bacterial chemotaxis receptors. *Nature communications*, *9*(1), 1-13.

Borkovich, K. A., Kaplan, N., Hess, J. F., & Simon, M. I. (1989). Transmembrane signal

transduction in bacterial chemotaxis involves ligand-dependent activation of phosphate group transfer. *Proceedings of the National Academy of Sciences*, *86*(4), 1208-1212.

Brown, D. A., & Berg, H. C. (1974). Temporal stimulation of chemotaxis in *Escherichia coli*. *Proceedings of the National Academy of Sciences*, *71*(4), 1388-1392.

Chen, K. C., Cummings, P. T., & Ford, R. M. (1998). Perturbation expansion of Alt's cell balance equations reduces to Segel's one-dimensional equations for shallow chemoattractant gradients. SIAM Journal on Applied Mathematics, 59(1), 35-57.

Clarke, S., & Koshland, D. E. (1979). Membrane receptors for aspartate and serine in bacterial chemotaxis. *Journal of Biological Chemistry*, *254*(19), 9695-9702.

Cluzel, P., Surette, M., & Leibler, S. (2000). An ultrasensitive bacterial motor revealed by monitoring signaling proteins in single cells. *Science*, *287*(5458), 1652-1655.

Dufour, Y. S., Fu, X., Hernandez-Nunez, L., & Emonet, T. (2014). Limits of feedback control in bacterial chemotaxis. *PLoS computational biology*, *10*(6).

Englert, D. L., Adase, C. A., Jayaraman, A., & Manson, M. D. (2010). Repellent taxis in response to nickel ion requires neither Ni2+ transport nor the periplasmic NikA binding protein. *Journal of bacteriology*, *192*(10), 2633-2637.

Ford, R. M., & Cummings, P. T. (1992). On the relationship between cell balance equations for chemotactic cell populations. *SIAM Journal on Applied Mathematics*, *52*(5), 1426-1441.

Ford, R. M., Phillips, B. R., Quinn, J. A., & Lauffenburger, D. A. (1991). Measurement of bacterial random motility and chemotaxis coefficients: I. Stopped-flow diffusion chamber assay. *Biotechnology and bioengineering*, *37*(7), 647-660.

Frymier, P. D., Ford, R. M., & Cummings, P. T. (1994). Analysis of bacterial migration: I. Numerical solution of balance equation. *AIChE Journal*, *40*(4), 704-715.

Gardina, P. J., Bormans, A. F., & Manson, M. D. (1998). A mechanism for simultaneous sensing of

aspartate and maltose by the Tar chemoreceptor of *Escherichia coli*. *Molecular microbiology*, 29(5), 1147-1154.

Hauri, D. C., & Ross, J. (1995). A model of excitation and adaptation in bacterial chemotaxis. *Biophysical journal*, *68*(2), 708-722.

Mercer, J. R., Ford, R. M., Stitz, J. L., & Bradbeer, C. (1993). Growth rate effects on fundamental transport properties of bacterial populations. *Biotechnology and bioengineering*, *42*(11), 1277-1286.

Middlebrooks, S. A. (1993). The chemotactic response of *Escherichia coli* to combined repellent and attractant stimuli. (M.S. Thesis) University of Virginia.

Park, H., Im, W., & Seok, C. (2011). Transmembrane signaling of chemotaxis receptor tar: insights from molecular dynamics simulation studies. *Biophysical journal*, *100*(12), 2955-2963.

Rivero, M. A., Tranquillo, R. T., Buettner, H. M., & Lauffenburger, D. A. (1989). Transport models for chemotactic cell populations based on individual cell behavior. *Chemical engineering science*, *44*(12), 2881-2897.

Strauss, I., Frymier, P. D., Hahn, C. M., & Ford, R. M. (1995). Analysis of Bacterial Migration. II. Studies with Multiple Attractant Gradients. *AICHE Journal*, *41*(2), 402-414.

Surette, M. G., Levit, M., Liu, Y., Lukat, G., Ninfa, E. G., Ninfa, A., & Stock, J. B. (1996). Dimerization is required for the activity of the protein histidine kinase CheA that mediates signal transduction in bacterial chemotaxis. *Journal of Biological Chemistry*, *271*(2), 939-945.

Chapter 3. *Escherichia coli* Chemotactic to Multiple Stimuli in a Microfluidic Device with a Constant Gradient

3.1 Abstract

Bacteria are exposed to multiple chemical stimuli in their natural environment. Chemotactic bacteria can accumulate near a higher concentration of chemoattractant, or swim away from a higher concentration of chemorepellent; this process is called chemotaxis. To relate the swimming response of individual bacteria to the chemotactic velocity of a bacterial population, we quantified chemotaxis by integrating signals from multiple stimuli at the kinase phosphorylation step in the chemosensory pathway. Experimental data was used to assess parameter values and to test model predictions for the chemotactic velocity of a bacterial population. To ensure that the migration of bacteria was solely in response to constant chemoeffector gradients, we exposed *Escherichia coli* to either a single stimulus (chemoattractant α-methylaspartate or chemorepellent nickel ion) or their combination in a uniquely designed microfluidic device. When facing competing chemoeffectors, their effects on bacterial distributions counteracted each other, but not necessarily as a simple summation. By using the parameters obtained from single stimulus experiments, we predicted bacterial responses to competing stimuli, providing information on bacteria migration in complex chemical environments. This study demonstrated the utility of multi-scale modeling to predict bacterial chemotaxis in the presence of two competing chemoeffectors and the power of combining theoretical models and experimental systems.

3.2 Introduction

Bacteria are exposed to multiple chemical stimuli in their natural environment. Facing a specific chemical gradient, a population of bacteria can direct their movement to swim toward or away from it, exhibiting a behavior termed chemotaxis. In some chemotactic responses, bacteria are attracted to a higher chemical concentration because they can use these chemicals as food and energy sources. Such compounds are called chemoattractants, while compounds bacteria swim away from are called chemorepellents. *Escherichia coli* (*E. coli*) show positive chemotaxis to amino acids and aromatic compounds, while sulfides and inorganic ions cause bacteria to exhibit negative chemotaxis (Terracciano et al., 1984, Pandey and Jain, 2002). Some industrial pollutants serve as carbon sources for bacteria and elicit a positive chemotactic response. Chemotaxis can thereby increase the mass transfer of bacteria to the pollutants. Upon arrival at the contaminant source, bacteria degrade pollutants to less toxic or nontoxic substances (Hoff, 1993, Das et al. 2011). This process is important in bioremediation, a promising technique that uses microorganisms to remove pollutants from contaminated groundwater sites (Pandey and Jain, 2002; Singh and Olson, 2008).

The physical mechanism for *E. coli* chemotaxis is well known (*e.g*. Sourjik, 2004): when the flagella rotate clockwise (CW), bacteria will tumble in place, while the counterclockwise (CCW) rotation of the flagella will lead to a "run" along a straight pathway. In the absence of chemoeffectors, bacteria perform a random walk similar to Brownian motion (Rivero et al., 1989) alternating between runs of ~1s and tumbles of ~0.1 s (Berg and Brown, 1972). In the presence of a chemoattractant gradient, bacteria extend their run times toward higher chemoattractant concentrations by decreasing the tumble probability. This results in the bacterial population showing a net drift velocity toward the chemoattractant. In contrast, in the presence of a chemorepellent gradient, cells increase their tumbling frequency when moving in an increasing chemorepellent concentration (Tso and Adler, 1974). Thereby, the bacterial population exhibit a net drift velocity

down the chemorepellent gradient.

The studies mentioned above measured bacteria chemotaxis in the presence of only one chemoeffector. However, bacteria encounter multiple chemicals in their native environments. Thus, it is important to study how bacteria respond to conflicting information from multiple chemical signals. Several researchers have studied bacterial chemotactic response in the presence of multiple stimuli. Mowbray and Koshland (1987) studied the response of aspartate and maltose stimuli on the Tar receptor. They suggested that the response was additive and independent since aspartate and maltose bind to separate sites on the Tar receptor. However, Strauss et al. (1995) argued that the response of fucose and α-methylaspartate were not addictive since the simple model predictions did not match the experimental results they performed with multiple stimuli and suggested that a more complex relationship which incorporated signal processing steps was required. Zhang et al. (2019) observed that a traveling escape band formed in opposing gradients of aspartate and tryptone broth. This phenomenon was explained by bacteria first responding to a strong attractant, that is a poor nutrient (aspartate) at one end of the channel. Then subsequently, the consumption of nutrient resulted in bacteria traveling toward a rich nutrient, that is a weak attractant (tryptone broth) at the other end of the channel. Kalinin et al. (2010) found that bacteria chemotactic response to the chemoattractants α-methylaspartate (MeAsp) and serine depended on the ratio of two receptors, which are the two most abundant of the five chemoreceptors. Their study demonstrated that bacteria may switch their preference from serine to MeAsp when the ratio of those two receptors Tar/Tsr is greater than 2. The study also showed that the binding of attractant to receptors is an important step in chemotaxis. Most studies measured the behavior of a population of bacteria, without emphasizing how the signal transduction mechanism functions inside an individual bacterium. However, to predict the response to multiple stimuli, it is important to relate the cellular-level signal transduction mechanism to population-scale chemotaxis behavior. By using multi-scale modeling, we can link

molecular reaction to individual cell level swimming behavior, and then relate that to population-scale dynamics. Therefore, we quantified chemotaxis using a mathematical model that integrates signal transduction kinetics from multiple inputs, starting from chemoeffector binding to chemotactic receptor, to the run and tumble behavior of individual cells to the population-scale chemotactic velocity.

Rivero et al. (1989) developed a theoretical model to describe chemotactic behavior at the individual cell level. They used the empirical correlation developed by Berg and Brown (1972), in which the logarithm of mean run time increases with respect to the rate of change in the number of bound receptors. The mean run time is the reciprocal of the tumbling probability, which is related to the change in concentration of signaling complexes inside the cell. The signaling response in *E. coli* chemotaxis depends on the phosphotransfer between a histidine kinase and a response regulator (Sourjik et al., 2010). In the absence of chemoattractant, the kinase CheA has autophosphorylation activity, and the CheA phosphoryl group is further transferred to response regulator CheY. The response regulator diffuses through the cytoplasm and transmits the signal to FliM of the flagellar motor, enhancing the probability of clockwise (CW) rotation and causing bacteria to tumble (Sourjik et al., 2010). The binding of chemoattractant inactivates the kinase, while the binding of chemorepellent increases the activity of the kinase (Grebe and Stock, 1998; Jasuja et al., 1999).

To facilitate a quantitative measure of the chemotactic response, it is beneficial to create a constant chemical gradient, which will serve as the driving force for chemotaxis. Middlebrooks et al. (2021) used a stopped flow diffusion chamber to analyze bacterial chemotactic response to the combination of aspartate and nickel ion. The device they used was able to create a sharp step change in the chemical concentration of chemoeffector that relaxed over time in a predictable way due to diffusion. However, the design did not maintain a constant chemical gradient during bacterial chemotactic response. In comparison, the microfluidic device in Wang et al. (2015) provides more

easily quantifiable results since it is able to reach a steady state condition with a constant chemical concentration gradient. We used this unique microfluidic device (Wang et al, 2015) to produce a constant concentration gradient in the channel that is also free of fluid convection. This design balances the pressure on opposite sides of the microchannel under laminar flow that is maintained in a separate layer above the cross channels.

In our work, we exposed bacteria to different chemicals (including attractants, repellents and their combination) with constant gradients using the design of Wang et al. (2015). We used *E. coli* to study bacterial chemotaxis with the presence of conflicting stimuli because that is more representative of their natural environments. We incorporated parameters from single-stimulus responses into our multiple stimuli model to gain a better picture of bacteria chemotactic response in a heterogeneous chemical environment. This process can further test our model on multiple stimuli. Experimental data were used to validate parameters in a mathematical model capturing bacterial motility and chemotaxis.

3.3 Mathematical Model

3.3.1 Bacteria transport processes at the population level

Bacterial transport in the cross channels on the bottom layer of the microfluidic device (Figure 3.1) was modeled using species mass conservation equations. A one-dimensional equation was deemed suitable following the work of Wang et al. (2015). They observed no dispersion in the cross channel for a tracer molecule. Thus, mass transfer between the vias through the cross channel was controlled by diffusion only; the convection term was eliminated from the equation as the device design prevents bulk fluid flow in the cross channel.

In the absence of chemoeffectors, the governing equation for bacteria concentration b under unsteady state conditions

$$\frac{\partial b}{\partial \mathrm{t}} = \mu_0 \frac{\partial^2 b}{\partial x^2} \tag{3.1}$$

where μ_0 is the bacterial random motility coefficient, which can be evaluated under unsteady state condition. Note that μ_0 will be cancel out at steady state and the bacteria distribution does not depend on μ_0. The boundary conditions are b (0, t) = b_0, b (L, t) = 0 and the initial condition is b (x, 0) = 0. The solution to Equation (3.1) is

$$\mathrm{b}(x,t) = 1 - \frac{x}{L} - \frac{2}{\pi}\sum_{n=1}^{\infty} \frac{\sin n\pi\frac{x}{L}}{n} \exp\left(-\frac{n^2\pi^2\mu_0 t}{L^2}\right) \tag{3.2}$$

In the presence of a chemoeffector, the governing equation for bacteria concentration b at steady state conditions is

$$0 = \mu_0 \frac{\partial^2 b}{\partial x^2} - \frac{\partial}{\partial x}(V_c b) \tag{3.3}$$

where V_c is the chemotactic velocity as derived in Middlebrooks et al. (2021) for multiple chemoeffectors. The equations for V_c under different conditions (attractant, repellent and their combination) are shown in Chapter 2. b was solved using finite difference method in MATLAB R2018b (MathWorks).

The governing equation for chemoeffectors at steady state is

$$0 = \frac{\partial^2 a}{\partial x^2} \tag{3.4}$$

where a is the chemoeffector concentration, and x is the position in the cross channel. *E. coli* do not metabolize α-methylaspartate or nickel, so a consumption term was not needed in the governing equation. The boundary conditions are a (x=0) =0 and a (x=L) = a_0, where L is the length of the channel. The solution of the equation is a linear concentration profile with a constant gradient (da /dx = a_0/L). The chemoeffector concentration and gradient are needed to evaluate the chemotactic velocity V_c term in Equation (3.3).

MATLAB R2018b was used to solve the equations, plot the bacterial concentration distribution in the cross channel, and fit parameters. The μ_0 value was obtained by using least square regression

analysis to fit Equation (3.2) to experimental data from unsteady state conditions without addition of chemoeffector. Equation (3.3) was solved using the chemoeffector concentration and gradient (from Equation 3.4) to get bacterial distributions given set of chemotaxis parameter values and then plot those distributions. Chemotactic parameters values were obtained by using least square regression analysis to fit Equation (3.3) to experimental data from steady state conditions in the presence of chemoeffectors.

3.3.2 Signal transduction kinetics for chemotaxis

In the absence of chemoattractant, the kinase CheA has autophosphorylation activity. The CheA phosphoryl group is further transferred to response regulator CheY as depicted in Figure 1.2. The response regulator diffuses through the cytoplasm and transmits the signal to a flagellar motor, enhancing the probability of CW rotation and causing bacteria to tumble.

In the presence of a chemoattractant, binding of the attractant causes CheA inactivation, decreases the probability of clockwise (CW) rotation and causes the bacterium to tumble less frequently, which leads to the bacterium continuing to move in the same direction. However, the binding of repellent does not inactivate CheA, and instead may increase the CheA activity, increase the probability of clockwise (CW) rotation and cause more frequent tumbles, resulting in bacteria tending to swim away from the repellent source.

Detailed equations are shown in Chapter 2. There are three parameters used in the model. The stimuli sensitivity coefficient σ captures the ratio of change in tumbling frequency to the change in the concentration of signaling complex $[CheA-P]$, and is only specific to the bacterium. The signaling efficiency γ represents the ratio of dissociation constant of $[CheA]$ phosphorylation to the concentration of phosphate, which is essentially the ratio of $[CheA]$ to $[CheA-P]$. γ can be seen as the inverse of the gain in the signaling process. The repellent sensitivity coefficient κ

represents the ratio of dissociation constant of phosphorylation reaction of $[CheA]$ to the dissociation constant of phosphorylation reaction of repellent bound $[CheA]$, and is specific to the repellent. κ represents the enhancement of repellent bound receptor in the phosphorylation signaling process compared to that in the absence of chemoeffector.

3.4. Experimental Methods

3.4.1 Preparation of bacteria cultures

E. coli HCB1 (Wolfe et al., 1987) were previously transformed to express green fluorescent protein (GFP). The transformation was performed using the protocols from the pGLO Bacterial Transformation Kit (Bio-Rad Laboratories, Hercules, CA). In each experiment, 100 μL of GFP-labeled *E. coli* HCB1 frozen stock was cultured in 50 mL Luria broth (Fisher Scientific, NY) in a 250 mL Erlenmeyer flask on a Thermo Scientific Incubated Shaker (MaxQ4000) with a rotation rate of 150 rpm at 30 ˚C. 10 μL ampicillin (100mg/mL, Sigma, MO) and 1 mL 100mg/mL D(-)-arabinose (Fisher Scientific, NY) were added into growth media to provide selective pressure for maintaining the plasmid and expressing GFP.

Bacteria were harvested when the optical density reached 1.20 at 590 nm (measured in spectrophotometer, Molecular Devices, Spectramax 384 plus), which corresponds to the mid-exponential phase of population growth; this also corresponds to the conditions when bacteria exhibit the greatest motility (Worku et al., 1999). Then bacteria were filtered from the culture media with 0.22 μm membrane filter (Millipore, MA) using vacuum filtration (Berg and Turner, 1990) and resuspended into 5% RMB (RMB, including 9.13 g/L Na_2HPO_4 (Fisher Scientific), 4.87 g/L $NaH_2PO_4{\cdot}H_2O$ (Amresco), and 0.029 g/L EDTA (Sigma, MO)) to an optical density around 1.0 (8×10^8 cells/mL). Before performing motility and chemotaxis experiments, the motility of the

bacteria was examined under Zeiss 100/1.25 oil lens with a Nikon microscope (Digital Sight DS-5Mc).

3.4.2 Microfluidic design, fabrication and operation

The uniquely designed microfluidic device is made up of three layers. Both the top and bottom channels are made of polydimethylsiloxane (PDMS). PDMS was chosen because of its oxygen permeability, allowing the bacteria to maintain motility inside the channel. The top layer has two inlets connected to the main channel and the dimensions of the main channel are 95 µm high, 3.3 mm wide, and 2 cm long. The centerpiece that fits between the two PDMS layers was made from black polystyrene material (Staples Inc.). The purpose of the black color is to block background fluorescence in the main channel from the signal in the bottom cross-channels. Double-sided tape (3M) was used to adhere the centerpiece to the top and bottom layers. As depicted in Figure 3.1 four pairs of vias were cut into the centerpiece using a laser cutter (VersaLaser, AZ). The vias connect the main channel in the top layer with the cross channels buried in the bottom layer. Because the pressures are equal in the vias at the cross positions perpendicular to the flow direction, no convection flow will occur in the bottom channels; there is only diffusion in the bottom channel. The dimensions for the cross channels were 100 µm high, 600 µm wide, and 1.5 mm long.

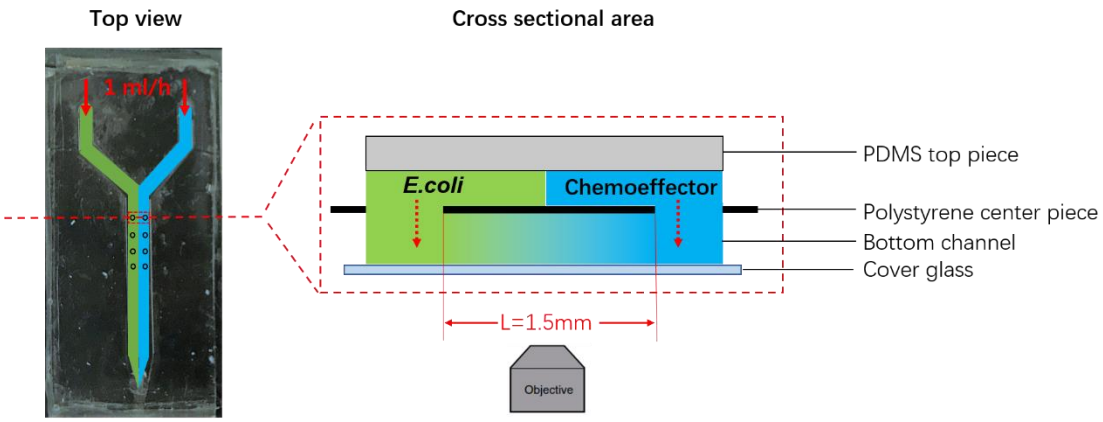

Figure 3.1 Photo of microfluidic device (top-down view) with *E. coli* flow path colored green and

chemoeffector colored blue and an enlarged cross-sectional view (not drawn to scale in order to emphasize the diffusion in the channel) showing connections between the top and bottom channels.

The bacteria suspension and chemoeffectors (or 5% RMB for control experiments) were introduced into opposite arms leading to the main channel. A syringe pump SP 220i (World Precision Instruments, LLC, FL) was used to control flow at a constant volumetric flow rate of 1.0 mL/h, which corresponds to a linear speed of 2.42 mm/s. The Reynolds number in the main channel with the connecting vias was 0.17, which means the two streams were under laminar flow.

3.4.3 Microscopy and image analysis

The fluorescence images were recorded using a Zeiss 780 confocal microscope with 10x objective lens in the Keck Center for Cellular Imaging at the University of Virginia. To observe the signal from bacteria, a MBS 488/561 filter was used and the detector was in the range of 502-607 nm. Images were collected at the speed of 1.94 seconds per frame, which gave us a 5.25 MB image. The 1.5 mm-long cross channel was taken in two images, and then stitched together with overlap percentage 0.01%. Bacterial intensity was recalibrated by automatic adjustment of the lighting as the microscope camera takes images tiles along the channel; this recalibration is programmed into the imaging software. Five images were collected for each region and superimposed together. For each image, the region was selected starting from the edge of the bacteria transported from the via. Since the distance between the scale markings is 0.4 mm, which corresponds to certain measurement in pixel on the image. Then 1.5 mm channel length was measured on the image. The gray level value in each region was collected by using the plot profile feature.

The following equation was used to normalize the fluorescence intensity for each image:

$$I_j^n = \frac{I_j - I_0}{I_F - I_0} \tag{3.5}$$

where I represents the gray level value, the superscript n represents the normalized value, subscript j corresponds to certain location along the channel, I_0 is the gray level value at the bacteria sink, I_F is the gray level value at the bacteria source.

3.5 Results and Discussion

Using the device and the model described before, bacteria motility coefficient was first measured without the presence of chemoeffectors (shown in the Appendix B). Then, attractant only and repellent only experiments were performed to obtain chemotactic parameters. These parameters were used to predict and compare to the experimental results when bacteria respond to the combination of chemoeffectors.

3.5.1 *E. coli* HCB1 chemotactic response to an attractant α-methylaspartate

A constant source of GFP-labeled chemotactic bacteria *E. coli* HCB1 was provided at the left end of the cross channel and a constant sink at the right end, while a constant source of the attractant 0.2 mM or 0.4 mM α-methylaspartate was provided at the right end of the channel with a constant sink at the left end. The distribution of bacteria after reaching steady state (two hours or longer) is shown in Figure 3.2a and Figure 3.3a; the normalized bacteria intensity is shown in Figure 3.2b and Figure 3.3b. A mathematical model for bacterial transport with chemotaxis (solved numerically with MATLAB software, The MathWorks, Inc.) was used to predict the bacterial distribution profile by solving the governing Equation (3.3) for bacteria and using the chemotactic velocity of Equation (2.23) for α-methylaspartate. The profile of chemotactic bacteria in Figure 3.2b shows a non-linear parabolic shape with positive deviation (with concave curvature) from the control case (without chemotaxis) because of the increased migration due to chemotaxis, which was captured by the chemotactic term in the governing equation. Compared to Figure 3.2b, the normalized bacteria

distribution profile increased above 1 (or b_0) around 0.5 mm at the channel location in Figure 3.3b. This suggests that the attractant concentration at this location is the optimal concentration, so bacteria migrate and accumulated at this concentration. This is reasonable as there is the constant source of bacteria at the 0 mm end. The set of parameter values used in the model are K_{dA}=0.64 mM (Clarke et al, 1979), K_{dN}=0.54 mM (Middlebrooks, 1993), γ=4, κ=9, σ=3 s, v=22 μm/s. The parameter values are consistent with others that have been previously reported (Middlebrooks et al., 2021; Middlebrooks, 1993; Clarke and Koshland, 1979). A non-linear least squares algorithm was used to regress the parameters in the theoretical model to align with experimental data. The experimental data collected from bacteria responses to two different concentrations of attractant (0.2 mM and 0.4 mM) were used to obtain the values of σ and γ. From Equation (2.23) for the chemotactic velocity, the maximum chemotactic velocity occurs when the K_{dA} value is equal to the concentration at the attractant source end. This explains the greater overall response of bacteria to 0.4 mM α-methylaspartate over 0.2 mM α-methylaspartate since K_{dA}=0.64 mM.

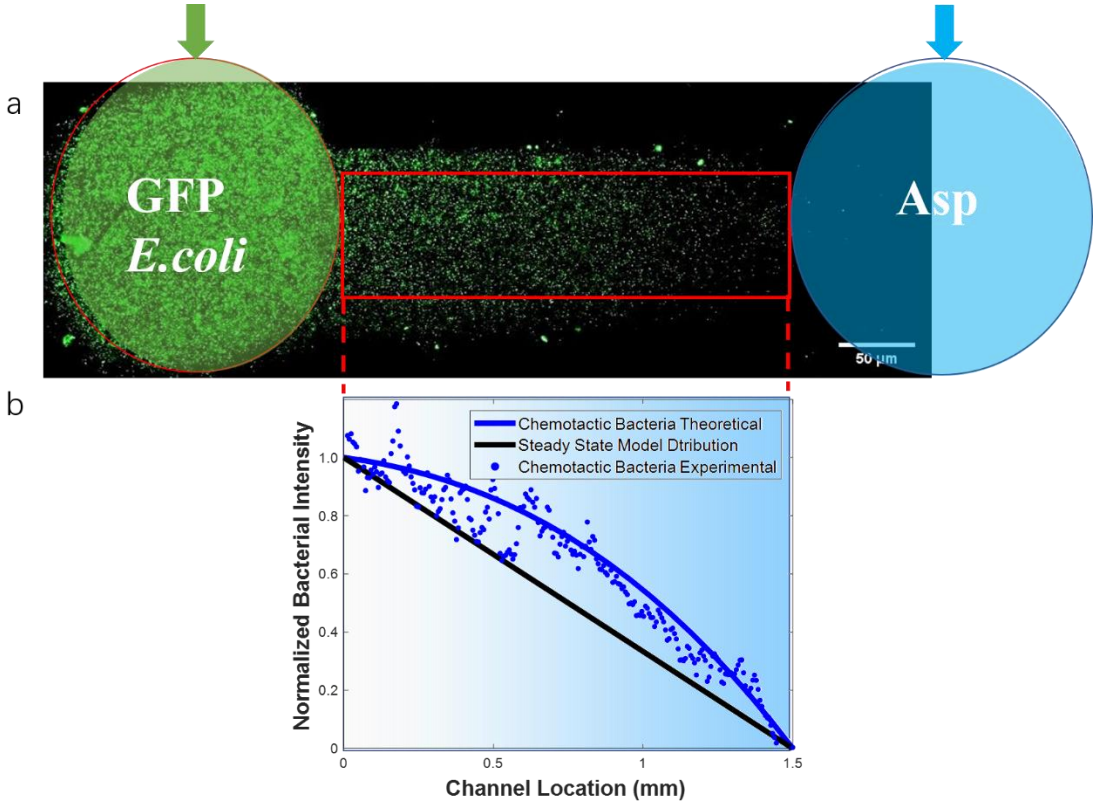

Figure 3.2 (a) GFP-labeled *E. coli* distribution in a cross channel at steady state. There is a constant source of bacteria on the left-hand side of the channel, and a constant attractant source of 0.2 mM α-methylaspartate on the right-hand side; the fluorescence intensity is proportional to bacterial concentration. Red rectangular box indicates the region over which data was analyzed. (b) Normalized bacteria intensity along the channel (scattered data) and the model results (solid lines). The black line indicates the expected bacterial distribution at steady state for the control case without chemoattractant. The blue shading from right to left represents the attractant gradient.

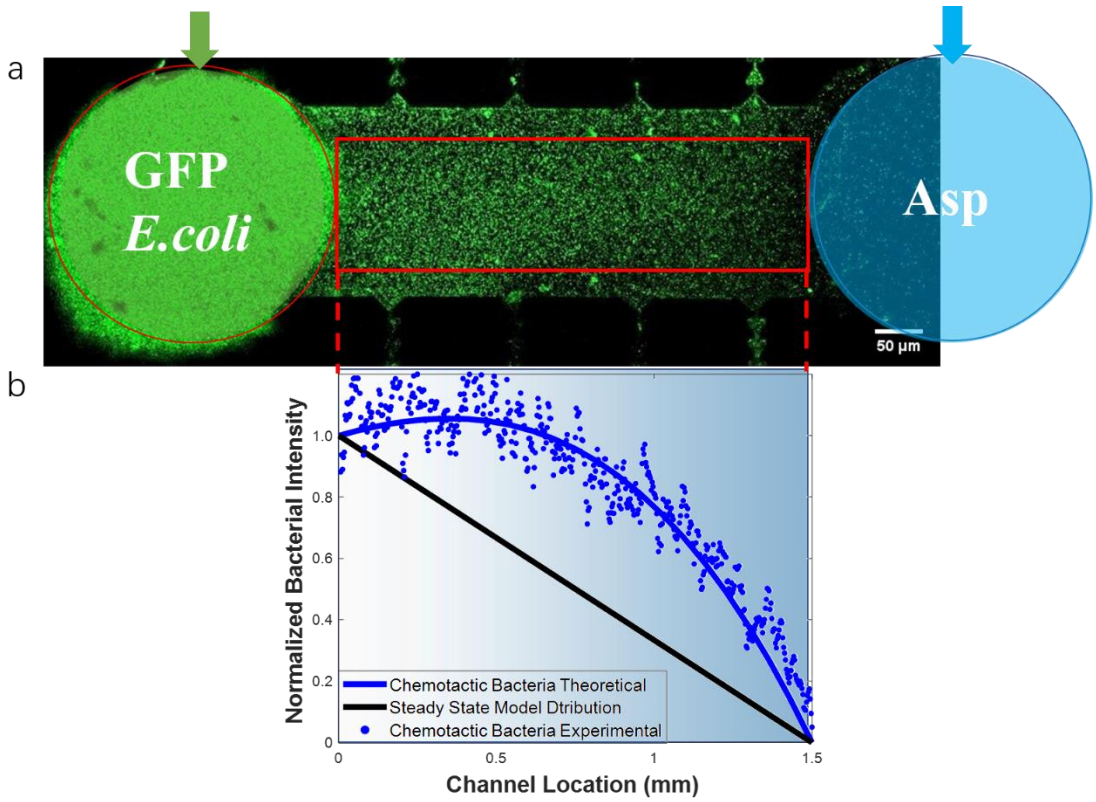

Figure 3.3 (a) GFP-labeled *E. coli* distribution in a cross channel at steady state. There is a constant source of bacteria on the left-hand side of the channel, and a constant attractant source of 0.4 mM α-methylaspartate on the right-hand side; the fluorescence intensity is proportional to bacterial concentration. Red rectangular box indicates the region over which data was analyzed. (b) Normalized bacteria intensity along the channel (scattered data) and the model results (solid lines). The black line indicates the expected bacterial distribution at steady state for the control case without chemoattractant. The blue shading from right to left represents the attractant gradient.

3.5.2 *E. coli* HCB1 chemotactic response to a repellent nickel

We measured the response of GFP-labeled *E. coli* HCB1 to repellent nickel ions in the cross channel. Bacteria were introduced in the left end of the channel and the repellent 0.01mM or 0.05 mM nickel sulfate was introduced into the right end of the channel. The distribution of the bacteria after at least two hours is shown in Figure 3.4 and Figure 3.5. Unlike the response in the previous

section, the concentration of bacteria in the channel is less because the existence of repellent. A mathematical model for bacterial transport with chemotaxis (solved numerically with MATLAB R2018b , The MathWorks, Inc.) was used to predict the bacterial distribution profile by solving the governing Equation (3.3) for bacteria and using the chemotactic velocity of Equation (2.28) for nickel. The model with the value of σ and γ obtained from the previous section was used to fit the experimental data of bacteria response to repellent to obtain value for κ. Figure 3.4b shows a non-linear parabolic shape with negative deviation (with concave curvature) from the steady state because of the decreased migration due to chemotaxis away from the nickel source, which was captured by the chemotactic term in the governing equation. Higher response of bacteria to 0.05 mM nickel over 0.01 mM nickel was observed since K_{dN}=0.54 mM.

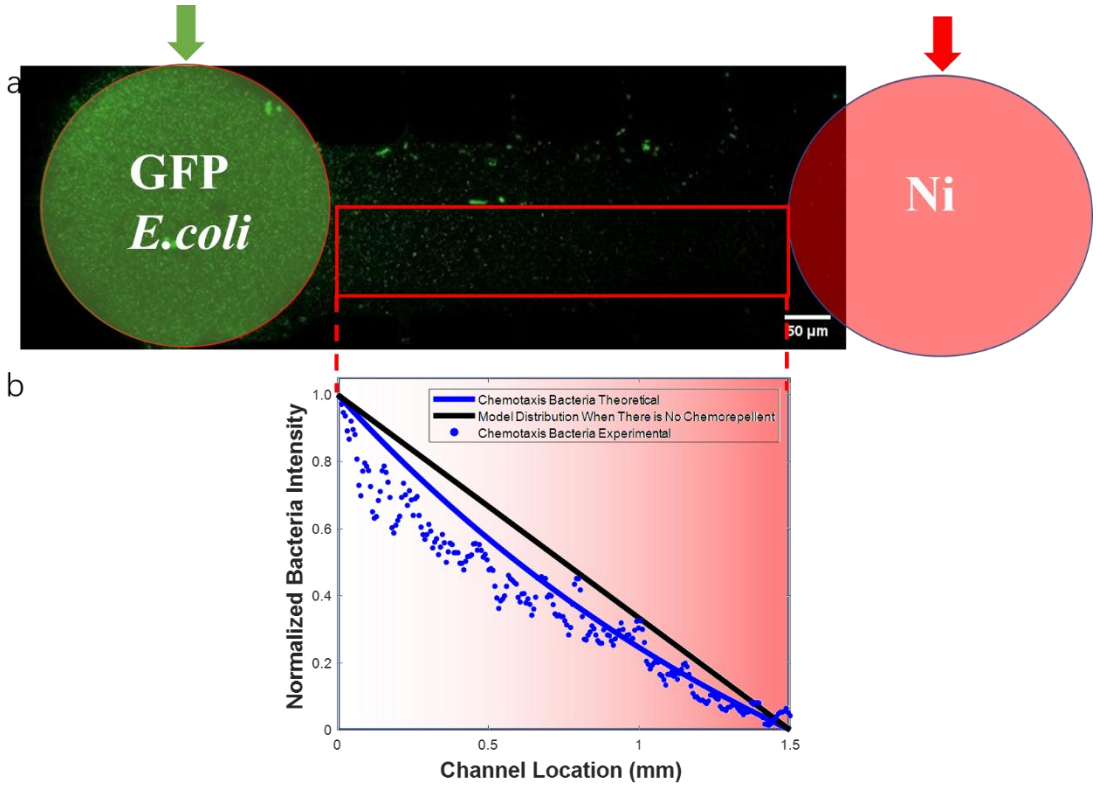

Figure 3.4 (a) GFP-labeled *E. coli* distribution in a cross channel at steady state. There is a constant source of bacteria on the left-hand side of the channel, and a constant repellent source of 0.01 mM nickel sulfate on the right-hand side; the fluorescence intensity is proportional to bacterial

concentration. Red rectangular box indicates the region over which data was analyzed. (b) Normalized bacteria intensity along the channel (scattered data) and the model results (solid line). The red line indicates the expected bacterial distribution at steady state for the control case without chemorepellent. The red shading from right to left represents the repellent gradient.

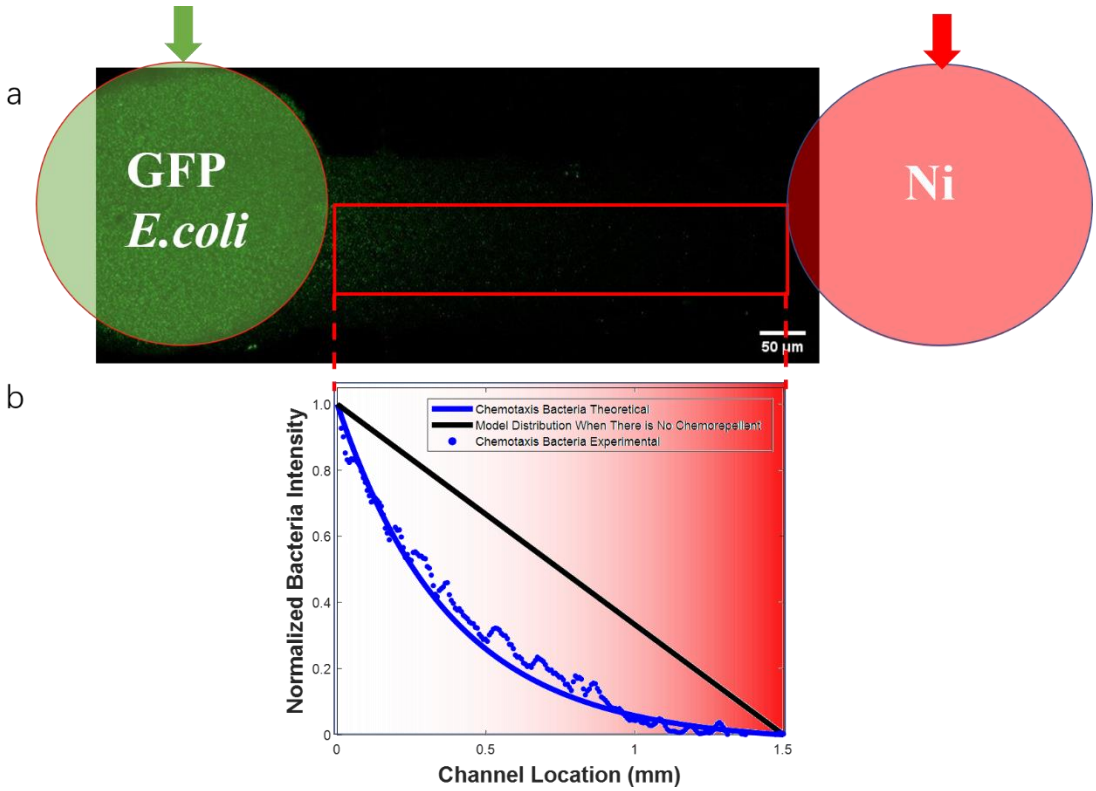

Figure 3.5 (a) GFP-labeled *E. coli* distribution in a cross channel at steady state. There is a constant source of bacteria on the left-hand side of the channel, and a constant repellent source of 0.05 mM nickel sulfate on the right-hand side; the fluorescence intensity is proportional to bacterial concentration. Red rectangular box indicates the region over which data was analyzed. (b) Normalized bacteria intensity along the channel (scattered data) and the model results (solid line). The red line indicates the expected bacterial distribution at steady state for the control case without chemorepellent. The red shading from right to left represents the repellent gradient.

3.5.3 *E. coli* response to chemoeffector mixtures

We measured the response of GFP-labeled *E. coli* HCB1 to different combinations of attractant α-methylaspartate and repellent nickel ion in the cross channel. There was a constant source of bacteria on the left-hand side of the channel. The attractant 0.2 mM (after mixing) α-methylaspartate and repellent 0.01 mM or 0.05 mM (after mixing) nickel sulfate were mixed to provide a constant source of chemoeffectors on the right-hand side. The distribution of bacteria to 0.2 mM α-methylaspartate after at least two hours is shown in Figure 3.6b. In the presence of both attractant and repellent, the normalized population density of bacteria in the channel falls between the distribution for the attractant only and repellent only cases because bacteria integrate the information taking into account both chemoeffectors. MATLAB software (The MathWorks, Inc.) was used to predict the bacterial distribution profile by solving the governing Equation (3.3) for bacteria and using the chemotactic velocity of Equation (2.30) for the combined case. Figure 3.6d also shows a non-linear parabolic shape with positive deviation (concave down) from the control case when bacteria respond to the combination of 0.2 mM α-methylaspartate and 0.01mM nickel sulfate, with decreased migration because of the addition of repellent. On the contrary, as we increase the nickel sulfate concentration to 0.05 mM as shown in Figure 3.6f, we can see a non-linear parabolic shape with negative deviation (concave up) from the control case. The decreased migration across the channel is due to the repellent response overwhelming the attractant response for this particular concentration combination. However, quantitively, the model over predicts the repellent effect compared to the experimental data, this suggests that the model can predict the response qualitatively, while the quantitively may depends on different concentration combination cases. For instance, Figure 3.6f shows the most deviation of the model from the experimental results, which can be explained by that the model results in the 0.05 mM nickel only case are stronger than the experimental results. This produces a stronger repellent response in the response to the mixture of 0.2 mM asp and 0.05 mM nickel.

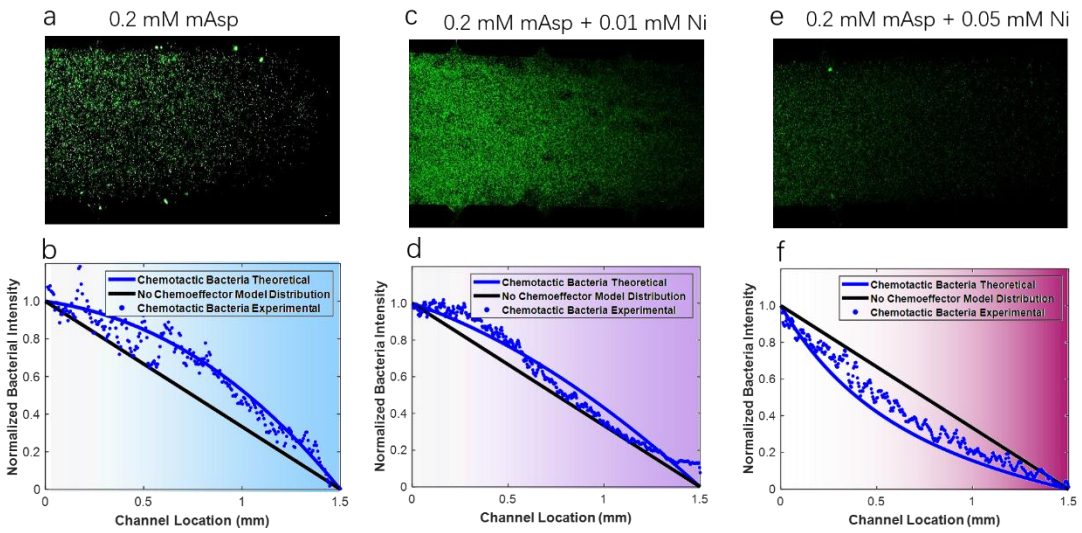

Figure 3.6 GFP-labeled *E. coli* distribution in a cross channel at steady state. There is a constant source of bacteria on the left-hand side of the channel, and a constant source of chemoeffector on the right-hand side: (a) 0.2 mM α-methyl aspartate, (b) 0.2 mM α-methyl aspartate and 0.01 mM nickel ions, and (c) 0.2 mM α-methyl aspartate and 0.05 mM nickel ions. The fluorescence intensity is proportional to bacterial concentration and is plotted as normalized intensity as a function of location for bacteria response to (d) 0.2 mM α-methyl aspartate, (e) 0.2 mM α-methyl aspartate and 0.01 mM nickel ions, and (f) 0.2 mM α-methyl aspartate and 0.05 mM nickel ions. Note that although the bacteria concentrations in the images are not the same, the gray level value in each image is calibrated itself using the methods described in 3.4.3.

Next, we studied the effect of adding different attractant concentrations to the repellent using the same method as described in the previous sections. Similar to previous section, there was a constant source of GFP-labeled chemotactic bacteria *E. coli* HCB1 on the left-hand side of the cross channel and the repellent 0.05 mM (after mixing) nickel sulfate and attractant α-methylaspartate 0.2 mM or 0.4 mM (after mixing) were mixed to provide a constant source of chemoeffectors on the right-hand side. The distribution of bacteria in response to 0.05 mM nickel sulfate repellent after at

least two hours is shown in Figure 3.7b. MATLAB software (The MathWorks, Inc.) was used to predict the bacterial distribution profile by solving the governing Equation (3.3) for bacteria and using the chemotactic velocity of Equation (2.30) for the combined case. When mixed with 0.2 mM α-methylaspartate, the bacteria distribution also shows a non-linear parabolic shape with negative deviation (concave up) in Figure 3.7d from the control case. As we increased the α-methylaspartate concentration to 0.4 mM as shown in Figure 3.7f, we also saw a non-linear parabolic shape with negative deviation (concave up) from the control case. The increased attractant concentration countered the repellent effect and moved the bacterial distribution closer to the control case, but never to the point of the combination crossing the diagonal line as an overall "attraction" response.

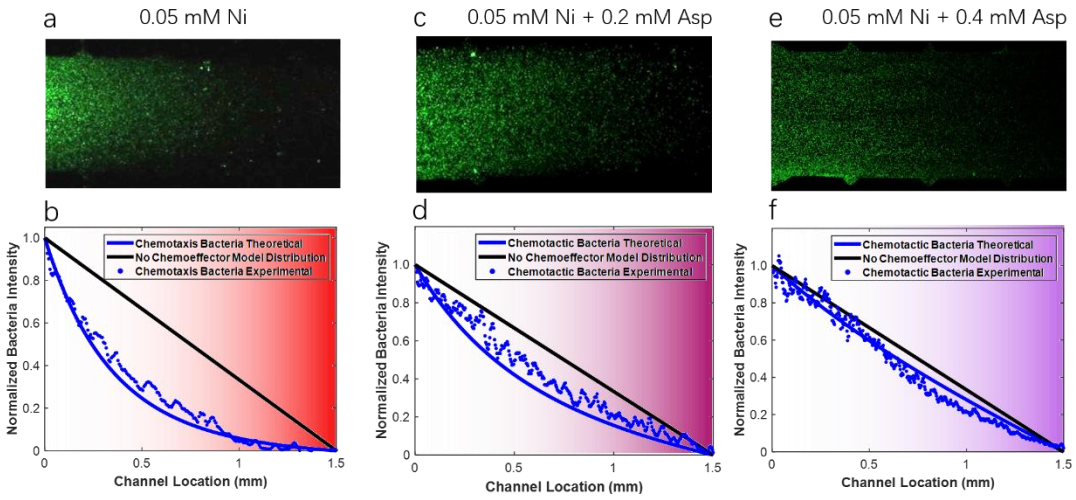

Figure 3.7 GFP-labeled *E. coli* distribution in a cross channel at steady state for a constant source of bacteria on the left-hand side of the channel and a constant source of chemoeffector on the right-hand side with (a) 0.05 mM nickel ions (b) 0.05 mM nickel ions and 0.2 mM α-methyl aspartate and (c) 0.05 mM nickel ions and 0.4 mM α-methyl aspartate). The fluorescence intensity is proportional to bacterial concentration and is plotted as normalized intensity as a function of location for bacteria response to (d) 0.05 mM nickel ions, (e) 0.05 mM nickel ions and 0.2 mM α-methyl aspartate, and (f) 0.05 mM nickel ions and 0.4 mM α-methyl aspartate. Note that although the bacteria concentrations in the images are not the same, the gray level value in each image is

calibrated itself using the methods described in 3.4.3.

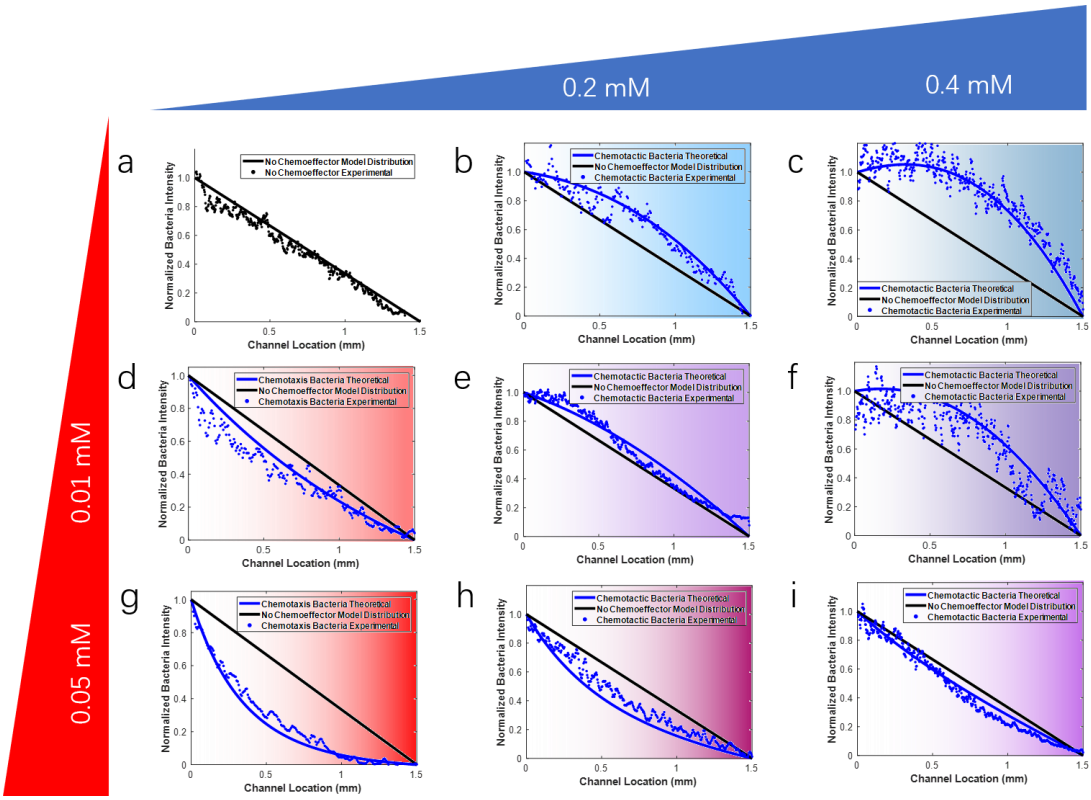

Figure 3.8 GFP-labeled *E. coli* distribution in a cross channel at steady state. There is a constant source of bacteria on the left-hand side of the channel, and a constant source of attractant α-methyl aspartate or/and repellent nickel ions on the right-hand side (a: buffer only; b-c 0.2 mM and 0.4 mM α-methyl aspartate; d-f 0.01 mM nickel ions, addition of 0.2 mM, and addition of 0.4 mM α-methyl aspartate; g-i 0.05 mM nickel ions, addition of 0.2 mM, and addition of 0.4 mM α-methyl aspartate). The fluorescence intensity is proportional to bacterial concentration.

We can see from the summary results in Figure 3.8 that the model and its parameters capturing bacteria chemotaxis signal transduction steps inside the cell provide a good description of bacterial population behavior. By fitting the model with the experimental data, we obtained parameters γ and σ from the attractant only experiment. We then used the same γ and σ value to fit the model

with the data in the repellent case, which is how we obtained κ. Then all the parameters were used to obtain to predict bacterial chemotaxis response to specific stimuli (α-methylasparate or nickel) given the concentration of the chemoeffector and compared to the experimental results. There are not many references about multiple stimuli response to compared with, but the shape of the combined case in our experiment is similar to that in Kalinin et al. (2010). They introduced two attractants separately in two ends of the channel to create the opposing effect of the attractants. While they concluded that the chemotactic response of *E. coli* depended on the ratio of the respective receptor number of Tar/Tsr, we are able to quantitively predict the bacteria distribution in the presence of multiple stimuli.

Here, we only considered cases where bacteria and chemoeffector sources were positioned on opposite sides of the channel, which means that two chemoeffectors were mixed first and then introduced into the top layer of the device. Chemoeffectors introdced from different sides were not considered as we assume that they would be mixed prior to exposure to bacteria in natural settings. This study suggests that mathematical model can be used to predict bacteria response to chemical mixture. It provides insights to tune bacteria chemotactic response by modulating the attractant/repellent concentration in a bioremediation scenario.

References

Ahmed, T., Shimizu, T. S., & Stocker, R. (2010). Bacterial chemotaxis in linear and nonlinear steady microfluidic gradients. Nano Letters, 10(9), 3379-3385.

Berg, H. C., Brown, D. A. (1972). Chemotaxis in *Escherichia coli* analysed by three-dimensional tracking. *Nature*, *239*(5374), 500-504.

Berg, H. C., Turner, L. (1990). Chemotaxis of bacteria in glass capillary arrays. *Escherichia coli*, motility, microchannel plate, and light scattering. *Biophysical Journal*, *58*(4), 919-930.

Clarke, S., & Koshland, D. E. (1979). Membrane receptors for aspartate and serine in bacterial chemotaxis. *Journal of Biological Chemistry*, *254*(19), 9695-9702.

Das, N., Chandran, P. (2011). Microbial Degradation of Petroleum Hydrocarbon Contaminants: An Overview. *Biotechnology Research International*, *201*, 1-13.

Diao, J., Young, L., Kim, S., Fogarty, E. A., Heilman, S. M., Zhou, P., Shuler, M. L., Wu, M., DeLisa, M. P. (2006). A three-channel microfluidic device for generating static linear gradients and its application to the quantitative analysis of bacterial chemotaxis. *Lab on a Chip*, *6*(3), 381-388.

de Sánchez, S. R., Schiffrin, D. J. (1996). Bacterial chemo-attractant properties of metal ions from dissolving electrode surfaces. *Journal of Electroanalytical Chemistry*, *403*(1-2), 39-45.

Ford, R. M., Harvey, R. W. (2007). Role of chemotaxis in the transport of bacteria through saturated porous media. *Advances in Water Resources*, *30*(6-7), 1608-1617.

Grebe, T. W., & Stock, J. (1998). Bacterial chemotaxis: the five sensors of a bacterium. Current Biology, 8(5), R154-R157.

Hoff, R. Z. (1993). Bioremediation: an overview of its development and use for oil spill clean up. *Marine Pollution Bulletin*, *26*, 476-481.

Jasuja, R., Trentham, D. R., & Khan, S. (1999). Response tuning in bacterial chemotaxis. Proceedings of the National Academy of Sciences, 96(20), 11346-11351.

Kalinin, Y., Neumann, S., Sourjik, V., & Wu, M. (2010). Responses of *Escherichia coli* bacteria to two opposing chemoattractant gradients depend on the chemoreceptor ratio. *Journal of Bacteriology*, *192*(7), 1796–1800.

Mears, P. J., Koirala, S., Rao, C. V., Golding, I., & Chemla, Y. R. (2014). *Escherichia coli* swimming is robust against variations in flagellar number. *Elife*, *3*, e01916.

Middlebrooks, S. A. (1993). The chemotactic response of *Escherichia coli* to combined repellent and attractant stimuli. (M.S. Thesis) University of Virginia.

Middlebrooks, S. A., Zhao, X., Ford, R. M., & Cummings, P. T. (2021). A mathematical model for *Escherichia coli* chemotaxis to competing stimuli. *Biotechnology and Bioengineering, 118*(12), 4678-4686.

Mowbray, S. L., & Koshland, D. E. (1987). Additive and independent responses in a single receptor: Aspartate and maltose stimuli on the tar protein. Cell, *50*(2), 171-180.

Pandey, G., & Jain, R. K. (2002). Bacterial chemotaxis toward environmental pollutants: role in bioremediation. *Appl. Environ. Microbiol.*, *68*(12), 5789-5795.

Rivero, M. A., Tranquillo, R. T., Buettner, H. M., & Lauffenburger, D. A. (1989). Transport models for chemotactic cell populations based on individual cell behavior. *Chemical Engineering Science*, *44*(12), 2881-2897.

Singh, R., & Olson, M. S. (2008). Application of bacterial swimming and chemotaxis for enhanced bioremediation. In Emerging environmental technologies (pp. 149-172). Springer, Dordrecht.

Sourjik, V. (2004). Receptor clustering and signal processing in E. coli chemotaxis. Trends in microbiology, 12(12), 569-576.

Sourjik, V., Armitage, J. P. (2010). Spatial organization in bacterial chemotaxis. *The EMBO journal*, *29*(16), 2724-2733.

Strauss, I., Frymier, P. D., Hahn, C. M., & Ford, R. M. (1995). Analysis of Bacterial Migration. II. Studies with Multiple Attractant Gradients. AICHE Journal, 41(2), 402-414.

Tso, W. W., Adler, J. (1974). Negative chemotaxis in *Escherichia coli*. Journal of bacteriology, 118(2), 560-576.

Wang, X., Atencia, J., Ford, R. M. (2015). Quantitative Analysis of Chemotaxis Towards Toluene by *Pseudomonas putida* in a convection-free device. *Biotechnology and Bioengineering*, *112*(5), 896-904.

Wolfe AJ, Conley MP, Kramer TJ, Berg HC. (1987). Reconstitution of signaling in bacterial

chemotaxis. *Journal of Bacteriology*, *169,*1878-1885.

Worku, M. L., Sidebotham, R. L., Walker, M. M., Keshavarz, T., Karim, Q. N. (1999). The relationship between *Helicobacter pylori* motility, morphology and phase of growth: implications for gastric colonization and pathology. *Microbiology*, *145*(10), 2803-2811.Yawata, Y., Cordero, O. X., Menolascina, F., Hehemann, J. H., Polz, M. F., & Stocker, R. (2014). Competition–dispersal tradeoff ecologically differentiates recently speciated marine bacterioplankton populations. *Proceedings of the National Academy of Sciences*, *111*(15), 5622-5627.

Zhang, X., Si, G., Dong, Y., Chen, K., Ouyang, Q., Luo, C., & Tu, Y. (2019). Escape band in *Escherichia coli* chemotaxis in opposing attractant and nutrient gradients. *Proceedings of the National Academy of Sciences*, 116(6), 2253-2258.

Chapter 4. Marine Bacteria *Halomonas* sp. 10BA Chemotactic to Multiple Stimuli

4.1 Abstract

Microorganisms played an important role in the degradation of hydrocarbons that were released into the Gulf of Mexico from the Macondo oil well blow-out. A process attracting bacteria toward higher hydrocarbon concentrations can increase biodegradation efficiency, which is termed chemotaxis. Marine bacteria chemotaxis is not well characterized. Therefore, we quantified the contribution of chemotaxis to the migration of marine bacteria toward a hydrocarbon. We exposed marine isolate *Halomonas* sp. 10BA to decane in a uniquely designed microfluidic device which maintained a constant concentration gradient across a channel. This design also ensured that the migration of bacteria was solely in response to decane. Inorganic ions, such as copper ions are repellent to marine bacteria. Therefore, the effect of copper ions on marine bacteria chemotaxis was tested. Experimental data was then used to quantify parameters in a mathematical model capturing bacteria motility and chemotaxis. We found that the random motility coefficient for marine bacteria in the model is within the same order of magnitude as that of *Escherichia coli*. In our model, *Halomonas* sp. 10BA used separate receptors for sensing attractant or repellent, an additional parameter was added to the model to account for using two receptors for attractant and one for repellent. Chemotaxis parameters values (stimuli sensitivity coefficient $\sigma = 2$ s ,signaling efficiency $\gamma = 4$, and repellent sensitivity coefficient $\kappa = 2.7$) were also reported. For *Halomonas* sp. 10BA response to multiple stimuli, qualitatively, the prediction correctly estimates the "attraction" or "repulsion" of bacteria to the stimuli mixture. However, the model predicts a stronger "repulsion response to the stimuli mixture. This overprediction may likely result from a high dissociation constant for the reaction of copper bound receptor and the phosphate group at higher Cu concentration, further changing the value for the repellent sensitivity coefficient κ. This work

suggests that the signaling pathway adapted from *E. coli* can be applied to qualitatively describe marine bacteria chemotactic response to multiple stimuli. However, further modification should be applied to the model to accurately predict the response quantitatively. Regardless, this model can provide qualitatively estimation on the naturally occurring marine bacteria respond to the oil given the oil composition. This can provide some information on whether bioremediation should be considered or the conventional interventions should be enforced in oil spill cleanup.

4.2 Introduction

The largest oil spill in U.S. waters, the *Deepwater Horizon* oil spill released around 780,000 m^3 crude oil into the Gulf of Mexico (Crone et al., 2010). To clean up the oil spill, strategies such as burning, filtering, collecting, and dispersing were used. During the dispersion process, 1.8 million gallons of chemical dispersants were released into the Gulf of Mexico. Dispersants created small oil droplets which provides greater surface area of oil for bacteria to be drawn to. However, the use of dispersants is controversial. Studies shown that dispersant Corexit 9500 can even decrease oil biodegradation rate (Almeda et al., 2014) and has greater environmental risk than crude oil alone (Kim et al., 2012). Therefore, it is necessary to find a way to degrade oil droplets, without using potentially harmful chemicals.

A promising technique is bioremediation, a technique that uses microorganisms to remove pollutants from contaminated sites. These organisms can use pollutants as a food source and degrade them to less toxic or nontoxic substances (Hoff, 1993, Das et al. 2011). King et al. (2015) studied the biodegradation process following the oil spill. They found that the bacterial density in a cloud of dispersed oil (10^5 cells/ml) was higher than outside of the cloud (10^3 cells/ml). In addition, they found genes for chemotaxis and motility were enriched and expressed in organisms isolated from this cloud. This finding indicates that marine organisms play a role in oil spill cleanup. Therefore, processes that increase bacteria accumulation in the cloud of dispersed oil would aid cleanup as greater numbers of bacteria have the capacity to degrade more oil droplets. Chemotaxis is one of these processes, in which bacteria are attracted to a higher chemical concentration because they can use the chemicals as food and energy sources. The chemical compounds attracting chemotactic bacteria are called chemoattractants, while compounds bacteria swim away from are called chemorepellents. *Escherichia coli* (*E. coli*) show positive chemotaxis to amino acids and aromatic compounds, while sulfides and inorganic ions cause negative chemotaxis (Pandey and Jain, 2002).

Studies show that common soil bacteria such as *Pseudomonas* sp. (Harwood, 1984) and *Azospirillum* sp. (Lopez-de-Victoria et al., 1993) have a positive chemotactic response to aromatic hydrocarbons. Other studies (Lanfranconi et al., 2003, Meng et al., 2017) reported that bacteria show positive chemotactic responses towards n-hexadecane. Most importantly, the presence of chemotactic genes in *Oceanospirillales* cells suggests that marine bacteria show chemotactic response to hydrocarbons in an oil plume (Mason et al., 2012). However, marine bacteria show different chemotactic responses to different hydrocarbons. Toluene, a major component of crude oil, has been reported as a negative chemoeffector for several marine *Pseudomonas* strains (Young and Mitchell, 1973). They also reported that inorganic copper ions act as chemorepellents to marine *Pseudomonas* strains. In contrast, de Sánchez and Schiffrin (1996) concluded that copper ions are strong chemoattractant to marine *Pseudomonas* strain H36-ATCC. Therefore, the effect of copper ions on different marine bacteria is still not clear and worth investigating.

Most studies in the field focus on soil bacteria chemotaxis, while the chemotaxis for marine bacteria is not well characterized. Furthermore, there is lack of study on quantitative bacteria chemotaxis, especially quantitative study on marine bacteria chemotaxis. Seymour et al. (2008) studied three marine bacteria chemotactic responses in the presence of five different chemoattractants. They used the chemotaxis index to quantify the responses. At the population level, two major parameters are used to characterize bacteria chemotactic response. Chemotactic sensitivity coefficient χ_0 [m^2/s] accounts for the strength of the chemotactic response of a population of bacteria and the chemotactic receptor constant K_c [mol/L] represents the apparent binding constant that characterizes the signal transduction process within the cell (Ford and Harvey, 2007). Wang et al. (2015) quantified the chemotactic parameters for soil bacteria *Pseudomonas putida* in the presence of toluene and reported an χ_0 value of $1.8 \pm 0.7 \times 10^{-4}$ cm^2/s and a K_c value of 1 ± 0.4 mM. Based on the diffusion profile of a population of bacteria, random motility

coefficient μ [m^2/s] can be obtained in the absence of chemoeffectors. One study from de Sánchez and Schiffrin (1996) on marine *Pseudomonas* strain H36-ATCC reported the apparent random motilty coefficient value of $1.5 \times 10^{-5} cm^2/s$. The lack of other quantitative studies prompts us to quantify chemotactic and motility parameters of marine bacteria.

In addition to studying marine bacteria chemotactic response to specific hydrocarbons, we are also interested in studying the chemotactic response to multiple stimuli. This is because bacteria are exposed to multiple compounds in their environment. When bacteria receive conflicting information from chemical signals, they decide how to respond and adjust their swimming behavior accordingly. At the individual bacterium level, chemotactic swimming is modulated by the directional change of rotation of the bacterium's flagella. Figure 4.1 shows flagellar arrangement of *Halomonas titanicae* BH1 electron micrographs. *Halomonas titanicae* BH1 is motile with the use of peritrichously flagella. However, there is a lack of study on the chemotactic mechanism of *Halomonas* sp. at the individual level, while the chemotactic mechanism for *E. coli* bacteria is well studied. For *E. coli*, when the flagella rotate clockwise, bacteria will tumble, while the counterclockwise rotation of the flagella will lead to bacteria to "run" in a straight pathway. In the absence of chemoattractant, bacteria would trace out a random walk similar to diffusive motion (Rivero et al., 1989). Specifically, they "run" for ~1 s and "tumble" for ~ 0.1s (Berg and Brown, 1972). In the presence of a chemoattractant, bacteria will migrate toward the higher chemoattractant concentration by decreasing the tumble probability when they run in a direction toward the higher chemoattractant concentration; while in the presence of a chemorepellent gradient, the cell decreases its tumbling frequency when moving in a decreasing chemorepellent concentration (Tso and Adler, 1974).

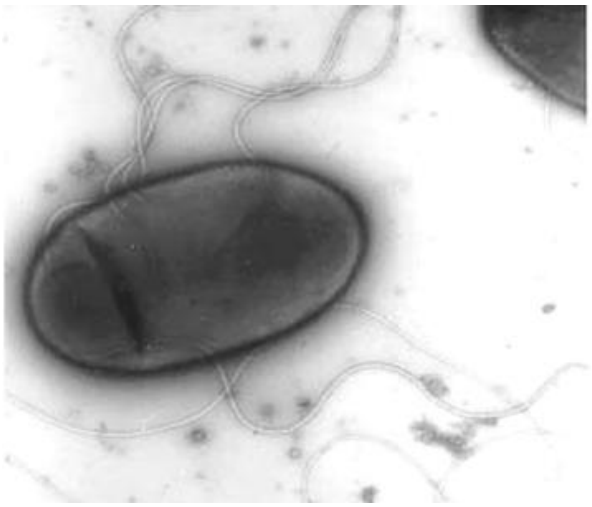

Figure 4.1 Transmission Electron Micrograph of *Halomonas titanicae* BH1, showing flagellar arrangement. (From Sánchez-Porro et al., 2010).

At the individual cell level, Rivero et al. (1989) developed a theoretical model to describe individual bacterium's chemotactic behavior. They used the empirical correlation developed by Berg and Brown (1972), in which the logarithm of mean run time is increased with respect to the rate of change in the number of bound receptors. The mean run time is the reciprocal of the tumbling probability which is related to the population's chemotactic movement velocity. Several researchers (Mowbray and Koshland, 1987; Strauss et al., 1995; Kalinin et al. 2010; Zhang et al., 2019) have studied bacterial chemotactic response in the presence of multiple stimuli. Kalinin et al. (2010) studied *E. coli* chemotactic response to the chemoattractants α-methyl-DL-aspartate (MeAsp) and serine, they found when the ratio of receptors (Tar/Tsr) is greater than 2, cells will change attraction from serine to MeAsp. For *Halomonas* sp. KHS3, three methyl-accepting chemotaxis proteins are included in chemosensory cluster (Gasperotti et al., 2018). It is possible for *Halomonas* sp. to use separate receptors for different compounds, e.g., receptor 1 for attractant and receptor 2 for repellent. Therefore, it is important to understand how the signal transduction mechanism functions inside an individual bacterium, integrating an individual bacterium's response in the presence of multiple

stimuli and relating it to the bacteria population response.

In order to measure the chemotactic response quantitatively, it is critical to create a well-defined chemical gradient since the chemical gradient is the driving force for chemotaxis. Middlebrooks et al. (1993) used a stopped flow channel to analyze bacterial chemotactic response to the stimuli α-methylaspartate and nickel ion. The device they used was able to create a step change in the chemical concentration for the bacteria, which then relaxed over time in a predictable way due to diffusion. In contrast, the device in Wang et al. (2015) maintained a constant chemical concentration gradient. The small scale of the microfluidic device has the advantages of low reagent consumption and decreased reaction time due to the short channel length. This design balances the pressure at opposite ends of the microchannel under laminar flow condition to eliminate convective flow in the cross channel. Stocker et al. (2008) also used microchannels to study the chemotaxis of marine bacteria *Pseudoalteromonas haloplanktis*. They measured and modeled bacteria population response to nutrient patches and plumes. They found that the chemotactic response of marine bacteria *P. haloplanktis* was ten times faster than *Escherichia coli*. However, they didn't report any parameters quantifying bacteria motility and chemotaxis.

In this paper, *Halomonas* sp. 10BA were exposed to attractants and repellents in the microfluidic device that forms a constant gradient. Decane was used as a chemoattractant. In addition to hydrocarbons, metallic ions (such as nickel, iron and copper) exist in all crude oil types in very small amounts. Copper is also known to be a chemoeffector to marine bacteria (Young and Mitchel, 1973). Experimental data was used to quantify transport parameters in a mathematical model capturing bacterial motility and chemotaxis. This work enables us to quantify the effect of bacterial chemotactic processes that facilitate accessibility of oil droplets to bacteria, further increasing degradation of dissolved hydrocarbons.

4.3 Methods and Model

4.3.1 Preparation of bacteria cultures

Marine bacteria *Halomonas* sp. Bead 10BA (Gasperotti et al., 2018) was obtained from Doug Bartlett (Scripps Institute of Oceanography). In each experiment, 100 μL of Bead 10BA frozen stock was cultured in 50 mL marine broth (Fisher Scientific, NY) with 100 μL decane added. Bacteria were cultured in a 250 mL Erlenmeyer flask on a Thermo Scientific Incubated Shaker (MaxQ4000) with a rotation rate of 150 rpm at 30 ◦C.

The bacteria were harvested when the optical density reached 1.20 (measured in spectrophotometer, Molecular Devices, Spectramax 384 plus) at 590 nm (corresponding to the mid-exponential phase of the growth phase); this also corresponds to the conditions when bacteria exhibit the greatest motility (Worku et al., 1999). Then the bacteria were separated from the culture media with 0.22 μm membrane filter (Millipore, MA) using vacuum filtration (Berg and Turner, 1990) and were ready to stain. Staining stock solution was prepared by dissolving the contents of one vial CFDA SE (Invitrogen, CA) in 90 μL of DMSO (Invitrogen, CA) to reach a concentration of 10 mM. Then 45 μL of the stock solution was diluted in the 5 mL of 5% random motility buffer (100% RMB, including 9.13 g/L Na_2HPO_4 (Fisher Scientific), 4.87 g/L $NaH_2PO_4 \cdot H_2O$ (Amresco), 0.029 g/L EDTA (Sigma, MO)). Bacteria were incubated in this working solution for at least 60 mins at 30°C, filtered twice to remove the dye, and then resuspended into 5% RMB to the optical density around 1.40. Before taking microscopy images, the motility of the bacteria was examined under Zeiss 100/1.25 oil lens with Nikon microscope (Digital Sight DS-5Mc).

In experiments designed to obtain the motility coefficient, 5% random motility buffer was injected in one arm of the Y-shaped channel as shown in Figure 3.1. To determine chemotaxis, 5% RMB was replaced by a decane solution that is at the solubility concentration in water (0.06 μM). Decane was chosen because it is the major compound in crude oil. The solubility of n-decane in water is 0.009 mg/L at 20 °C (Verschueren, 2001), which corresponds to a concentration of 0.06

μM. However, in salt water, the solubility is increased to 0.087 mg/L at 20 °C (Verschueren, 2001). Therefore, it is feasible to test the response of *Halomonas* sp, 10BA to different concentrations of decane. The recipe for synthesized sea water used in this study is: Trzima base 5 g/L, KCl 0.75 g/L, NH_4Cl 1 g/L, $MgSO_4.7H_2O$ 3.91 g/L, $MgCl_2.6H_2O$ 5.08 g/L, $CaCl_2$ 1.5 g/L, and NaCl 23 g/L. Then HCl was used to adjust pH to 7.5. For repellent, copper is chosen because copper is known to be a repellent for marine bacteria (Young and Mitchell, 1973). Copper concentration of 0.05 mM was tested at first, but no obvious response was observed. Therefore, the concentration of 0.5 mM and 2 mM were selected. Note that Grey and Steck (2001) observed *E. coli* growth on agar plates of LB medium and of LB medium containing 4 mM $CuSO_4$. Therefore, 2 mM Cu won't be toxic for bacteria.

4.3.2 Mathematical Model

Signal transduction kinetics

In order to understand how an individual bacterium reacts to chemoeffectors, we need to understand the bacteria signal transduction mechanism. The signaling response in *E. coli* chemotaxis depends on the phosphotransfer between a histidine kinase and a response regulator (Sourjik et al., 2010). In the absence of chemoattractant, the kinase CheA has autophosphorylation activity, and the CheA phosphoryl group is further transferred to response regulator CheY. The response regulator diffuses through the cytoplasm and transmits the signal to flagellar motor, enhancing the probability of clockwise (CW) rotation and causing bacteria to tumble. For *Halomonas sp*. KHS3, Gasperotti et al. (2018) found that three methyl-accepting chemotaxis proteins are included in chemosensory cluster. However, the chemotactic mechanism for *Halomonas* sp. is still unknown. Since *Halomonas* sp. have the same flagella arrangement as that of *E. coli*, we first assumed they have the same chemotactic mechanism. However, the competitive

model for the multiple stimuli of *E. coli* didn't fit the experimental results of *Halomonas* sp. 10BA. We then assumed that the chemotactic response of *Halomonas* sp. 10BA to decane and copper are independently. We also assumed that each receptor regulates the response for either attractant or repellent, with m designated to sense one chemical (e.g. A) and n (e.g. B) for another, as shown in Figure 4.2.

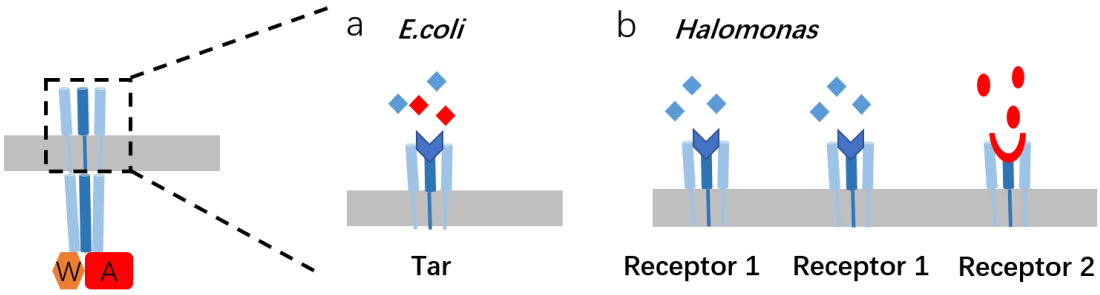

Figure 4.2 Schematic of the signal transduction mechanism in (a) *E. coli*, where the Tar receptor is used to sense both stimuli (blue indicates attractant and red indicates repellent); (b) *Halomonas* sp., where there are two Receptor 1s (m=2) for sensing attractant, and for each Receptor 2 (n=1), which is associated with sensing repellent.

Similar to the model for *E. coli*, in the absence of chemoeffector, we assume that there is an autophosphorylation reaction when the receptor complex is unbound, represented as

$$A + P_i \overset{K_1}{\Leftrightarrow} A\text{-}P_i \tag{4.1}$$

$$A_T = A + A\text{-}P_i \tag{4.2}$$

$$B + P_i \overset{K_1}{\Leftrightarrow} B\text{-}P_i \tag{4.3}$$

$$B_T = B + B\text{-}P_i \tag{4.4}$$

$$R_T = A_T + B_T \tag{4.5}$$

where R_T, a fixed value, is the summation of A_T and B_T, where A_T is the summation of A, the unbound receptor complex, and A-P_i, the phosphorylated receptor, and K_1 is the dissociation constant of phosphorylation of the unbound receptor complex and in the absence of any other evidence, we assigned the same dissociation constant value for the phosphorylation reaction of A and B.

We assume that in the presence of a chemoattractant, binding of the attractant causes A inactivation (indicated as the red cross in Figure 1.2), decreases the probability of clockwise (CW) rotation and causes the bacterium to tumble less frequently, which leads to the bacterium continuing to move in the same direction. In the opposite case, the binding of repellent does not inactivate B, and instead may increase the B activity, which increases the probability of clockwise (CW) rotation and results in more frequent tumbles, causing bacteria to swim away from the repellent source. We assume that decane (D) binds specifically to receptor A and copper ion (Cu) binds specifically to the receptor B, represented as

$$A + D \overset{K_{dD}}{\Longleftrightarrow} D\text{-}A \tag{4.6}$$

$$B + Cu \overset{K_{dC}}{\Longleftrightarrow} Cu\text{-}B \tag{4.7}$$

$$Cu\text{-}B + P_i \overset{K_2}{\Leftrightarrow} Cu\text{-}B\text{-}P_i \tag{4.8}$$

$$[R_T] = [A] + [B] + [D\text{-}A] + [Cu\text{-}B] + [A\text{-}P_i] + [B\text{-}P_i] + [Cu\text{-}B\text{-}P_i] \tag{4.9}$$

In the above Equations (4.6-4.9), D-A and Cu-B represent bound receptor complexes of decane and copper ions, respectively, R_T is the total amount of receptor and is a fixed number, K_{dD} is the dissociation constant of decane binding and K_{dC} is the dissociation constant of copper ions binding.

We assume the signaling complex transfers information through phosphorylation

$$A\text{-}P_i \overset{k}{\rightarrow} Y\text{-}P_i \tag{4.10}$$

where Y-P_i is the phosphorylated Y.

The concentration of phosphorylated Y in the absence of chemoattractant could be obtained since the total amount of receptor is fixed, and is shown in Equation (4.11)

$$[\text{Y-P}_\text{i}]_0 = \frac{R_T k}{\gamma+1} \tag{4.12}$$

where k is the reaction rate constant of the phosphate transfer reaction, and $\gamma = \frac{K_1}{[P_i]}$ is the signaling efficiency.

Similarly, the amount of signal in the presence of decane alone and copper alone are expressed in Equations (4.13) and (4.14)

$$[\text{Y- P}_\text{i}]_\text{D} = \frac{[A_T]}{1+\gamma+\gamma\frac{[Decane]}{K_{dD}}} + \frac{[B_T]}{\gamma+1} \tag{4.13}$$

$$[\text{Y- P}_\text{i}]_\text{Cu} = \frac{R_T k}{1+\gamma(1+\frac{[Cu]}{K_{dC}})/(1+\kappa\frac{[Cu]}{K_{dC}})} \tag{4.14}$$

where $A_T = \frac{m}{m+n}R_T, B_T = \frac{n}{m+n}R_T$, and $\kappa = \frac{K_1}{K_2}$ is the repellent sensitivity coefficient.

We further related the receptor concentration to the tumbling probability (more details are provided in Section 2.2) and obtained Equations (4.15) (4.16) (4.17) for the chemotaxis velocity in the presence of decane, copper and both together:

$$V_{c,D} = \frac{1}{3}\sigma v^2\left(\frac{m}{m+n}\frac{\left(\frac{\gamma+1}{\gamma}\right)K_{dD}}{\left(\left(\frac{\gamma+1}{\gamma}\right)K_{dD}+[Decane]\right)^2}\frac{\partial([Decane])}{\partial x}\right) \tag{4.15}$$

$$V_{c,C} = -\frac{1}{3}\frac{n}{m+n}\sigma(\kappa-1)v^2\frac{\left(\frac{\gamma+1}{\gamma}\right)K_{dC}}{\left(\left(\frac{\gamma+1}{\gamma}\right)K_{dC}+\left(\frac{\kappa+\gamma}{\gamma}\right)[Cu]\right)^2}\frac{\partial([Cu])}{\partial x} \tag{4.16}$$

$$V_{c,T} = -\frac{1}{3}\sigma v^2\left(\frac{n}{m+n}\frac{\left(\frac{\gamma+1}{\gamma}\right)(\kappa-1)Kdc}{\left(\left(\frac{\gamma+1}{\gamma}\right)KdC+\left(\frac{\kappa+\gamma}{\gamma}\right)[Cu]\right)^2}\frac{\partial[Cu]}{\partial x} - \frac{m}{m+n}\frac{\left(\frac{\gamma+1}{\gamma}\right)KdD}{\left(\left(\frac{\gamma+1}{\gamma}\right)KdD+[Decane]\right)^2}\frac{\partial[Decane]}{\partial x}\right) \tag{4.17}$$

Note that Equation (4.15) can be simplified into the chemotactic velocity equation in Wang et al. (2015) given 1) $\frac{\gamma+1}{\gamma}$ is close to 1 (or large γ), 2) $\frac{m}{m+n}$ is close to 1 (or n is small), and 3) $\chi_0 = \sigma v^2$, where χ_0 is the chemotactic sensitivity coefficient, accounting for the strength of the

chemotactic response of a population of bacteria. Different terms dominate the equation when the chemoeffector concentration is low or high. Since K_{dD} is at least one order of magnitude higher than the decane concentration in this study, the effect of decane concentration doesn't change $\frac{\left(\frac{\gamma+1}{\gamma}\right)K_{dD}}{\left(\left(\frac{\gamma+1}{\gamma}\right)K_{dD}+[Decane]\right)^2}$, but $V_{c,D}$ increases as the decane concentration gradient $\frac{\partial([Decane])}{\partial x}$ increases. However, K_{dC} is at the same order of magnitude as the copper concentration in this study, so the concentration affects both terms in Equation (4.16). It is obvious that Equation (4.17) is the form of the addition of Equation (4.15) and Equation (4.16), which is the case of our assumption that the response of bacteria to attractant and repellent are independent to each other.

4.4 Results and Discussion

4.4.1 *Halomonas* sp. 10BA chemotactic response to decane

CFDA SE labeled *Halomonas* sp. 10BA were introduced from the left-hand side of the channel, and decane from the right-hand side. This provides a constant concentration gradient of 0.06 μM or 0.2 μM decane (calculated based on the solubility level). Microscopic images of the cross channel were taken after the system reached steady state (at least two hours), as shown in Figure 4.3a and Figure 4.4a. Both distribution profiles show positive deviation from the control case when no chemoeffector was introduced. This positive deviation indicates that decane is an attractant to *Halomonas* sp. 10BA. Bacteria distribution profiles were also predicted by solving the governing Equation (3.3) for bacteria and using the chemotactic velocity of Equation (4.15) for decane. Parameters used in the model were the stimuli sensitivity coefficient $\sigma = 2$ s, signaling efficiency $\gamma = 4$, and the dissociation constant of decane binding $K_{dD} = 1.0\ \mu$M. Since there were no literature values for the parameters γ and σ for *Halomonas* sp. 10BA, the values of these parameters for *E. coli* were used as the initial estimates. For the dissociation constant K_{dD}, a value

of order of magnitude 10^{-6} was used because we assumed this value is close to the maximum availability value (or the solubility level) in the water. In addition, a study by Xie et al. (2015) also reported a dissociation constant in the order of magnitude of 10^{-6} for marine bacteria chemotactic response.

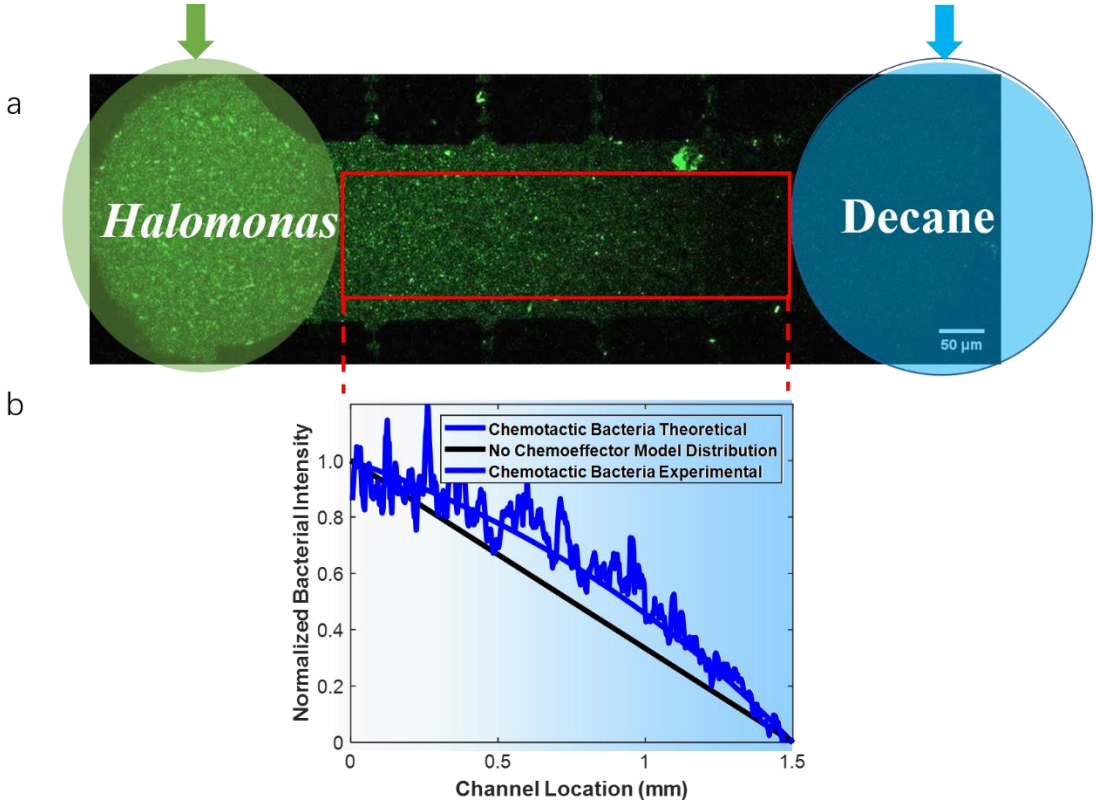

Figure 4.3. (a) Microscopic images of the cross channel in the microfluidic device, where *Halomonas* sp. 10BA migrate from a constant source at the left-hand side toward 0.06 μM decane from a constant source at the right-hand side. The red rectangular box indicates the region over which the data was analyzed. (b) Normalized bacterial intensity profile from the experiment (scattered blue line) and model results (solid blue line). The blue shading indicates the concentration of decane which decreases from right to left.

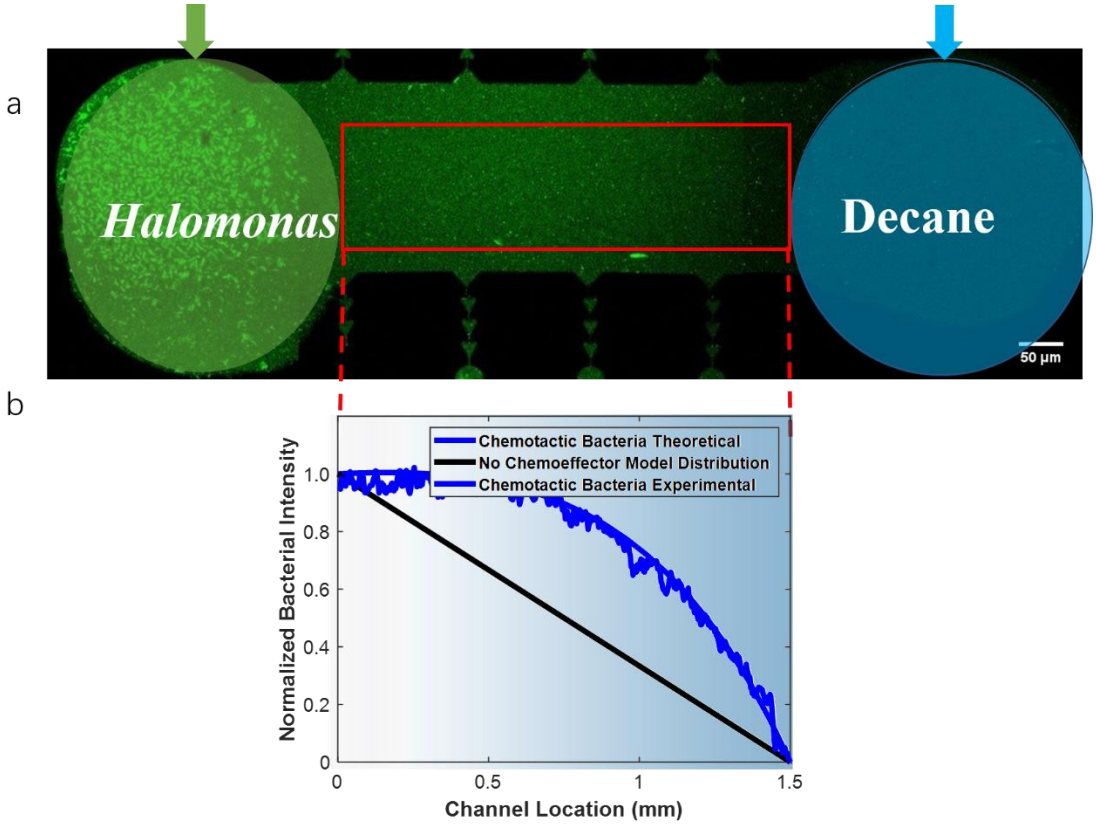

Figure 4.4 (a) Microscopic images of the cross channel in the microfluidic device, where *Halomonas* sp. 10BA form a constant source at the left-hand side and 0.2 μM decane form a constant source at the right-hand side. The red rectangular box indicates the region over which the data was analyzed. (b) Normalized bacterial intensity profile from the experiment (scattered blue line) and model results (solid line). The blue gradient shade indicates the constant gradient of decane from right to left.

4.4.2 *Halomonas* sp. 10BA chemotactic response to copper

Similar to the previous section, CFDA SE labeled *Halomonas* sp. 10BA were introduced from the left-hand side of the channel, and Cu from the right-hand side. This provides a constant gradient of source of 0.5 mM or 2 mM Cu concentration. Microscopic images of the bottom channel were taken after the system reached steady state after at least two hours, as shown in Figure 4.5b and Figure 4.6b. Both distribution profiles show negative deviation from the control case when no

chemoeffector is introduced. This indicates that Cu is a repellent to *Halomonas* sp. 10BA. Bacteria distribution profiles were also predicted by solving the governing Equation (3.3) for bacteria and using the chemotactic velocity of Equation (4.16) for Cu. The value of γ, σ for *Halomonas* sp. 10BA were used directly from the results in the previous section. The value of repellent sensitivity coefficient κ was fitted staring from the value determined for *E. coli* as an individual guess and $\kappa = 2.7$ was obtained to characterize repellent response of *Halomonas* sp. 10BA. For the dissociation constant K_{dC}, a value in the order of magnitude of 10^{-3} was used because this value indicates the concentration where bacteria have the most "repulsion" response to Cu, and it should be close to the toxic concentration for bacteria. The value of $K_{dC} = 3.5$ mM was obtained after fitting the model with the experimental results.

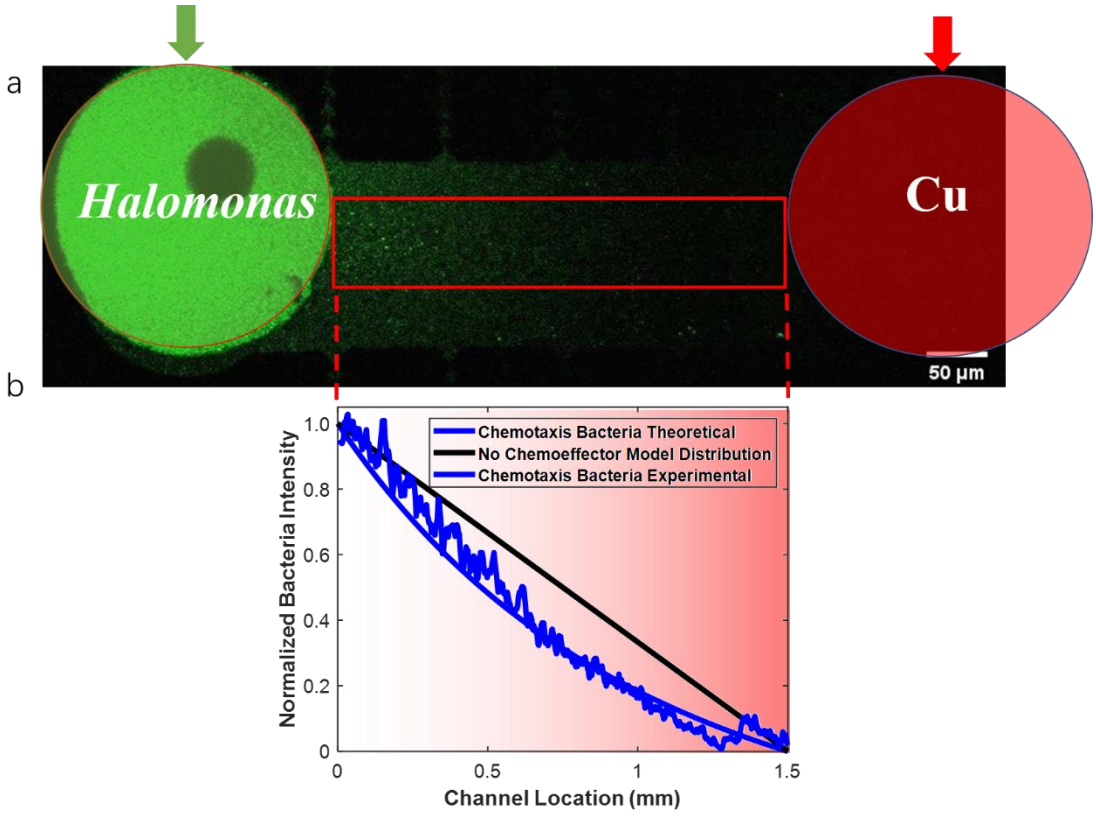

Figure 4.5 (a) Microscopic images of the bottom channel in the microfluidic device, where *Halomonas* sp. 10BA form a constant source at the left-hand side and 0.5 mM Cu form a constant source at the right-hand side. The red rectangular box indicates the region over which the data was

analyzed. (b) Normalized bacterial intensity profile from the experiment (scattered blue line) and model results (solid line). The blue gradient shade indicates the constant gradient of Cu from right to left.

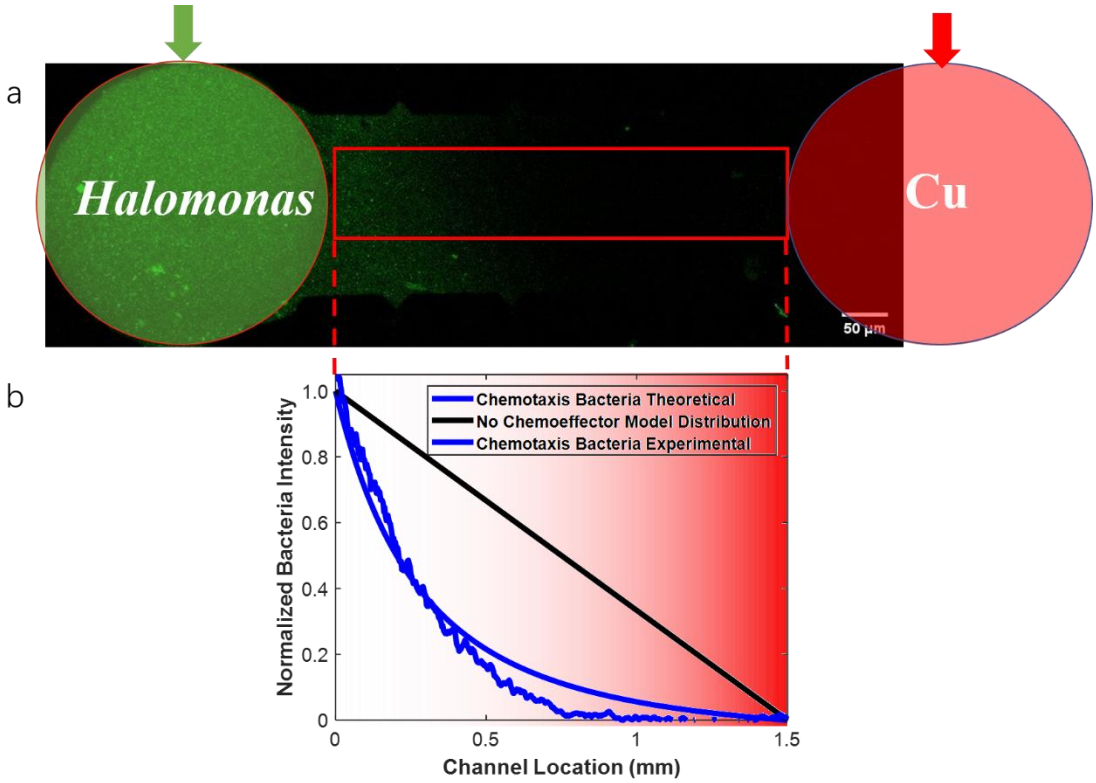

Figure 4.6 (a) Microscopic images of the bottom channel in the microfluidic device, where *Halomonas* sp. 10BA form a constant source at the left-hand side and 2 mM Cu form a constant source at the right-hand side. The red rectangular box indicates the region over which the data was analyzed. (b) Normalized bacterial intensity profile from the experiment (scattered blue line) and model results (solid line). The blue gradient shade indicates the constant gradient of Cu from right to left.

4.4.3 *Halomonas* sp. 10BA chemotactic response to chemoeffector mixtures

CFDA SE labeled *Halomonas* sp. 10BA were introduced from the left-hand side of the channel, and different concentrations of decane and Cu were introduced from the right-hand side. This

provides a constant gradient of source of chemoeffector mixture. Microscopic images of the cross channel were taken once the system reached steady state (after at least two hours), as shown in Figure 4.7 and Figure 4.8. By comparing the Figure 4.7b and Figure 4.7d, it is suggested that the addition of Cu to 0.2 μM decane decreased the migration of *Halomonas* sp. 10BA. As the concentration of Cu increased from 0.5 mM to 2 mM, bacteria response eventually shifts from attraction to repulsion to the chemoeffector mixture, as shown in Figure 4.7f. Bacteria distribution profiles were also predicted by solving the governing Equation (3.3) for bacteria and using the chemotactic velocity of Equation (4.17) for the chemoeffector mixture. The value of γ, σ, κ for *Halomonas* sp. 10BA were used directly from the results in the previous section. This indicates that the model successfully predicts bacteria response to chemoeffector mixture. For bacteria response to the mixture of 0.2 μM decane and 0.5 mM Cu, the model captures bacteria response both quantitively and qualitatively. However, the model only predicts qualitatively the response of marine bacteria to the mixture of 0.2 μM decane and 2 mM Cu. This may due to the decreased κ value at high Cu concentration, which corresponds to a larger dissociation constant for the reaction of copper bound receptor with the phosphate group. This may correspond to a lower binding affinity of copper bound receptor to the phosphate group, which may likely because the conformational change of the cytoplasmic domain on the transmembrane receptor following Cu binding to the periplasmic domain of the receptor (Park et al., 2011).

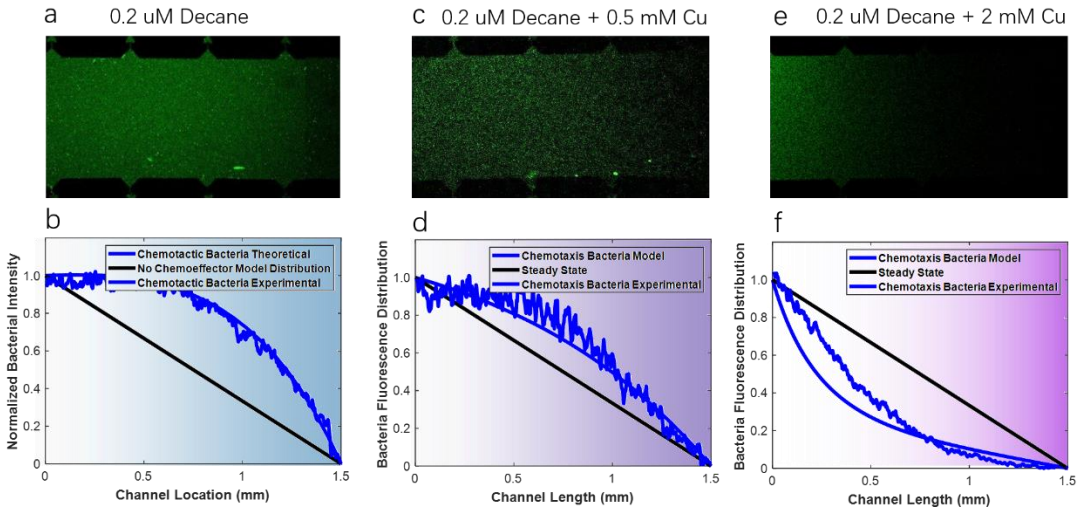

Figure 4.7 Effect of the addition of Cu to *Halomonas* sp. 10BA response to chemoeefector. Microscopic images of the bottom channel in the microfluidic device, where *Halomonas* sp. 10BA form a constant source at the left-hand side and (a) 0.2 μM decane (b) 0.2 μM decane and 0.5 mM Cu (c) 0.2 μM decane and 2 mM Cu form a constant source at the right-hand side; normalized bacterial intensity profile from the experiment (scattered blue line) and model results (solid line). The blue gradient shade indicates the constant gradient of chemoeffector from right to left.

Next, the effect of addition of decane to Cu was shown in Figure 4.8. By comparing the Figure 4.8b and Figure 4.8d, it is suggested that the addition of decane to 0.5 mM Cu increased the migration of *Halomonas* sp. 10BA to the chemoeffector. As the concentration of decane increased from 0.06 μM to 0.2 μM, *Halomonas* sp. 10BA switched the response from repulsion to attraction to the chemoeffector mixture. The model correctly predicts the response both quantitatively and qualitatively.

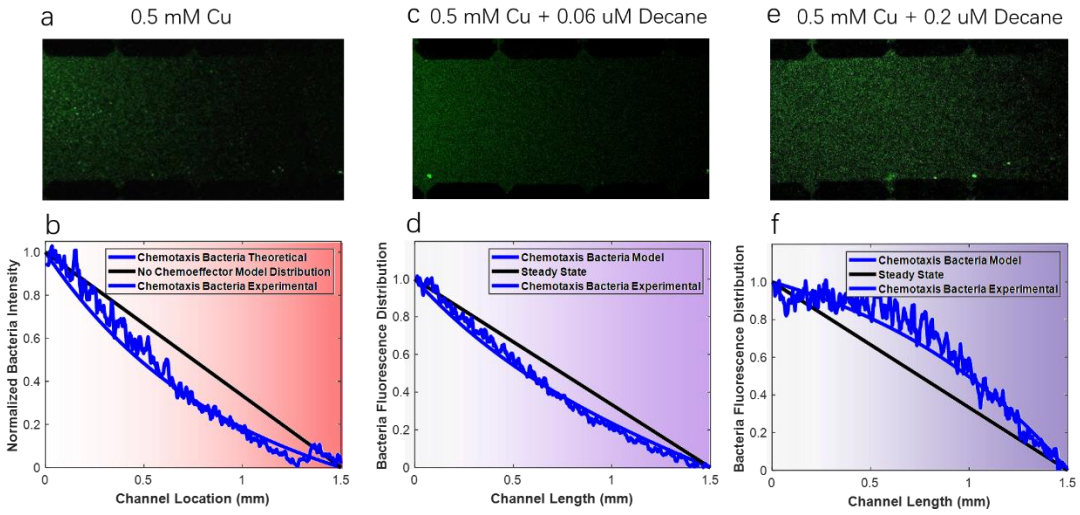

Figure 4.8 Effect of the addition of decane to *Halomonas* sp. 10BA response to chemoeefector. Microscopic images of the bottom channel in the microfluidic device, where *Halomonas* sp. 10BA form a constant source at the left-hand side and (a) 0.5 mM decane (b) 0.5 mM Cu and 0.06 μM decane and (c) 0.5 mM Cu and 0.2 μM decane form a constant source at the right-hand side; normalized bacterial intensity profile from the experiment (scattered blue line) and model results (solid line). The blue gradient shade indicates the constant gradient of chemoeffector from right to left.

In summary, the model incorporates three chemotactic receptors for *Halomonas* sp. 10BA chemotaxis. As shown in the methods section, two receptors are used for decane binding and one receptor is used for Cu binding. The experimental results and the model prediction for different scenarios are shown in Figure 4.9. The model predicts the experiment results successfully except for the cases with 2 mM Cu. This overprediction may likely result from the conformational change of the receptor at high Cu concentration, altering the affinity of copper bound receptor to phosphate group, further changing the value for the repellent sensitivity coefficient κ.

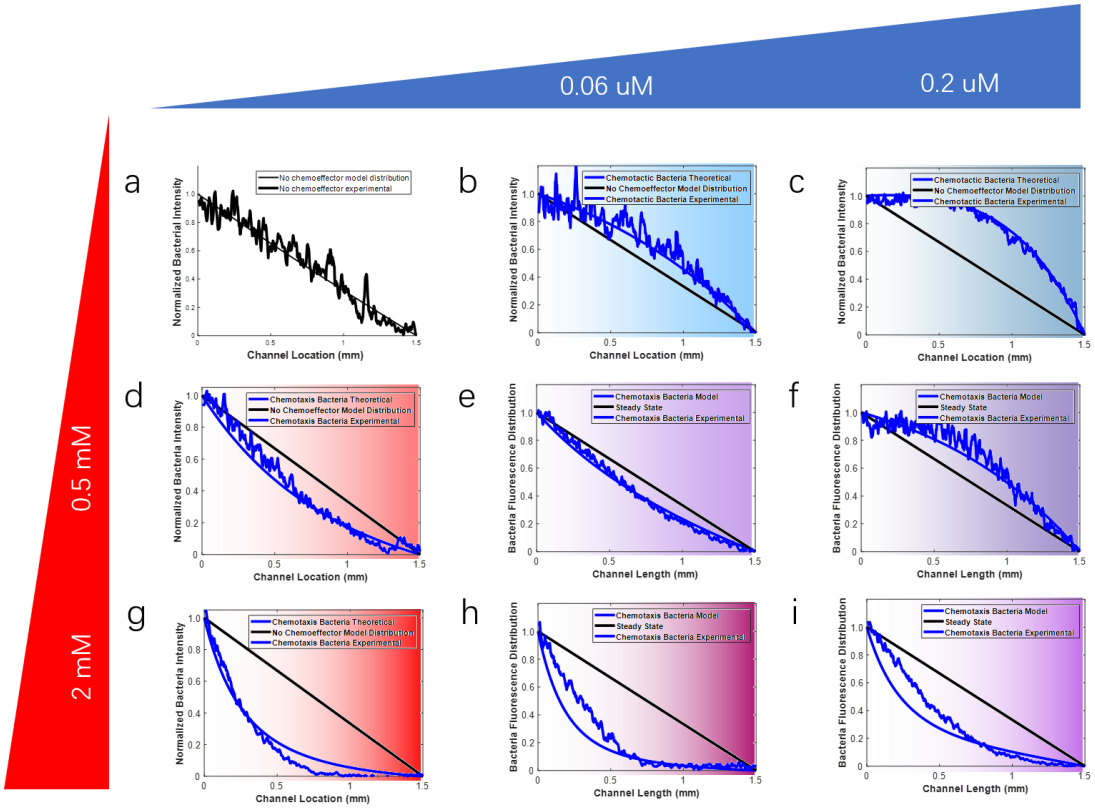

Figure 4.9 Normalized bacterial intensity profile from the experiment (scattered blue line) and model results (solid line). (a) buffer only; (b-c) 0.06 μM decane and 0.2 μM decane; (d) 0.5 mM Cu; (e) 2 mM Cu; (f) 0.06 μM decane and 0.5 mM Cu; (g) 0.2 μM decane and 0.5 mM Cu; (h) 0.06 μM decane and 2 mM Cu; (i) 0.2 μM decane and 2 mM Cu. The blue gradient shade indicates the constant gradient of chemoeffector from right to left.

In conclusion, a mathematical model was presented in this paper to capture *Halomonas* sp. 10BA chemotaxis response to attractant and repellent. The model was first used to fit bacteria response to single stimulus to obtain the value for parameters $\gamma, \sigma, \kappa, K_{dD}, K_{dC}$. Then the model was used to predict the response of *Halomonas* sp. 10BA to the mixture of decane and Cu. This prediction captures the response well at low Cu concentration at 0.5 mM, while under predicts bacteria migration at high Cu concentration of 2 mM, which may likely due to the high dissociation constant of Cu bound receptor to the phosphate group at high Cu concentration, corresponding to a

lower κ. Under the case with 0.06 μM decane and 0.5 mM Cu, *Halomonas* sp. 10BA exhibited "attraction" response to the combination, meaning chemotaxis will bring more bacteria to the mixture and likely further increase the biodegradation of hydrocarbons.

References

Almeda, R., Hyatt, C., Buskey, E. J. (2014). Toxicity of dispersant Corexit 9500A and crude oil to marine microzooplankton. *Ecotoxicology and environmental safety*, *106*, 76-85.

Berg, H. C., Brown, D. A. (1972). Chemotaxis in *Escherichia coli* analysed by three-dimensional tracking. *Nature*, *239*(5374), 500-504.

Berg, H. C., Turner, L. (1990). Chemotaxis of bacteria in glass capillary arrays. *Escherichia coli*, motility, microchannel plate, and light scattering. *Biophysical Journal*, *58*(4), 919-930.

Crone, T. J., Tolstoy, M. (2010). Magnitude of the 2010 Gulf of Mexico oil leak. *Science*, *330*, 634.

Das, N., Chandran, P. (2011). Microbial Degradation of Petroleum Hydrocarbon Contaminants: An Overview. *Biotechnology Research International*, *201*, 1-13.

De Sánchez, S. R., Schiffrin, D. J. (1996). Bacterial chemo-attractant properties of metal ions from dissolving electrode surfaces. *Journal of Electroanalytical Chemistry*, *403*(1-2), 39-45.

Ford, R. M., Harvey, R. W. (2007). Role of chemotaxis in the transport of bacteria through saturated porous media. *Advances in Water Resources*, *30*(6-7), 1608-1617.

Gasperotti, A. F., Revuelta, M. V., Studdert, C. A., Seitz, M. K. H. (2018). Identification of two different chemosensory pathways in representatives of the genus *Halomonas*. *BMC genomics*, *19*(1), 266.

Grey, B., & Steck, T. R. (2001). Concentrations of copper thought to be toxic to Escherichia coli can induce the viable but nonculturable condition. Applied and Environmental Microbiology, 67(11), 5325-5327.

Harwood, C. S., Rivelli, M., Ornston. L. N. (1984). Aromatic acids are chemoattractants for *Pseudomonas putida*. *Journal of Bacteriology*, *160*, 622-628.

Hoff, R. Z. (1993). Bioremediation: an overview of its development and use for oil spill clean up. *Marine Pollution Bulletin*, *26*, 476-481.

Kalinin, Y., Neumann, S., Sourjik, V., & Wu, M. (2010). Responses of *Escherichia coli* bacteria to two opposing chemoattractant gradients depend on the chemoreceptor ratio. *Journal of Bacteriology*, *192*(7), 1796–1800.

Kim, J. N., Kim, B. S., Kim, S. J., Cerniglia, C. E. (2012). Effects of crude oil, dispersant, and oil-dispersant mixtures on human fecal microbiota in an in vitro culture system. *Mbio*, *3*(5), e00376-12.

King, G. M., Kostka, J. E., Hazen, T. C., Sobecky, P. A. (2015). Microbial Responses to the *Deepwater Horizon* Oil Spill: From Coastal Wetlands to the Deep Sea. *Annual Review of Marine Science*, *7*(1), 377-401.

Lanfranconi, M. P., Alvarez, H. M., Studdert, C. A. (2003). A strain isolated from gas oil-contaminated soil displays chemotaxis towards gas oil and hexadecane. *Environmental microbiology*, *5*(10), 1002-1008.

Lopez-de-Victoria, G., Lowell, C. R. (1993). Chemotaxis of *Azospirillum* species to aromatic compounds. *Applied and Environmental Microbiology*, *59*, 2951-2955.

Mason, O. U., Hazen, T. C., Borglin, S., Chain, P. S., Dubinsky, E. A., Fortney, J. L., … & Mackelprang, R. (2012). Metagenome, metatranscriptome and single-cell sequencing reveal microbial response to Deepwater Horizon oil spill. *The ISME journal*, *6*(9), 1715.

Meng, L., Li, H., Bao, M., Sun, P. (2017). Metabolic pathway for a new strain *Pseudomonas synxantha* LSH-7′: from chemotaxis to uptake of n-hexadecane. *Scientific reports*, *7*, 39068.

Middlebrooks, S. A. (1993). The chemotactic response of *Escherichia coli* to combined repellent

and attractant stimuli. (M.S. Thesis) University of Virginia.

Mowbray, S. L., & Koshland, D. E. (1987). Additive and independent responses in a single receptor: Aspartate and maltose stimuli on the tar protein. *Cell*, *50*(2), 171-180.

Pandey, G., & Jain, R. K. (2002). Bacterial chemotaxis toward environmental pollutants: role in bioremediation. *Applied and Environmental Microbiology*, *68*(12), 5789-5795.

Park, H., Im, W., Seok, C. (2011). Transmembrane signaling of chemotaxis receptor tar: insights from molecular dynamics simulation studies. *Biophysical journal*, *100*(12), 2955-2963.

Rivero, M. A., Tranquillo, R. T., Buettner, H. M., & Lauffenburger, D. A. (1989). Transport models for chemotactic cell populations based on individual cell behavior. *Chemical Engineering Science*, *44*(12), 2881-2897.

Sánchez-Porro, C., Kaur, B., Mann, H., Ventosa, A. (2010). *Halomonas titanicae* sp. nov., a halophilic bacterium isolated from the RMS Titanic. International journal of systematic and evolutionary microbiology, 60(12), 2768-2774.

Seymour, J. R., Ahmed, T., Stocker, R. (2008). A microfluidic chemotaxis assay to study microbial behavior in diffusing nutrient patches. Limnology and Oceanography: Methods, 6(9), 477-488.

Sourjik, V., & Armitage, J. P. (2010). Spatial organization in bacterial chemotaxis. *EMBO Journal*, *29*(16), 2724-2733.

Stocker, R., Seymour, J. R., Samadani, A., Hunt, D. E., Polz, M. F. (2008). Rapid chemotactic response enables marine bacteria to exploit ephemeral microscale nutrient patches. *Proceedings of the National Academy of Sciences of the United States of America*, *105*(11), 4209-4214.

Strauss, I., Frymier, P. D., Hahn, C. M., & Ford, R. M. (1995). Analysis of Bacterial Migration. II. Studies with Multiple Attractant Gradients. *AICHE Journal*, *41*(2), 402-414.

Tso, W. W., Adler, J. (1974). Negative chemotaxis in *Escherichia coli*. Journal of bacteriology, 118(2), 560-576.

Verschueren, K. Handbook of Environmental Data on Organic Chemicals. Volumes 1-2. 4th ed. John Wiley & Sons. New York, NY. 2001, p. 655

Wang, X., Atencia, J., Ford, R. M. (2015). Quantitative Analysis of Chemotaxis Towards Toluene by *Pseudomonas putida* in a convection-free device. *Biotechnology and Bioengineering*, *112*(5), 896-904.

Worku, M. L., Sidebotham, R. L., Walker, M. M., Keshavarz, T., Karim, Q. N. (1999). The relationship between *Helicobacter pylori* motility, morphology and phase of growth: implications for gastric colonization and pathology. *Microbiology*, *145*(10), 2803-2811.

Xie, L., Lu, C., Wu, X. L. (2015). Marine bacterial chemoresponse to a stepwise chemoattractant stimulus. *Biophysical journal*, *108*(3), 766-774.

Young, L. Y., & Mitchell, R. (1973). Negative chemotaxis of marine bacteria to toxic chemicals. Applied microbiology, 25(6), 972-975.

Zhang, X., Si, G., Dong, Y., Chen, K., Ouyang, Q., Luo, C., & Tu, Y. (2019). Escape band in *Escherichia coli* chemotaxis in opposing attractant and nutrient gradients. *Proceedings of the National Academy of Sciences*, *116*(6), 2253-2258.

Chapter 5. Conclusions and Future Directions

The work presented in this dissertation focused on measuring motility and chemotactic parameters for *E. coli* and marine bacteria *Halomonas* sp. 10BA by using a constant-gradient microfluidic device and a mulit-scale model capturing the signal sensing process inside the cell. The advantage of the microfluidic device is that it creates a constant concentration gradient of a chemical stimulus. Fitting the model with the experimental results allows us to obtain parameters capturing the chemotactic response. The integration of the individual level sensing mechanism to the population scale chemotactic velocity provided insight about the fundamental cellular reaction when bacteria perform chemotactic behavior.

For the experimental device, a few upgrades were incorporated into the previous manifestation of the device. First, the orientation of the bottom channel was changed to directly face the light source, largely improving the image quality. Second, an opaque polystyrene material was used as an alternative for the glass centerpiece, which improved the maintenance of the device. Fluorescent labeling was chosen to visualize and quantify bacteria concentration in the device. CFDA SE cell tracer was selected label marine bacteria *Halomonas* sp. because this cell tracer provides a high and stable fluorescence intensity over others.

The multi-scale model incorporated the phosphorylation reaction when stimuli bind to the receptor on the cell membrane where the chemotactic response is initiated. This model relates the cellular level reaction to the chemotactic response at the populational level. Motility and chemotactic parameters were obtained by comparing the model predictions with the experimental results. The random motility coefficient obtained from this study was $\mu_0 = 1.4 \pm 0.46 \times 10^{-10}\ m^2/s$ for *E. coli*, and $\mu_0 = 2.5 \pm 0.20 \times 10^{-10}\ m^2/s$ for marine bacteria *Halomonas* sp. 10BA. The random motility coefficient for *E. coli* was in the same order of magnitude as that from a previous study (Wang et al., 2015). The higher random motility coefficient for *Halomonas* sp.

10BA was expected due to the faster swimming speed of marine bacteria compared to *E. coli*, which matches the observations from previous studies.

Three parameters were used to quantify the cellular level chemotactic response. Stimuli sensitivity coefficient σ, signaling efficiency γ, and repellent sensitivity coefficient κ were obtained for both *E. coli* (σ=3 s, γ=4, κ= 9) and *Halomonas* sp. 10 BA (σ=2 s, γ=4, κ= 2.7). The resulting parameters were in the same order of magnitude as those previously reported in the scientific literature, though these parameters of *E. coli* were slightly lower compared to those in (Middlebrooks et al., 2021). We believe that the value measured in this constant gradient device may be more accurate as the gradient, which drive that chemotaxis response, is better defined compared to the results from the stopped-flow diffusion chamber.

Furthermore, these parameters evaluated independently for bacteria chemotactic responses to single stimulus allow us to make prediction for responses to multiple stimuli. We then compared the prediction with experimental results. For *E. coli*, qualitatively, the model predicted correctly the overall attraction or repulsion outcomes of the mixture. However, the prediction showed a higher repellent response of the mixture than the experimental results in some conditions, which was also the case in Middlebrook et al. (2021).

Since the chemosensory mechanism for *Halomonas* sp. was not well-studied, we assumed *Halomonas* sp. to have the same run-and-tumble chemotactic mechanism as *E. coli* based on 1) the same peritrichous flagella arrangement, and 2) similar organization of chemotactic genes compared to *E. coli*. We also started by assuming that chemotactic receptors for *Halomonas* sp. 10BA were independent for attractant or repellent. However, this initial simple approach did not yield predictions that matched the experiments results. Therefore, we further modified the model with that *Halomonas* sp. 10BA use two receptors for sensing attractant decane and one for sensing repellent copper. This modification achieved good agreement with the experimental results.

Similar to the model prediction for *E. coli* in the case of stimuli mixtures, qualitatively, the prediction for *Halomonas* sp. correctly estimates the attraction or repulsion of bacteria to the stimuli mixture. However, the model predicted a stronger repellent response to the stimuli mixture at high copper concentration. In order for the model to fit in these situations, a lower κ value was necessary, especially at higher copper concentrations. We suspected this discrepancy was due to a lower affinity of copper bound receptor to the phosphate group at a high copper concentration. Another possible explanation is that *Halomonas* sp. swim at a faster speed at higher repellent concentrations, which would change the strength of the chemotactic response to both repellent and attractant.

In this study, the alignment of the microfluidic device layers was important to achieve good results. Even though the alignment marker was introduced to the design, but there is still room for improvement. In our work, bacteria diffuse into the channel from the via connecting to the top channel, another configuration to consider is one where bacteria are preloaded in the channel at the beginning. Then multiple stimuli are introduced on opposite sides to see whether bacteria migrate preferentially toward one chemical gradient over another in the channel, using a device similar to the one in Kalinin et al. (2010). For the model part, it is suggested that the parameter value for repellent response κ may need to be altered at a higher repellent concentration to fit the experimental results better. Therefore, it is possible that another parameter should be introduced in order to capture this possible change in affinity of the repellent-bound receptor to the phosphate group.

Since the swimming speed of bacteria at various constant temperatures is increasing with temperature, the effect of temperature on chemotaxis should also be investigated. Past oil spills happened in both cold and warm temperature, such as the Exxon Valdez Oil Spill in Alaska or the Deepwater Horizon Oil Spill in the Gulf of Mexico. Therefore, the temperatures should also be considered to enrich the knowledge for chemotaxis under different temperatures. Since motility is decreased at low temperature, we expected the chemotactic response also decrease. However, cell

growth is also reduced at low temperature, therefore, chemotactic might be more advantages for increase bacteria population near the contamination sites.

Though the microfluidic device used in this study provided a well-defined constant gradient for modeling chemotaxis, the situation in the ocean is more complex. Chemical gradients especially can fluctuate quickly as the nutrients are dissipated rapidly by ocean currents. Therefore, it is important to consider the temporal change by designing a device that can introduce a pulse stimulus gradient for evaluating the temporal component in bacteria chemotactic response, which might be related to the adaptation in the chemotaxis signaling pathway, which is bacteria's ability to make temporal comparisons of the stimuli concentration in the environment by modulating sensory sensitivity of the chemoreceptors. A potential device might be the microfluidic device used by Stocker et al. (2008).

References

Kalinin, Y., Neumann, S., Sourjik, V., & Wu, M. (2010). Responses of *Escherichia coli* bacteria to two opposing chemoattractant gradients depend on the chemoreceptor ratio. *Journal of Bacteriology*, *192*(7), 1796-1800.

Middlebrooks, S. A., Zhao, X., Ford, R. M., & Cummings, P. T. (2021). A mathematical model for *Escherichia coli* chemotaxis to competing stimuli. *Biotechnology and Bioengineering, 118*(12), 4678-4686.

Stocker, R., Seymour, J. R., Samadani, A., Hunt, D. E., Polz, M. F. (2008). Rapid chemotactic response enables marine bacteria to exploit ephemeral microscale nutrient patches. *Proceedings of the National Academy of Sciences of the United States of America*, *105*(11), 4209-4214.

Wang, X., Atencia, J., Ford, R. M. (2015). Quantitative Analysis of Chemotaxis Towards Toluene

by *Pseudomonas putida* in a convection-free device. *Biotechnology and Bioengineering*, *112*(5), 896-904.

Appendix A: Validation of diffusion only in the device using 10% uranine solution

A.1 Validation of diffusion only in the device using 10% uranine

To test the accuracy of the microfluidic device, fluorescein uranine and buffer were injected from each end of the inlet. Microscopic pictures of the channel at different time were taken and the images were shown in Figure A.1 The gradually increasing trend of the fluorescence intensity in the cross channel was corresponding to the diffusion of the fluorescein uranine.

Einstein relation was used to estimate the time required to reach steady state:

$$L^2 = 2Dt \tag{A1}$$

where L is the channel length is 1.5mm and $D = 0.49 \times 10^{-9}$ m^2/s is the diffusion coefficient for uranine. Solving Equation (A1), t = 38min was the time used to reach the steady state in the channel.

The experimental data in Figure A.1 only showed the fluorescence intensity values from 0.45 to 1.5mm in the channel since the intensity close to the vias was too high. The experimental observation and the theoretical prediction at different times matches well as shown in Figure A.1. This confirms that there is only diffusion in the cross channel in this microfluidic device.

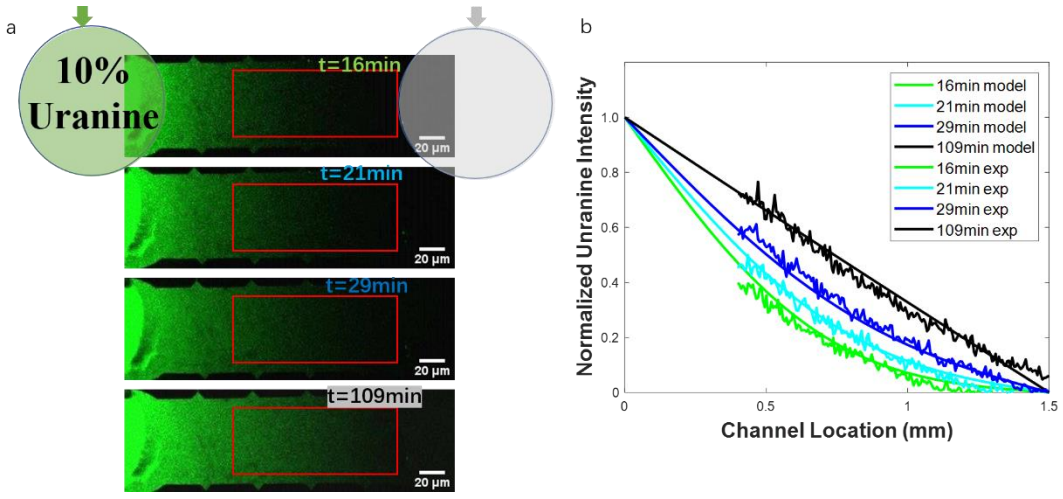

Figure A.1 (a) 10% uranine distribution in a cross channel at different times. There is a constant source of 10% uranine on the left-hand side of the channel and a constant sink on the right-hand side; the fluorescence intensity is proportional to fluorescein concentration. Red rectangular box indicates the region over which data was analyzed. (b) Normalized uranine intensity along the channel (scattered data) and the model results (solid lines) at different times.

Appendix B: Random Motility Coefficient for *E. coli* HCB1

B.1 Random motility coefficient for *E. coli* HCB1

To evaluate the bacterial diffusivity (*i.e.* random motility coefficient), a constant source of GFP-labeled chemotactic bacteria *E. coli* HCB1 was maintained at one end of the cross channel and a constant sink of random motility buffer at the opposite end. The distribution of bacteria as they migrated through the cross channel is shown in Figure B.1 at several times; the corresponding normalized bacteria fluorescence intensity is plotted in Figure B.1b. A best-fit of the mathematical model (Equation 3.2, n=10) to experimental data using nonlinear regression yielded a random motility coefficient of $\mu_0 = 1.4 \pm 0.46 \times 10^{-10}\, m^2/s$ (averaged over three replicates). This motility coefficient value is similar in magnitude to others that were previously reported ($2.4 \times 10^{-10}\, m^2/s$) for *E. coli* (Wang et al., 2015). Theoretical predictions from Equation (3.2) are shown in Figure B.1b for comparison to experimental observations. The qualitative shape of bacterial profiles follows the expected exponential decay in concentration from the constant source at x=0 as well as the increasing degree of penetration into the cross channel over time. At long times the normalized bacterial distribution approaches a decreasing linear distribution as expected once steady state has been achieved.

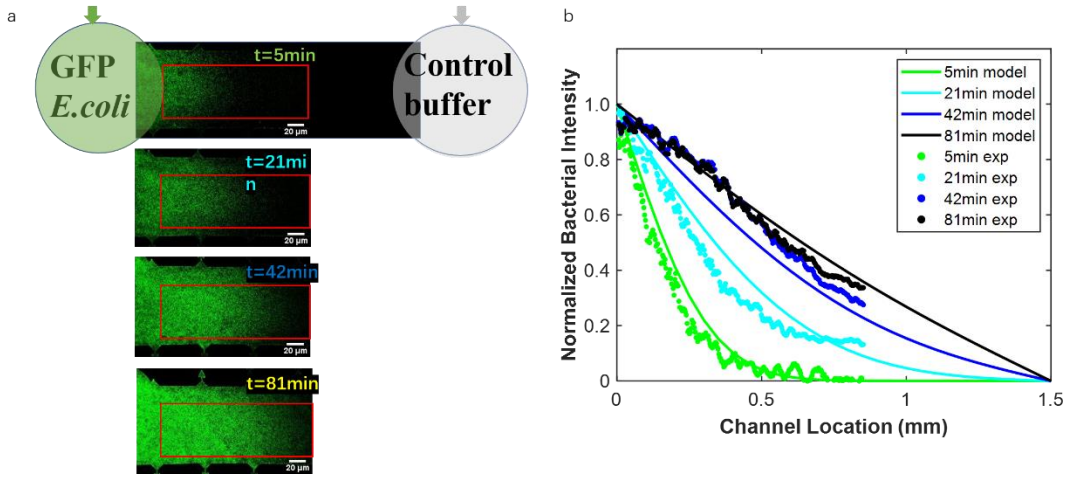

Figure B.1 (a) GFP-labeled *E. coli* distribution in a cross channel at several times. There is a constant

source of bacteria on the left-hand side of the channel and a constant sink on the right-hand side; the fluorescence intensity is proportional to bacterial concentration. Red rectangular boxes indicate the region over which data was analyzed. Only a portion (0 mm - 0.8 mm) of the channel was analyzed; this distance corresponds to the width of a single tile in the imaging process and was used to avoid recalibration of image intensity due to automatic lighting adjustment by the software controlling the camera settings (see Methods section for details). (b) Normalized bacteria intensity along the channel (scattered data) compared with model results (solid lines) at several times. The random motility coefficient obtained was $\mu_0 = 1.0 \times 10^{-10}\, m^2/s$

In order to compare the experimental results and model predictions at multiple times, following the Boltzmann's transformation, the normalized bacteria fluorescence intensity was plotted with respect to the that combines the dependence on time and space into a single variable. The model curves at different times follow the equation below

$$\frac{b}{b_0} = \operatorname{erfc}\left(\frac{1}{2\sqrt{D}}\frac{x}{\sqrt{t}}\right) \tag{B1}$$

where $\varepsilon = \frac{x}{\sqrt{t}}$. The overlaping of the plots into one curve at unsteady state indicated that it was a diffusion process.

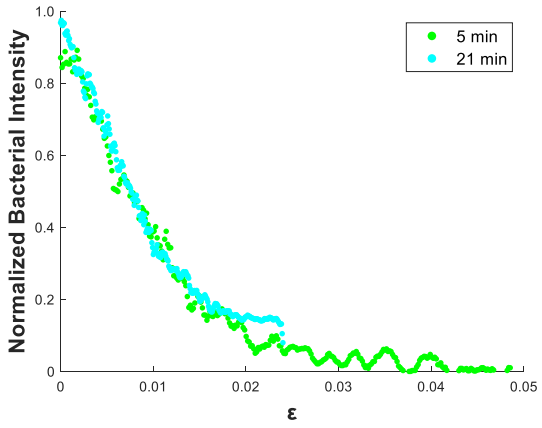

Figure B.2 Normalized bacteria intensity with respect to $\varepsilon = \frac{x}{\sqrt{t}}$ at the unsteady state time point (5 minutes and 21 minutes).

Appendix C: Random Motility Coefficient for *Halomonas* sp. 10BA

C.1 Random motility coefficient for *Halomonas* sp. 10BA

To evaluate the bacterial diffusivity (*i.e.* random motility coefficient), a constant source of CFDA FE-labeled chemotactic bacteria *Halomonas* sp. 10BA was maintained at one end of the cross channel and a constant sink of random motility buffer at the opposite end. The distribution of bacteria as they migrated through the cross channel is shown in Figure C.1 at several times; the corresponding normalized bacteria fluorescence intensity is plotted in Figure C.1b. A best-fit of the mathematical model (Equation (3.2), n=10) to experimental data using nonlinear regression yielded a random motility coefficient of $\mu_0 = 2.5 \pm 0.20 \times 10^{-10}\ m^2/s$ (averaged over three replicates). This motility coefficient value is slightly higher than that of *E. coli* as measured in the previous section, this would likely due to the faster swimming speed of *Halomonas* sp. 10BA compared to *E. coli*. Theoretical predictions from Equation (3.2) are shown in Figure C.1b for comparison to experimental observations. The qualitative shape of bacterial profiles follows the expected exponential decay in concentration from the constant source at x=0 as well as the increasing degree of penetration into the cross channel over time. At long times the normalized bacterial distribution approaches a decreasing linear distribution as expected once steady state has been achieved.

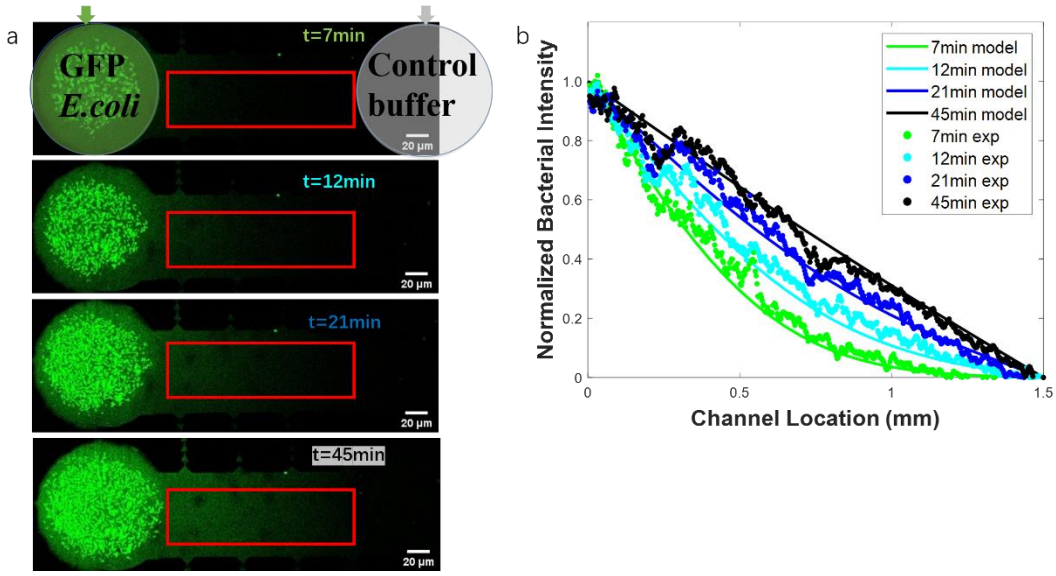

Figure C.1 (a) CFDA SE-labeled *Halomonas* sp. 10BA distribution in a cross channel at several times. There is a constant source of bacteria on the left-hand side of the channel and a constant sink on the right-hand side; the fluorescence intensity is proportional to bacterial concentration. Red rectangular boxes indicate the region over which data was analyzed. (b) Normalized bacteria intensity along the channe compared with model results at several times. The random motility coefficient obtained was $\mu_0 = 2.7 \times 10^{-10}\ m^2/s$.